Max Planck Institute für Kolloid und Grenzflächenforschung
Abteilung für Kollide; Prof. M. Antonietti

Mesoporous organosilica materials with amine functions: surface characteristics and chirality

Dissertation
zur Erlangung des akademischen Grades
"doctor rerum naturalium"
(Dr. rer. nat.)
in der Wissenschaftsdisziplin "Chemie"

eingereicht an der
Mathematisch-Naturwissenschaftlichen Fakultät
der Universität Potsdam

von
Rebecca Voß

Potsdam, den 23.03.2005

1 Introduction and motivation

By taking into consideration the adverse effects of pollution on the global weather and on the health of human beings, chemistry, as an applied science, is compelled to find solutions for the reduction and cleansing of wastes.

As a materials chemist one way to pursue this objective is to find materials having a high surface area and a tailorable functionalization. These materials could then be used as catalysts in industrial processes increasing the energy to product ratio, or they could be employed as filters to clean water or air through adsorption of heavy metals from waste water or of volatile organic compounds from the air, as well as membranes for fuel cells or electrolytes or electrodes for solid state batteries. These materials should be harmless to the environment by themselves, synthesizable under green chemistry conditions and usable in multiple cycles.

One class of materials that might combine these qualities are mesoporous silicas. These materials have been found in 1992 by Kresge and coworkers[1] using the self-assembly of templating surfactants to micelles combined in a sol-gel process with silica precursors. The sol-gel process, a condensation reaction between silanol groups to from siloxane bridges, was at that point already well known and used to form xero- or aero-gels with unconnected and unordered micropores as well as the ordered microporous zeolites. These materials are prepared in an aqueous or ethanolic solution with the help of acid or base as a catalyst. The structure-inducing molecules can then be extracted with the help of a solvent like ethanol or thermally by calcination. There are two general methods used for the condensation of silica precursors: the first is working in a dilute solution of all the components (micellation route) while the second employs the lyotropic phase of the surfactant in a more concentrated sol (nanocasting).

The behavior of these mesoporous materials can now be influenced through different factors. First of all the templates used can be changed to give different pore structures. This method has been widely employed to give pore sizes in a wide range between 2 nm and 500 nm, employing amphiphilic molecules as well as polymers[2-6] and colloids.[7-9]

A second way to influence the properties is to use different precursors in the synthesis. Instead of using only the chemically inert silica, organic groups can be incorporated into the pore walls to change the physical and chemical properties of the material. This has been done by different groups leading to materials with simple alkyl functions as well as complicated metal complexes.[10-13] However, there have only been few chiral mesoporous organosilica materials and to our knowledge none of them showed separation. So the incorporation of chirality into mesoporous organosilica and the separation of racemates on these solids will be one topic of this work. Especially precursors with two siloxyl groups bridged by a chiral organic function will be considered here.

One factor that has not received much consideration in the field of mesoporous materials is that a lot of the functional groups which can be incorporated into the silica framework are hidden in the walls and therefore not accessible for any interaction or reaction. In this work we devise a new approach that ensures that the organic function tailored for catalysis and adsorption will be on the pore surface of the material. We use two precursors in a way that while one of them is functionalizing the surface of the pores, the other is creating the skeleton of the structure by forming the pore walls. In this way the bulk properties of the material can be made independent of the surface properties and vice versa. This would allow an unprecedented degree of control on the physical and chemical properties of such class of mesoporous materials.

The mesoporous materials could also find applications in separation science[14-19] and in environmental remediation.[20, 21] In this context, the properties of organically modified

mesoporous silicas towards water will be tested. Water is used in many applications and industrial processes and effective materials for waste water clean-up have to be found. Organosilica materials with high surface areas could be used for this task, since with the right modification they are able to bind metal ions or other pollutants from this waste water.[22, 23] Also our atmosphere is becoming more polluted and needs to be protected. In this case it is not metal ions but gaseous organic molecules that are in need to be removed from air. Since the atmosphere contains water vapor in combination with organic molecules, their interaction has to be considered in any separation scheme.[24] The first step in this thesis work is to get an idea about the behavior of pure water towards different mesoporous organosilica (MO) materials.

2 Introduction to PMO materials and the sol-gel process

2.1 History of PMO materials

In the last decade, a of lot interest has been put into the synthesis of well defined porous materials, because of their potential applications in catalysis,[25-32] separation science[14-19] and environmental remediation.[20, 21] Porous materials can be classified by size, network forming material and degree of order. A material will be called microporous if the pores are smaller than 2 nm, macroporous if they are over 50 nm and mesoporous for all the sizes in between.

In this work mesoporous materials with a silica framework will be considered in more detail. One of the methods to synthesize these materials is to use a surfactant-templated sol-gel system, which was reported for the first time by Kresge and coworkers in 1992,[33] who discovered surfactant-assembled silica mesostructures. Unfortunately pure silica materials are not that interesting chemically, and different synthetic methods have been examined to create materials with chemical functionality.

One way is to anchor a functional group on the surface of the pores in a post synthesis procedure. After the removal of the surfactant the silica surface contains a certain amount of hydroxyl groups, which can function as chemical tethering sites for a wide range of organic molecules with interesting functionality. The disadvantages of this approach are that the organic groups are dangling into the pore void and therefore blocking off space and sometimes even clogging the entire pore. Also not every silanol is modified creating a none uniform distribution of grafted organics. Nevertheless, amine functions,[34-37] ephedrine,[38, 39] and organometallic complexes[40] have been introduced into mesoporous silica materials by this method.

Another way is to change the framework itself by introducing organic groups in the precursor. This can be done by using molecules containing R'-Si-$(OR)_3$ during the condensation.[41-45] This has been successful for alkyl, aryl, thiol, amine and other side chains as well as metal and chiral complexes.[22, 41-48] However, only about 25% of the modified precursor could be used in the synthesis without causing collapses of the framework. Another potential disadvantage of this method is the uneven distribution of organic groups on the surface. This problems may be exacerbated by microphase separation, which leads to some parts of the material containing more of the function than the others.[49]

In 1999 three different research groups independently introduced organically bridge-bounded precursors for the synthesis of mesoporous hybrid organic-inorganic silica compounds.[50-55] This method enabled materials to be made exclusively from organically modified precursors, leading to a uniform distribution of organic functionality in the solid. These materials have been labeled "periodic mesoporous organosilica" (PMO). Some of the organic groups included into PMOs are alkyl bridges like ethene and methene, double bond containing molecules like ethylene, phenylene, benzene and derivatives thereof, also heteroatoms functionalities like ferrocene, thiophene, 4-phenyl ether and 4-phenyl sulfide and amines.[50-53, 55-60] The incorporation of organic groups inside the channel walls of silica-based materials leads to the possibility to fine tune the chemical, physical and mechanical properties of the compound through synthetic chemistry. And, compared to the methods described above, the groups do not take space from the pores and pure organic precursor can be condensed without compromising the mechanical stability of the material as well as its short and long range order.

2.2 Formation of mesoporous materials by the surfactant–templated sol-gel method

For a standard synthesis of PMO materials non-covalently bound templates are used, including molecules, supramolecular arrays, polymers[2-6] and colloids.[7-9] When dissolved in solution these species can template small inorganic precursors via electrostatic, van de Waals, and hydrogen bonding interactions to form nanostructured materials with tailorable pore shapes and sizes.

Surfactant templates consist of bi-functional molecules with a hydrophilic head group and a hydrophobic tail. As a result of their amphiphilic nature, surfactants can self-assemble into supramolecular arrays. These molecules exist as monomers when the solution is dilute, but when their concentration exceeds a certain minimum (the so-called "critical micellar concentration" cmc) the monomers organize spontaneously, forming aggregates of colloidal dimensions, the micelles.

The formation of micelles in aqueous media is generally seen as a compromise between the tendency for the hydrophobic groups to avoid the energetically unfavorable contacts with water and the desire for the polar parts to maintain contact with the aqueous environment. Depending on the size ratio between the hydrophobic chain and the head group of a surfactant different superstructures can be formed (Figure 2-1).

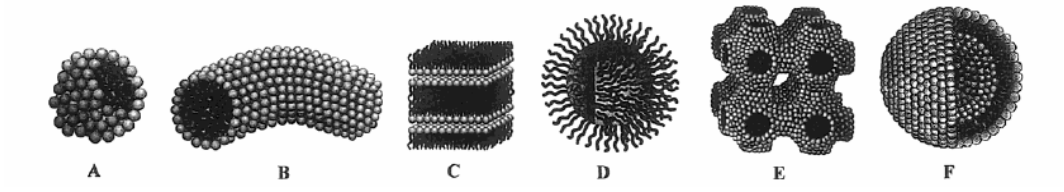

Figure 2-1: Supramolecular structures for surfactants. A = sphere, B = cylinder, C = planar bilayer, D = reverse micelle, E = bicontinous phase, F = liposomes.[61]

Since these supramolecular structures are in thermodynamic equilibrium they are often called “phases”, and a phase diagram can be constructed for each surfactant-solvent system. These phase diagrams allow prediction of the shape of the micelles depending on the thermodynamic conditions, involved in the system under consideration. For example, cetyltrimethylammonium bromide (CTAB) in water will form spherical micelles above the cmc in which the hydrophilic head group forms the outer surface and the hydrophobic tails point towards the center.

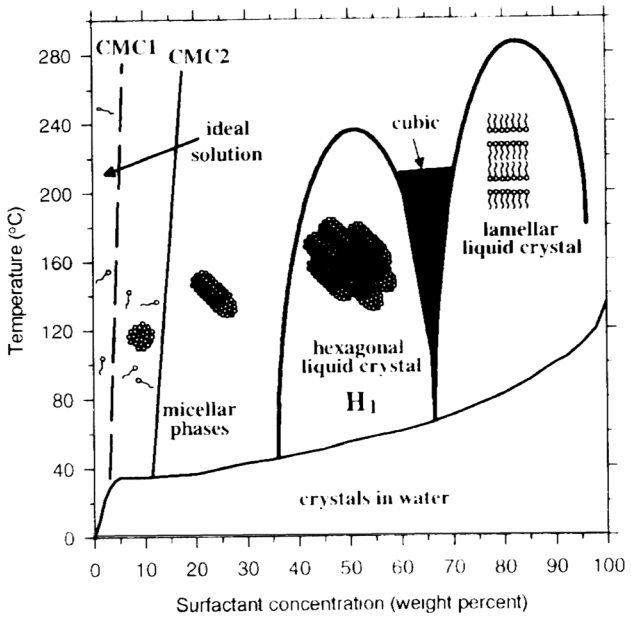

Figure 2-2: Schematic phase diagram for CTAB in water.[62]

As the concentration of the surfactant increases, the spherical micelles can coalesce to form cylindrical micelles (cmc2). Further increasing the surfactant concentration leads to liquid-crystalline (LC) phases. The rod like micelles aggregate and form hexagonal close packed LC arrays. A further increase of the surfactant concentration can produce cubic bicontinuous LC phases and even leads to LC lamellar phases. At very high concentrations, in

some systems, inverse phases can exist, in which the water is inside the micelle, with the head group pointing inwards.

There are two different pathways for the preparation of mesoporous silica materials the synthetic co-assembly mechanism introduced by Kresge *et al.*[63] and the nanocasting or true liquid crystal mechanism introduced by Attard and Goeltner.[64-66] While the co-assembly works in a concentration range below the cmc of the surfactant and the assembly takes place due to the interaction of the surfactant with the precursor forming a molecule with a bigger head group, the true liquid crystal mechanism employs concentrations in which the surfactant forms LC phases. This process, which is also called nanocasting, therefore leads to a 1:1 replica of the surfactant phase in the final material as has been shown by X-ray diffraction.[64, 65, 67] The scheme of the procedure of nanocasting with some possible templates is shown in Figure 2-4. An organic template is dissolved in the precursor and an organic solvent, usually alcohol. The concentrations are set in such a way that the template is in one of its LC phases. The precursor assembles around the template due to van de Waals or Coulomb interactions, after condensation the template is removed to give the porous solid. The condensation is a two step reaction in which first the alkoxyl groups of the precursor are hydrolyzed by the water in the reaction mixture and then the silanol group condenses with either an alkoxyl or a silanol group of another precursor (Figure 2-3).

1. Hydrolysis

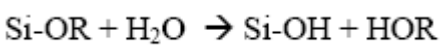

2. Condensation

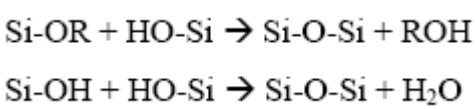

Figure 2-3: Reaction steps in a silica condensation.

The hydrolysis and condensation are taking place at different rates depending on the pH of the solution. At a pH between 2 and 5 the hydrolysis is faster leading to the formation of hydrolyzed monomeric units, which then slowly form small particles.[68, 69] At a pH higher than 5 the condensation is instead favored, leading to the formation of larger condensed particles, which will slowly grow into a 3D network.[69-71] The nanocasting process is usually performed at a pH lower than 5 therefore leading to monolithic materials, whereas the co-assembly is often done at higher pH leading to powders although procedures have been developed for controlling the morphology of the materials in the form of films, fibres and spheres to name a few.

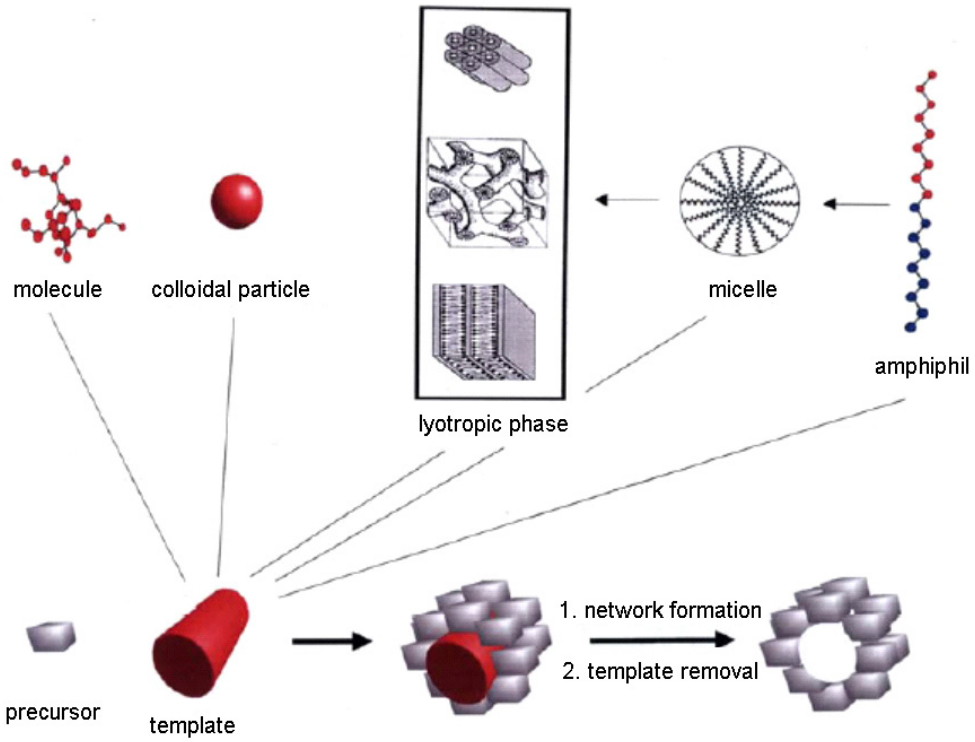

Figure 2-4: Scheme of the nanocasting process.

3 Analytical methods

3.1 Adsorption behavior of PMO materials

The adsorption of gases and vapors is one of the main methods used for characterization of the materials described in this thesis and will therefore be illustrated in more detail here.

Adsorption of nitrogen or argon on PMO materials is the standard analytical method to measure the surface area, the total pore volume and the pore size distribution.[72] It is also possible to use other gases and vapors for the adsorption analysis of porous materials. For example Mikhail *et al*.[73] exposed microporous and mesoporous silica gels to vapors of different organic solvents to investigate the physical and chemical interactions of adsorbates with silica hydroxyl groups. Bambrough *et al*.[74-76] used organic solvents and water for adsorption on mesoporous silica, which was co-polymerized with phenyltriethoxysilane. They were able to show differences in the influence of the hydrophobic modification on adsorbate molecules.

In this work, besides the standard nitrogen adsorption experiments, water vapor adsorption on PMOs is used to get information about the hydrophilicity of the surface and the influence of different organic groups on it.

3.1.1 Nitrogen adsorption on PMOs

The simplest model of a porous material is that of non-intersecting cylindrical tubes. There are two possible modes of filling (empting) these pores with a liquid like adsorbate. The first model is “adsorptive filling” (Figure 3-1a). A multilayered film of the liquid is formed on the wall of the capillary and with increasing thickness of this layer it gradually fills. In the “bulk

filling" model, a thin monolayer is formed, but then additional adsorbate fills the capillary completely at one point. The addition of more liquid causes the meniscus to gradually move filling the pore.

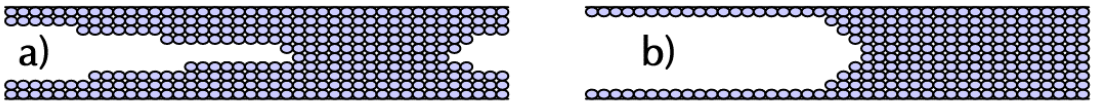

Figure 3-1: Models for pore filling with vapor in cylindrical pores. a) adsorptive filling, b) bulk filling.

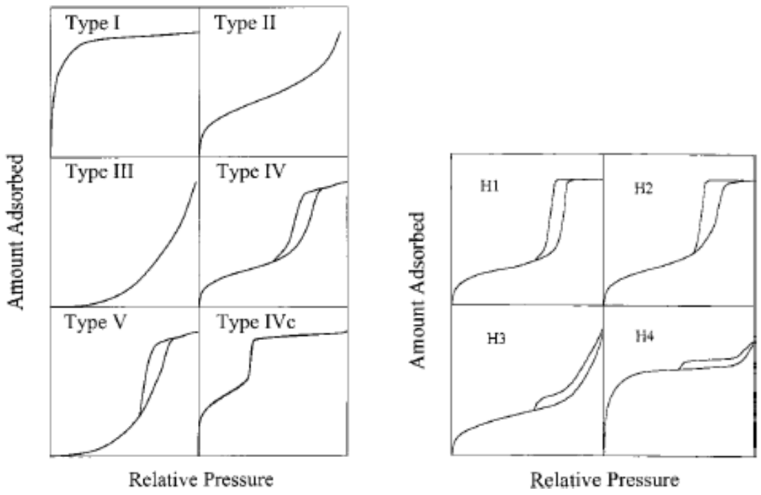

Figure 3-2: Classification of gas adsorption isotherms and of adsorption-desorption hysteresis loops.[77, 78]

Gas adsorption isotherms generally fall in six categories (Figure 3-2).[77, 78] Type I isotherms are an indication for microporous materials as well as strong adsorbent-adsorbate interactions. However Type I isotherms can also be found in mesoporous materials with cylindrical pores, which have a pore size close to the microporous range.

Type II isotherms are found in many macroporous solids, which show a gradual increase in the amount of adsorbate with relative pressure due to multilayer formation following the "adsorptive filling" model. A material showing a Type II isotherm exhibits a pronounced monolayer formation, whereas in the case of a Type III isotherm no monolayer formation is observed. This is due to the lack of monolayer formation resulting from strong lateral

interactions between the adsorbed molecules compared to weak adsorbent surface-adsorbate interactions.[79]

Type IV and Type V isotherms are found in mesoporous materials. At low pressures the materials show isotherms similar to macroporous materials, but at higher pressures the amount adsorbed rises steeply due to capillary condensation in the pores ("bulk filling" model). The difference between Type IV and Type V isotherms is the same as between Type II and Type III. The capillary condensation and evaporation are usually taking place at different pressures giving rise to the formation of a hysteresis loop. If the capillary condensation-evaporation in the mesopores is reversible, then an isotherm with a Type IVc occurs. This is often the case for materials with a pore diameter close to the micropore range.

The origin of the hysteresis loop in mesoporous materials is usually attributed to thermodynamic and/or network effects. [77, 80-84] The hysteresis loops can be classified into four types (Figure 3-2),[78] depending on their shape, which is related to the form of the pores in the material. Type H1 loops are found for cylindrical pores with a high degree of uniformity,[79, 85] where as type H2 shapes can come from ink-bottle-shaped ones.[83] Slit-like pores show a type H3 hysteresis and a type H4 loop is observed for mesopores, which are embedded in a matrix of smaller pores.[86, 87] Some porous materials also show a low pressure, non-closing hysteresis loop, which arises when the adsorbent is swollen or deformed by the adsorbate or when reversible or irreversible chemisorption takes place in the material.

The specific surface area, pore volume and pore size distribution can be calculated by the Brunauer-Emmet-Teller (BET) method.[77, 78, 80, 88, 89] The BET method is based on the monolayer capacity, which is found by fitting the gas adsorption data to the BET equation (Equation 3-1). The monolayer capacity is then multiplied by the cross sectional area of the adsorbed molecule, which for nitrogen is 16.2 $Å^2$.

$$\frac{1}{W\left(\left(P_0/P\right)-1\right)} = \frac{1}{W_m C} + \frac{C-1}{W_m C}\left(\frac{P}{P_0}\right)$$

Equation 3-1: BET equation. W: weight of adsorbed gas; P/P_0: relative pressure; W_m: weight of adsorbate constituting a monolayer of surface coverage; C: BET constant

The total pore volume of a material is calculated from the amount adsorbed at a relative pressure close to the saturation vapor pressure. This is done by converting the amount adsorbed into the corresponding volume of liquid adsorbate at the analysis temperature. In the case of nitrogen at liquid nitrogen temperature, this conversion value is 0.0015468.[90] Hereby it is assumed that the density of the condensed adsorbate is the same as the one of the bulk liquid.

The pore size distribution can be evaluated in many different ways, which are either based on the Kelvin Equation[91-97] or the Horvath-Kawazoe method.[98, 99] The method usually employed for PMO materials and utilized in this work is that of Barrett, Joyer and Halenda (BJH)[91].

3.1.2 Water vapor adsorption

A lot of work has been done on the adsorption of either hydrophilic[100-107] or hydrophobic[100, 102] molecules on pure[106, 107] and surface modified silica materials.[100-105, 108-110]

Cauvel *et al*. and Nano *et al*. applied water adsorption to mesoporous silica materials prepared from different templates.[106, 107] These materials show different isotherms depending on the temperature of calcination and out-gassing. A higher temperature leads to a decrease of surface hydroxyl group concentration and a concommitant higher hydrophobicity.[106, 107] A

second water adsorption on a material treated at high temperature changes the isotherm (Figure 3-3). This can be explained by the rehydroxylation of the surface during the first water adsorption and the formation of more hydroxyl groups. [106, 107, 111]

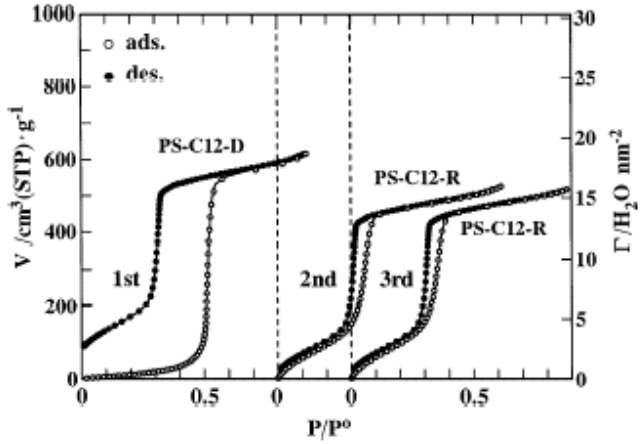

Figure 3-3: Adsorption–desorption isotherms of water vapor at 298 K for dehydroxylated CTAB based MCM-41 sample (PS-C12-D) and rehydroxylated CTAB based MCM-41 sample (PS-C12-R).[107]

Water adsorption is also applied to many organic-inorganic nanocomposite materials.[112-118] These materials have been post-treated with alkyl chain organosilanes,[112-114] with hydrocarbon alcohols[115, 117] or with organometallic compounds.[116, 117] Their isotherms changed from type IV for an untreated to a type V or III for a treated silica, showing the higher hydrophobicity in the latter materials. Depending on the size[114, 115] and the structure[114] of the organic groups the uptake of water in these materials decreased.[111] This is due to the sensitivity of water molecules to the environment. They are able to physically adsorb on surfaces, e.g. through hydrogen bonding interactions of different types, but they can also form chemical bonds with the surface species. In the case of hydroxyl groups, water vapor interacts either through electric dipoles or through hydrogen bonding.[113] PMO materials therefore can physically and/or chemically adsorb water.

The shape of a water vapor isotherm can give an indication of the hydrophilicity of a substance. In the case of hydrophobic porous materials, which show no tendency to

chemically interact with the water molecules, the adsorption branch will show type III shape and the hysteresis will close at low pressures. For hydrophobic materials that chemically interact with water a type V adsorption and a low pressure hysteresis is observed. This is for example the case in dehydrated silicas, which result in dissociative chemisorption with the formation of new surface hydroxyl groups.[107, 111] Also for hydrophilic materials with a type IV isotherm, the hysteresis might not close, because some of the water molecules are too tightly bound to the surface to be removed at low pressure alone. Also a swelling of the material with water and along with this a much slower release of the water[119] as well as a change of the surface water to bulk water at higher pressures, which leads to higher surface tension, can hinder the removal of water molecules from the pores at low pressures.

As in nitrogen adsorption, the BET surface area can be calculated, however in this case it only shows the hydrophilic portion of the surface, if no other interactions like rehydroxylation or inclusion are taking place. If the surface area for water is the same as the one for nitrogen, the whole material is considered hydrophilic. If the surface area for water is instead smaller than the one for nitrogen, the surface consists of both hydrophilic and hydrophobic sites.[120] In the case of a hydroxyl-group-containing surface the following adsorption mechanism is assumed. On a fully hydroxylated surface, each molecule in the first layer of water is considered to be doubly hydrogen bonded to two surface silanol groups (Figure 3-4). On sparsely hydroxylated surfaces, the water molecules cluster in the hydrophilic areas to form the tetrahedrally bound water like in liquid water and ice, before hydrophobic parts or isolated silanols groups take up water.[104, 121]

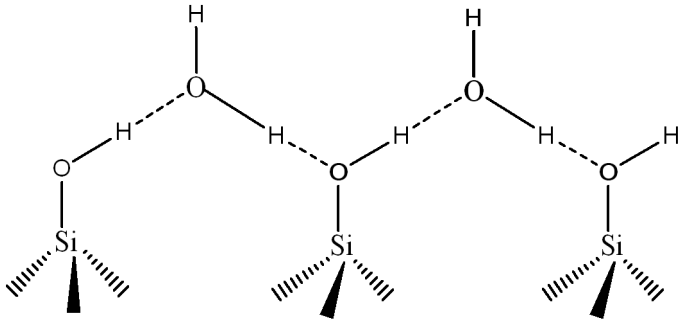

Figure 3-4: Scheme of water adsorption on a fully hydroxylated surface.

For water in confined spaces there is a difference in dynamical behavior and structure depending on the size of the pore size and temperature. Generally the water molecules exist in the state of bulk water,[122] however they are more strongly hydrogen bonded under confinement compared to free bulk water.[123] They exhibit structures that are equivalent to free water at lower temperature.[124] Also there is a difference in the conformation of the molecules depending on the amount of water in the system. Whereas for low concentrations (near the monolayer formation) the structure of water is deformed from the one of bulk water,[125] the behavior of water at high concentrations is more like bulk water. Whether there are layers close to the surface which are deformed or whether water molecules are behaving like bulk water is still a controversial topic.[123, 125-127]

3.2 Isothermal titration calorimetry

Isothermal titration calorimetry (ITC) provides a direct route to a complete set of thermodynamical data for interactions that are non-covalent under equilibrium conditions. The molar calorimetric enthalpy change ΔH and the equilibrium binding constant K_B can be determined by the direct measurement of the heat of interaction as one component is titrated

into the other. With these two values the rest of the thermodynamical data is calculated from the following equations:

$$K_B = \exp(\frac{-\Delta G}{RT})$$

$$\Delta H = \Delta G + T\Delta S$$

Where as ΔG is the free energy change, ΔS the entropy change, R the gas constant and T the temperature in Kelvin.

Standard ITC instruments consist of two identical cells, which are housed in an isothermal jacket (Figure 3-5). The jacket is cooled in such a way, that energy is required to keep the cells at experimental temperature. One cell is filled with solvent and the other with one component of the interaction. The second component is added to the solution in a series of aliquots up to the desired total volume. Depending on the type of interaction (exothermic or endothermic) less or more heat is required to keep the two cells at the same temperature and this temperature is measured over time. The raw data is plotted as the power required to maintain the sample cell at the desired temperature *versus* time (Figure 3-6). The molar enthalpy is found by integrating these peaks with respect to time and these data are plotted against total concentration of compound titrated into the solution or molar ratio of the components. The equilibrium binding constant is found by a nonlinear regression of this curve, which also gives the stoichiometry of the interaction.

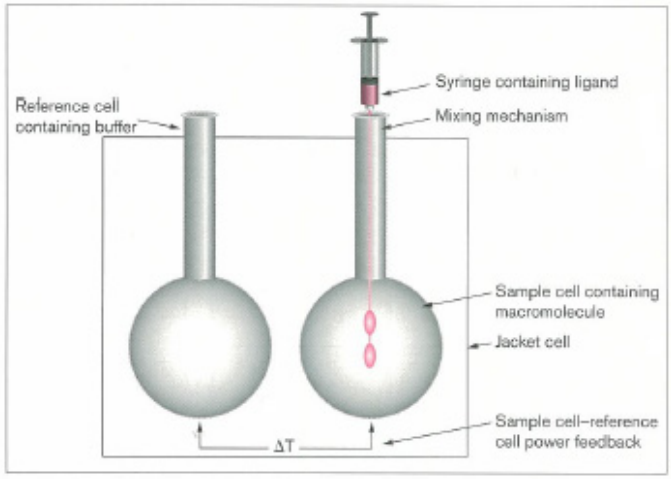

Figure 3-5: Schematic drawing of an ITC measurement cell for a ligand titrated into a macromolecular solution.[128]

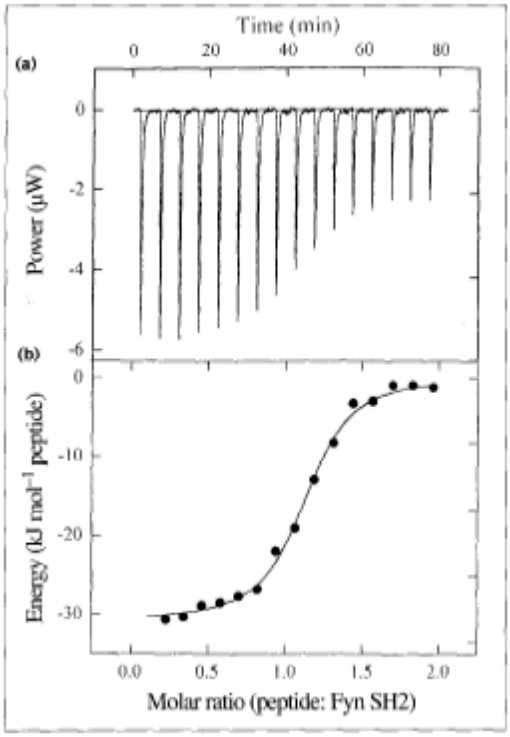

Figure 3-6: Sample ITC data for the interaction between a specific phosphotyrosyl peptide and Fyn SH2 domain at 20 °C. a) raw data, b) titration plot.[128]

The enthalpy observed with this method is a global property of the whole system. All contributions that are not due to the analyzed interaction need to be removed from this value. Already the dilution of the compound in the measuring cell or the dilution of the compound titrated into the pure solved leads to a change in enthalpy. To find the normalized heat of

interaction these dilutions have to be measured in separate experiments and their heats of dilution are than subtracted from the one found in the desired interaction. The final graph then contains all the information needed to calculate the molar enthalpy, the equilibrium binding constant and the stoichiometry if the initial concentrations of the compounds are known.[129, 130] The temperature dependence of the heat capacity at constant pressure ΔC_p can be found if several experiments at different temperatures are done. This is achieved by using the following formula:

$$\Delta C_P = \frac{d\Delta H}{dT}.$$

4 MO materials produced from silsesquioxane surfactant precursors

4.1 Introduction

PMO materials have been prepared from a variety of silsesquioxane precursors with bridging organic groups based on saturated hydrocarbons[10, 131-133] like methene, ethene and propene, and unsaturated hydrocarbons[13, 59, 60, 134-137] like vinyl, benzyl, phenyl ethylene and phenylene.[56, 57] However these materials show no other functionality than the hydrophobicity of the hydrocarbons included within. To further modify the silica framework, silisesquioxane precursors containing functional groups like amine,[12, 138-142] and metal complexes[11] either pure or mixed with another silica precursor have been incorporated into PMOs. However a common problem in these functional PMO materials is that not all of the organic functional groups are accessible from the pores. This has been observed by Ozin *et al.*[10] during bromination of an ethylene PMO. It took 8 days in solution to complete the reaction. Stein *et al.*[132] tried the same reaction in the vapor phase and did not achieve completion even after 18 hours, while a terminal vinyl group grafted onto a PMO only needs 40 minutes to undergo conversion under the same conditions. Since most PMO precursors are synthesized *via* time consuming procedures it is important to develop a strategy to optimize the accessibility of the functional groups. Different methods to locate the organic groups on the surface of the pores have thus been explored.

The first technique to be employed for the functionalization of mesoporous silicas used terminally bonded organic groups and was called the ‘grafting’ approach. Up till the present time, acidic, basic, hydrophobic and chiral functions have been incorporated in mesoporous materials by this method,[34, 35, 37, 40, 143-145] but the approach has some disadvantages. To

amplify, it is a two step procedure: first the mesoporous silica host is synthesized and then a trialkoxylorganosilane with the terminally bound organic functionality is reacted with surface silanol groups of the mesoporous silica. This leads to an uneven distribution of the organics due to the irregular spacing of the surface hydroxyl groups and an incomplete reaction of them. Moreover, under the reaction conditions employed condensation between two or more trialkoxyorganosilanes is also possible leading to the partial or complete clogging of some of the pores. A maximum loading of 25 mol% of organic groups can be achieved while the pore diameter and the total pore volume decrease, because the organic groups are dangling into the pore spaces and take up room.[146, 147]

An improvement of this method is the newly found ‘painting’ of silsesquioxane precursors onto the pore surface of mesoporous silicas.[148] It is similar to the grafting method the only difference being that bis-trialkoxyorganosilanes with bridge-bonded organic groups are employed in the post synthetic step. This provides the possibility of having the organic functional group ‘laying down’ on the pore surface thereby occupying less of the pore space. So far, ethane, ethene and p-xylene bridged silisesquioxanes have been painted on the pore surfaces of mesoporous silicas. These groups are accessible for reactions like hydroboration of double bonds with 70% percent conversion. This approach still involves a two step reaction in which the mesoporous silica host is prepared first, the template extracted and then the bridging organic function is introduced in a second step of anchoring the silisesquioxane to the surface of the pores of the host.

Figure 4-1: Methods to locate organic groups to the surface of the pores in mesoporous silica. Grafting on the left and painting on the right.

4.2 Non-chiral "all-in-one" method

4.2.1 Precursor preparation

It is the objective of the present work to simplify these procedures by discovering a way to prepare a functionalized PMO in a one step synthesis that ensures the bridging organic group is located mainly on the surface of the pore wall where it is accessible for subsequent chemical reactions. If successful, this approach would reduce the amount of precursor required in the synthesis of a PMO because none of it is lost in inaccessible sites buried within the wall of the pores. Hence the bridge bonded organic group is placed exactly where one wants it, namely on the surface and not within the pore wall.

For this idea to be reduced to practice one needs to synthesize a silsesquioxane surfactant, that is a hybrid precursor where the head group of the surfactant contains the organic functionality bonded to two polymerizable trialkoxysilane groups and the tail of the surfactant is comprised of an alkane chain bonded to the bridging organic. Such a silsesquioxane surfactant under aqueous synthesis conditions can in principle self-assemble into a mesophase in which the polymerizable silsesquioxane head group is located exclusively at the interface of the microphase separated region. Synthesis conditions have to be selected such the silicon-carbon-bond remains intact throughout the self-assembly condensation-polymerization reaction used to make the desired PMO. At the same time, the bond linking the silsesquioxane head group and the surfactant tail (covalent or ionic) has to be weak enough to be easily cleaved in a final step to produce the PMO in which the pores are open and accessible to chemical reagents.

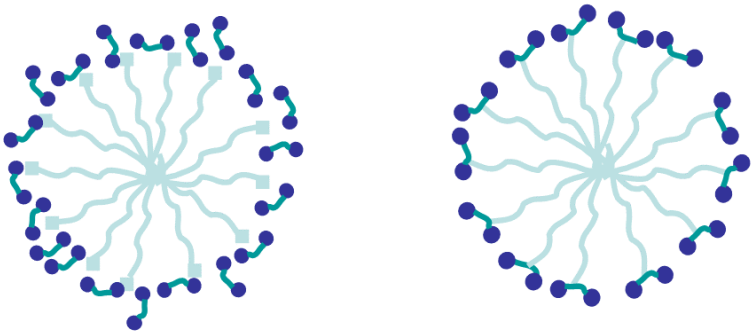

Figure 4-2: Scheme of the micelles formed from the proposed hybrid silisesquioxane surfactant precursor (right) and traditional silsesquioxane surfactant mixtures (left).

We opted to employ both covalent bonding and ion-pair interactions for the formation of the hybrid "all-in-one" silsesquioxane surfactant precursor (see chapter 4.2 and chapter 4.3). With such a precursor it is possible to create a PMO in one step in which the surfactant tail is chemically removed and the bridge bonded organic functional group is located mainly on the surface of the pore wall where it is required. In the case of covalent bonding between the bridge bonded organic in the silisesquioxane head group and the surfactant tail, a boron-carbon-bond seems to be the most interesting, for a number of reasons. On one hand the chemistry of the boron-carbon bond is well known and understood. Especially hydroboration of double bonds can be achieved with a wide variety of hydroboration agents under quite different and sometimes very mild conditions. Furthermore, there are numerous reactions that allow cleavage of a boron-carbon-bond under mild conditions providing a pathway to a variety of bridging organic functional groups in the targeted PMO.

After evaluating the possibilities we decided on using the commercially available bis(triethoxysilyl)ethene, which can also be easily synthesized,[149] as the precursor part and a propylboronhydride for hydroboration.[150] We decided against a BH_3 complex, because the two left over protons may cause complications from side reactions. This could lead to a mixture of hybrid silsesquioxane surfactants, which cannot be easily separated. In a typical

synthesis 2-propyl-1,2,3-benzodioxaborole in dry THF is cooled down to 0 °C and then $LiAlH_4$ in THF is added to free the hydroboration agent. After 1 hour at this temperature the ethylene bridged silsesquioxane is added and the whole mixture is stirred at room temperature overnight. Then hexadecene as the surfactant part is added to the solution and the mixture is stirred at 45 °C for 24 hours. Hexane is then added to the mixture and the solid so formed is removed by filtration. From the clear colorless solution the solvent is removed to give the pure "all-in-one" hybrid precursor molecule in good yield (Figure 4-3).

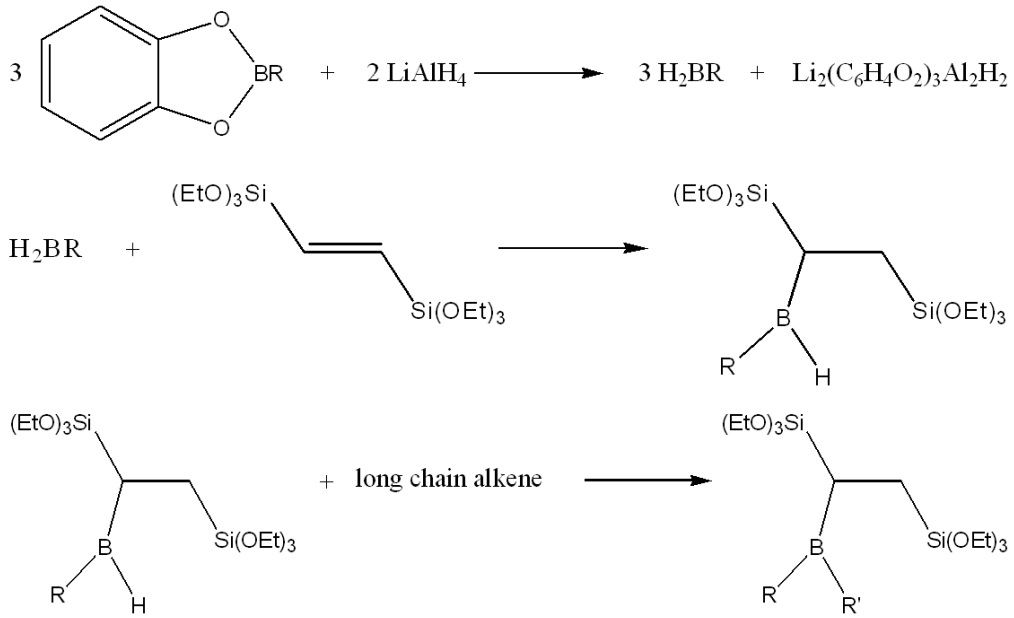

Figure 4-3: Reaction scheme for the preparation of the "all-in-one" hybrid silsesquioxane surfactant precursor.

4.2.2 PMO preparation and analysis

For the PMO preparation the "all-in-one" hybrid molecule is diluted with ethanol, and a second condensable silica precursor is added. The addition of this second silica source is necessary because the "all-in-one" precursor alone is not able to form PMOs with mechanically stable walls. The maximum thickness of pore walls in this instance could only

be at the length scale of a Si-O-Si bond, which is insufficient to form a mechanically stable PMO. A second polymerizable precursor, like tetraethoxyorthosilicate (TEOS), a purely silica-based molecule, or bis(triethoxysilyl)ethane (BTSE), a PMO precursor, is used. This second precursor in the synthesis mixture provides the opportunity not only to tune the chemical behavior of the desired PMO, through variations of the "all-in-one" precursor but also its physical properties. Furthermore the second silica source should be mainly located within the pore walls and therefore not accessible to guest molecules in the pores. In the MO synthesis the reaction is performed under HCl acidic conditions. After homogenization of the synthesis mixture, the ethanol is removed in vacuum to give the solid product.

To remove the surfactant tail in order to open the pore space different boron-carbon-bond cleavage reactions had to be explored. First of all the reaction to hydroxyl groups through the use of tetraethylamine N-oxide dihydrate as a cleavage agent can be done.[151] A second group that can be introduced into the material during extraction is iodide.[152] The latter seems more interesting since a lot of other functionalities can be easily obtained through subsequent reactions of the MO. In this work, a reaction that leads to primary amine functional groups on the pore wall surface is employed.[150] Like the iodide, this functionality provides an entry to further reactions of the MO and is intrinsically interesting. Conversion to the amine is achieved by heating the MO in diglyme with hydroxylamine-O-sulfonic acid, followed by washing and drying of the sample.

The so-formed MO material is then analyzed for structure and function. The usual instrumental analytical methods for structure characterization of MOs are nitrogen adsorption, SAXS and TEM. To probe the amine functionality in the MO the Kaiser test is employed as a fast qualitative probe for primary amines and copper adsorption as a quantitative diagnostic of the amine. ^{29}Si solid state NMR is used to check that the integrity of the Si-C-bond of the "all-in-one" precursor during the nanocasting and extraction processes is maintained. As well ^{11}B

solid state NMR is performed to check the degree of extraction of boron during the aminolysis step.

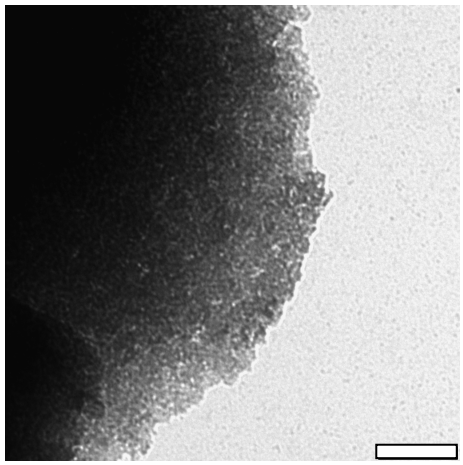

Figure 4-4: TEM picture of an amine functionalized MO prepared from the “all-in-one” precursor. Scale bar 100 nm.

For the “all-in-one” MO material a TEM image is shown in Figure 4-4. It can be seen that a highly porous material with a so-called “wormhole structure” with disordered pores is produced. This behavior is not unexpected for mesoporous silica and organosilica materials prepared from non-ionic surfactants. The “all-in-one” precursor used for the MO preparation is analogous to a T-type non-ionic surfactant.[3, 153]

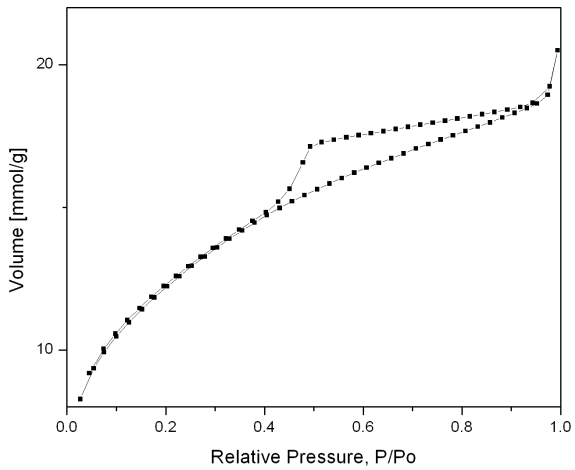

Figure 4-5: Nitrogen adsorption isotherm of the amine functionalized MO material after removal of the alkane tail from the poly-condensed silsesquioxane head group.

The high porosity and narrow pore size distribution are confirmed by nitrogen adsorption measurements. In Figure 4-5, the isotherm shows a diagnostic type IV shape indicative of the existence of mesopores in the amine MO. In this isotherm, capillary condensation in the adsorption branch is missing, which is another typical behavior for channel architectures templated from the micelles of non-ionic surfactants. The featureless shape of the adsorption branch can be due to a difference between the adsorption behavior of the here analyzed material compared to the pure silica MCM 41, which is the model system for the adsorption of nitrogen on mesoporous silica containing solids. The missing capillary condensation step in the adsorption branch of the isotherm could be due to a layer by layer filling as described in chapter 4.2.2. Whereas during desorption, a bulk emptying of the pores takes place, which may be explained by the existence of a small amount of micropores in the solid, that leads to pore blocking. Another possible explanation for the missing capillary condensation is the position of the organic groups in the material. All known PMOs do not force the organic to the surface but leave the possibility for them to be hidden in the walls. In the “all-in-one” PMOs the organic molecules build a layer on the pore wall, which may be more flexible than the TEOS in the wall interior. This gives the possibility of some swelling of the more flexible surface layer, which also could hinder capillary condensation. The emptying of pores during desorption in this model could induce a sudden deswelling of the surface layer. Unfortunately models for nitrogen adsorption on this type of material do not currently exist. Taking the standard model for adsorption of nitrogen the surface area is calculated by the BET approach to be 974 m^2/g. From analysis of the desorption branch the pore size is found to be 3.9 nm by the BJH method with a narrow pore size distribution. The total pore volume found from the adsorption branch is 0.65 cm^3/g. Both from the shape of the isotherm and from the surface area it can be concluded that the material also contains some smaller pores probably below

1nm in diameter. This implies that condensation not only traps micellar aggregates, but likely also monomeric species and solvent molecules.

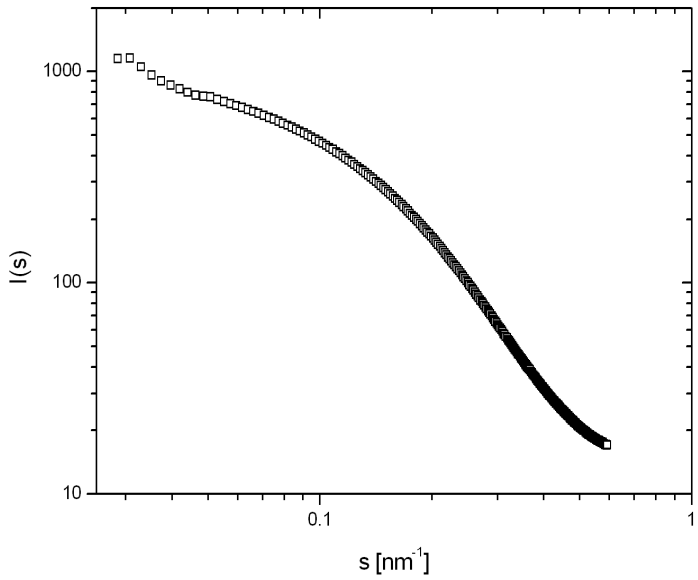

Figure 4-6: SAXS curve of the amine MO in the double logarithmic scale.

Since the shape of the adsorption isotherm with its few features does not allow for a good interpretation of the pore structure, SAXS measurements have been performed. The double logarithmic scattering curve of the amine functionalized MO is shown in Figure 4-6. From this it can be seen that there is a defined pore system in the MO, because otherwise there would be no pronounced scattering intensity distribution to be found. However the broad more plateau-like maximum of the curve leads to the conclusion that there is no long range order in the system. With the help of a mathematical algorithm the cord-length distribution (CLD) and from the maximum of this plot (Figure 4-7), the "Porod-length" (l_P) can be determined to be 2.4 nm.[154-157] With the help of the total pore volume (V_{Pore}) known from nitrogen adsorption and the density of the material, which is taken as 1.5 cm^3/g, the average pore diameter, which is independent of the shape of the pore can be calculated from Equation 4-1 to be approximately 4.7 nm. This value is higher than the value of 3.9 nm found from nitrogen adsorption. This is because the analysis calculates not only the shortest distances

across a pore but all possible lengths are taken into account. So the higher value found for the diameter as well as the shape of the CLD, with its shoulder to higher diameters, lead to the conclusion that in this MO an elongated pore system, such as cylinders, likely exists. Also the steep decrease in CLD going from the maximum to lower diameters and the low value for the radius close to zero is a good indication for only a few micropores in the MO.

$$D = \frac{l_P}{1-\phi} \qquad \phi = \frac{V_{Pore}}{V_{Pore} - V_{Material}} \qquad V_{Material} = \frac{1}{\rho}$$

Equation 4-1: Equation to calculate the average pore diameter from the 'Porod-length'. D: average pore diameter; l_P: 'Porod –length'; V_P: total pore volume; ρ: density of the material.

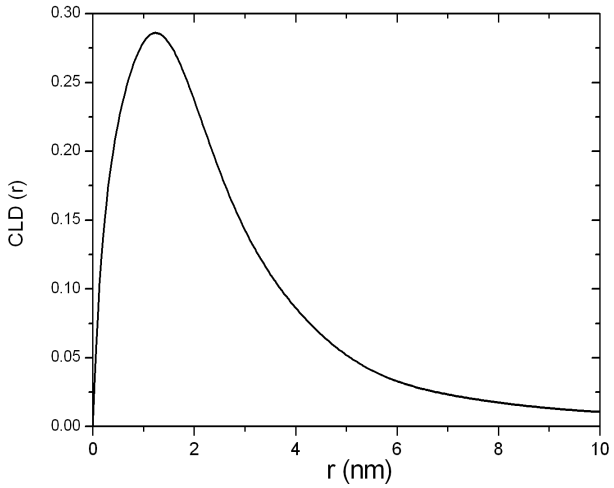

Figure 4-7: Cord-length distribution calculated from the SAXS curve shown in Figure 4-6.

On summarizing the results from the structural analyses presented in this chapter it appears that the "all-in-one" silsesquioxane surfactant precursor forms a MO material with an elongated worm-like pore structure.

The chemical composition and stability of the material during and after the preparation is analyzed with the following methods. The comparison of the ^{13}C NMR of the as-prepared and the extracted sample (Figure 4-8) show removal of the long chain surfactant from the amine functionalized MO is almost complete. These results imply high conversion to the amine function and good accessibility of the boron-carbon-bond.

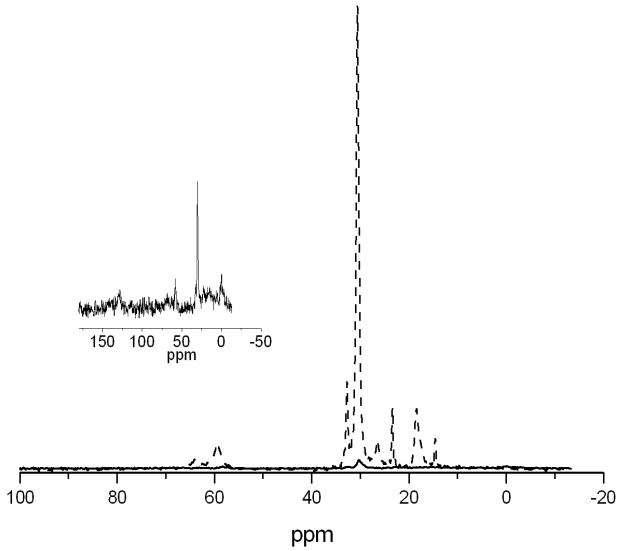

Figure 4-8: ^{13}C NMR for the as-prepared and the extracted amine functionalized MO. Dashed line: as-synthesized sample; solid line: amine functionalized PMO.

This fact can be confirmed by ^{11}B NMR. The peaks at -0.15 and 5.62 ppm in the as-prepared sample, best assigned to boron atoms attached to 3 carbon atoms and a water ligand vanish in the spectra of the extracted sample, indicating a complete removal of the boron moiety from the material. The ^{29}Si NMR shows about 10% Si-C bond cleavage occurred during the assembly of the silsesquioxane surfactant to form the amine MO or the extraction chemistry that led to the amine (Figure 4-10). The T sites are centered at -60 ppm and the Q sites are at -104 ppm. This amount of Si-C bond cleavage has little effect on the structural stability of the material as well as the amine functionality.

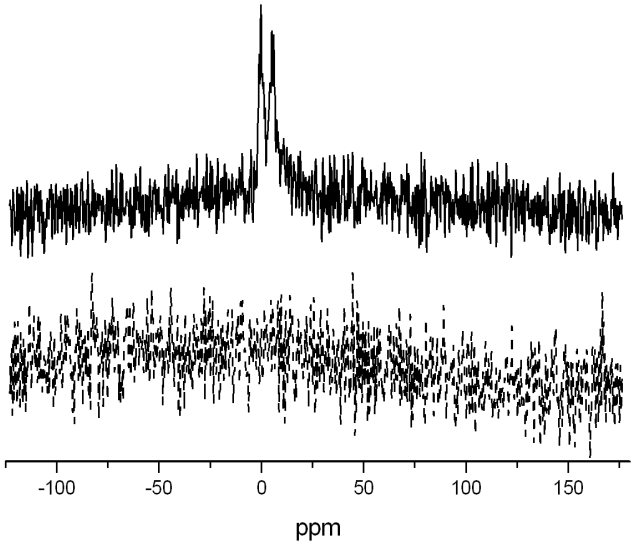

Figure 4-9: ^{11}B NMR: Solid line as-synthesized sample; dashed line: amine functionalized MO.

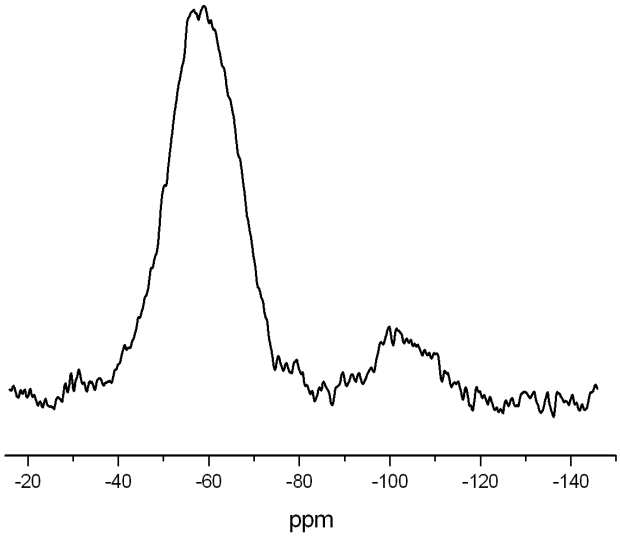

Figure 4-10: ^{29}Si NMR of an amine MO with bis(triethoxysilyl)ethane as co-precursor.

Confirmation of the presence of primary amine groups in the amine MO is established by the Kaiser test, a color reaction with Ninhydrin[158] exposure to which caused the entire sample to turn deep blue. However this test only gives a qualitative impression about amine groups so for quantitative analysis other methods have to be devised. The basic amine function could be titrated with an acid but this method has limitations for colloidal dimension particles of the type prepared for the amine MO materials due to the hydrogen "sponge" effect. So instead it was decided to use copper ion binding to the MO as a means of defining

the presence and number density of amine functional groups.[138, 159] To this end, the sample was first suspended in 0.1M ammonia solution for one hour, washed with clean water, and then a 0.03M Cu(II) nitrate solution was added. The copper loaded particles were isolated, rinsed two times with water, dried, and then the copper content was determined by AAS of the solution. Based on the theoretically estimated content of primary amine groups, 27 mol% of copper have been adsorbed from a 1:1 reaction. This represented about one quarter of the loading of the amines, which together with the blue coloration of the solid indicates formation of a tetrahedral copper complex, a not unexpected result for the reaction between copper ions and primary amines. Significantly, this amount of adsorbed copper is much higher than previously observed in mesoporous organosilica materials. Mercier *et al.* have seen up to 6.5% loading for a BTSPEA material and Im *et al.* found 7.1% for grafted ethylendiamine groups.

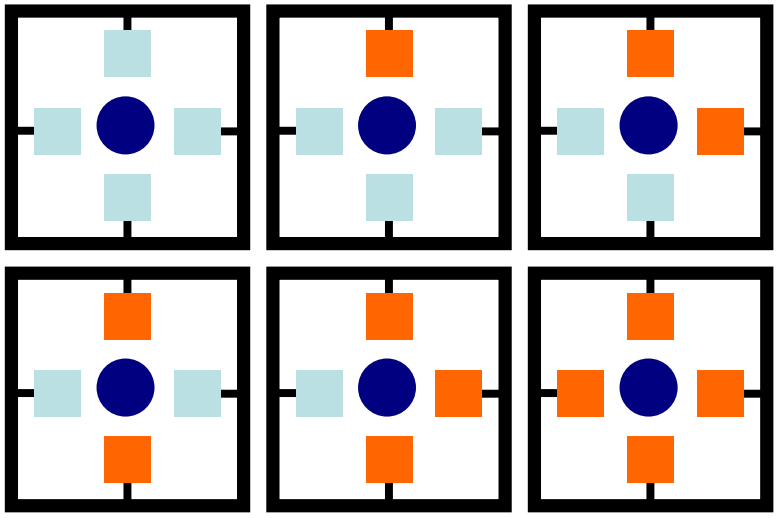

Figure 4-11: Scheme of the possible interactions of a copper ion to form tetrahedral complexes with the functional groups found in a four-ring of SiO_2 and $SiRO_{1.5}$ building blocks. Every corner is representing an oxygen atom. The light blue squares are silanol groups and the orange ones primary amine functions. The dark blue circle represents the bonded copper ion.

This higher loading compared with the values found in literature can be explained by the fact that the amine functions are located on the pore wall surface. The blue coloration can be

explained in terms of a simple model involving the smallest ring building unit found for solid silica materials and the different possible tetrahedral ligand arrangements around the copper ions. An illustration of these four-rings with all binding sites for the copper 2+ ion to be found on the surface of the solid is shown in Figure 4-11. This is a simplification of the actual interactions taking place in the material, since there are also water molecules that could take up vacant binding sites as well as larger rings like five- or six-rings to be found in MO materials. However it gives a good idea about the mode of binding of copper 2+ ions in mesoporous hybrid organosilica materials and is considered a reasonable model to explain copper ion adsorption.

In a four-ring a copper ion can find from zero to four primary amine functionalities on the surface. Some of these sites will exhibit tetrahedral conformation and a copper ion can be adsorbed. If there are not four surface groups with the right conformation some of the vacant binding sites can be filled by water molecules, also not all amine function may be accessible. This explains that if more copper ions are offered to the solid, like a 1:2 ratio between estimated amine functions in the solid and copper ions in the aqueous solution, a higher uptake of 36% of the organic groups can be seen.

That the amount of copper adsorbed in solid mesoporous materials is highly depended on the conformation of the functional groups has been shown by Zhu *et al.* and Dai *et al.*. Both groups used terminal trialkoxysilanes with amine functionalities, which were co-condensed or grafted to form mesoporous hybrid materials. During the synthesis copper ions were added so that the condensation of the organic groups would take place in tetrahedral order. Adsorption of copper ions on the extracted samples shows a nearly quantitative binding of the ions as well as a high selectivity for it.[138, 159]

That the adsorption of copper is specific to the organic functions and not only due to interactions with the surface silanol groups is checked by adsorbing the same amount of ions

on a comparable pure silica material, which shows no blue coloration and very low uptake at both concentrations. To better understand the mode of copper 2+ binding in the MO, UV/VIS spectroscopy of the solids would need to be done, since copper ions show specific peaks in the spectra for the different coordination geometries. Unfortunately this was not possible in the limited timeframe of this work but will be the subject of future studies.

In conclusion, “all-in-one” silsesquioxane surfactants with polymerizable head groups and chemically cleavable alkane tails have been synthesized and self-assembled in a template free preparation to form high surface area narrow pore size distribution MO materials in which the bridge bonded organic groups are located on the surface of the pores. This type of MO is to be contrasted with all known MO materials in which the bridging organics are located both on the surface of the pores and buried within the pore walls. In the particular case presented in this chapter, the precursor organic and sol-gel chemistry is designed to create the first example of an amine MO where the amine functionality is bonded to a bridging ethane group and intentionally positioned on the surface of the mesopores.

4.3 MOs for chiral separation

4.3.1 Introduction

Chirality and chiral discrimination are fundamental concepts of nature and life. Chiral separation is often performed in biological systems by molecular recognition. Because of the relevance of chirality in biological processes, pharmaceutical compounds, when chiral, have to be enantiopure. If the synthesis of enantiomerically pure materials is not possible, a cheap and effective separation of chiral molecules is or would be of high significance. Highly

selective adsorbent materials are thus required for this purpose, and they are already commonly used in liquid chromatography.

Natural polysaccharides or proteins as well as synthetic polymers like polyacrylates, polyamides or helical polymers are used for such chiral stationary phases (CSPs). All these materials however present the drawback that the elution order and the separability of the enantiomers are largely unpredictable and have to be found by experiment.

Chiral compounds bound to a solid substrate are also able to selectively bind one enantiomer and have been developed for HPLC.[160] Not only small chiral organic compounds, but also biologically derived materials such as oligopeptides, amino acids, sugars, or even larger biological entities can be coupled to a solid substrate and used as the stationary phase in chiral chromatography. It is well known that such systems can exhibit very high performance in special polar organic solvents, but are badly performing in water which is the most common environment.[161] One of the most selective and molecularly flexible systems for chiral adsorption is based on teicoplanin, a cage-like antibiotic with at least 20 active chiral centers,[162] but it also shows lower performance in water.

A way to increase the chiral separation performance in water is to use imprinted polymers, which are prepared by polymerizing a functional polymer around a target molecule to form specific cavities around the template. The extraction of the target molecule leads to molecular recognition sites for the target. These polymers are prepared as micron sized particles and filled into chromatography columns. Molecular imprinted polymers (MIPs) do presumably hold the record for selective adsorption in water (selectivity factor $\alpha \sim 7$), but are compound-specific.[163] They also exhibit drawbacks like shrinkage or swelling of the formed cavities which decrease the selectivity.

Although these chromatographic techniques show high chiral discrimination, none of them is yet applicable for the resolution of enantiomers on a large scale due to capacity and flow-

through reasons; therefore large-scale separation technology is still based on the classical crystallization methods and increasing perfection of chiral organic synthesis.

Hereafter the incorporation of a chiral amine group into a mesoporous silica network in a way to ensure that the chiral function is on the pore wall surface is described. For this purpose, the "all-in-one" method described in chapter 4.2 is extended to a chiral hydroboration agent. Next to the very high surface area, high capacity and technical accessibility this material should also exhibit a higher mechanical and thermal stability than the molecularly imprinted polymers.

The preparation of chiral-moieties-containing PMOs has been described before, but to the best of our knowledge none of the systems was effective in chiral separation. Alvaro *et al.*[48] used a chiral binaphthyl precursors in co-condensation with TEOS. This led to materials showing an optical rotation of linearly polarized light, but the loading of functional groups was very low and the optical rotation value decreased after extraction. Corma *et al.* used chiral trialkoxysilanes grafting them onto mesoporous silica materials forming a whole range of chiral catalyst.[164-167] They also prepared a bridged-bonded catalytic precursor, which they then co-condensed with TEOS in low loadings.[134]

4.3.2 Preparation and analysis of the precursor

The method described for the boron-containing precursor (chapter 4.2.1) is slightly modified to produce MOs having chiral amine groups on the pore wall surface. Starting from the commercially available S-monoisopinocamphenylborane tetramethyl-ethyldiamine complex, the hydroboration agent S-monoisopinocamphenylborane ($IpcBH_2$) is liberated with the help of BF_3.[168] A bis(triethoxysilyl)ethene precursor is added to this molecule and after 24 hours the remaining active protons are reacted with hexadecanol to give the "all-in-one"

silsesquioxane surfactant precursor. Compared to the synthesis described in chapter 4.2.1 here a more reactive alcohol has to be used for the reaction on the second boron-hydrogen bond, because of the higher steric demand of the monoisopinocamphenyl group. The new chiral center formed in the silsesquioxane surfactant precursor has R-configuration.

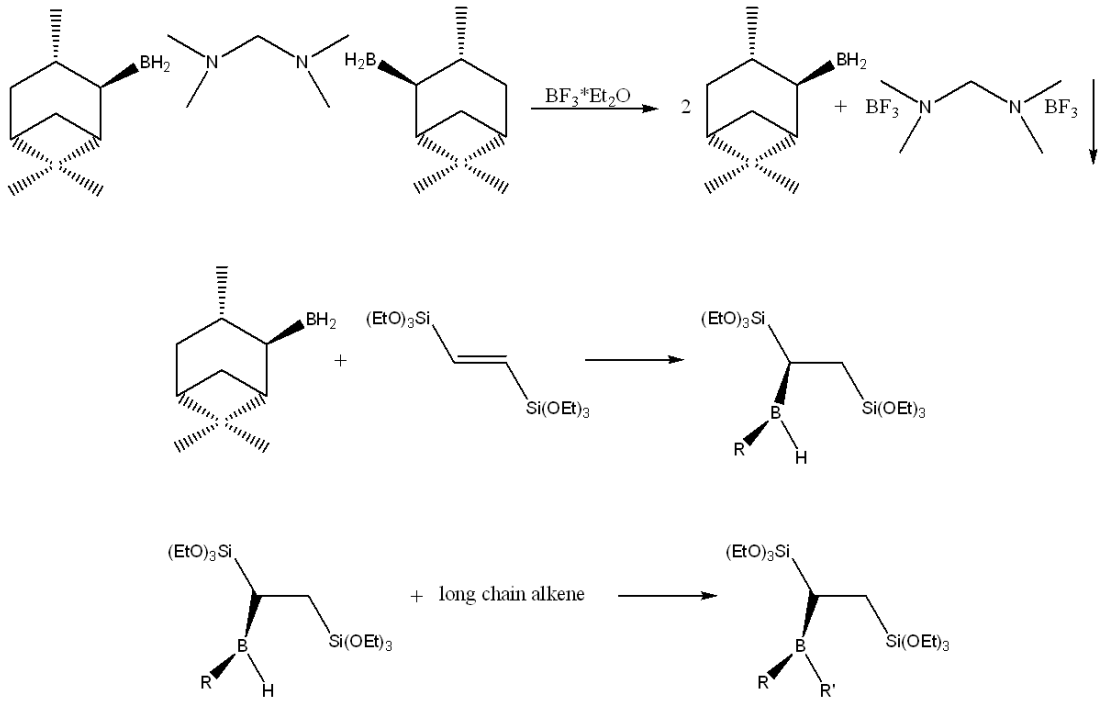

Figure 4-12: Reaction scheme of the preparation or a chiral boron containing MO precursor.

The precursor is analyzed with solution NMR and CD spectroscopy. The ^{1}H NMR of the intermediate after hydroboration of the bis(triethoxysilyl)ethene shows no peaks in the double bond region indicating complete conversion of the unsaturated bond. The ^{13}C NMR of the final product only shows peaks belonging to the desired compound and some residual THF (Figure 4-13).

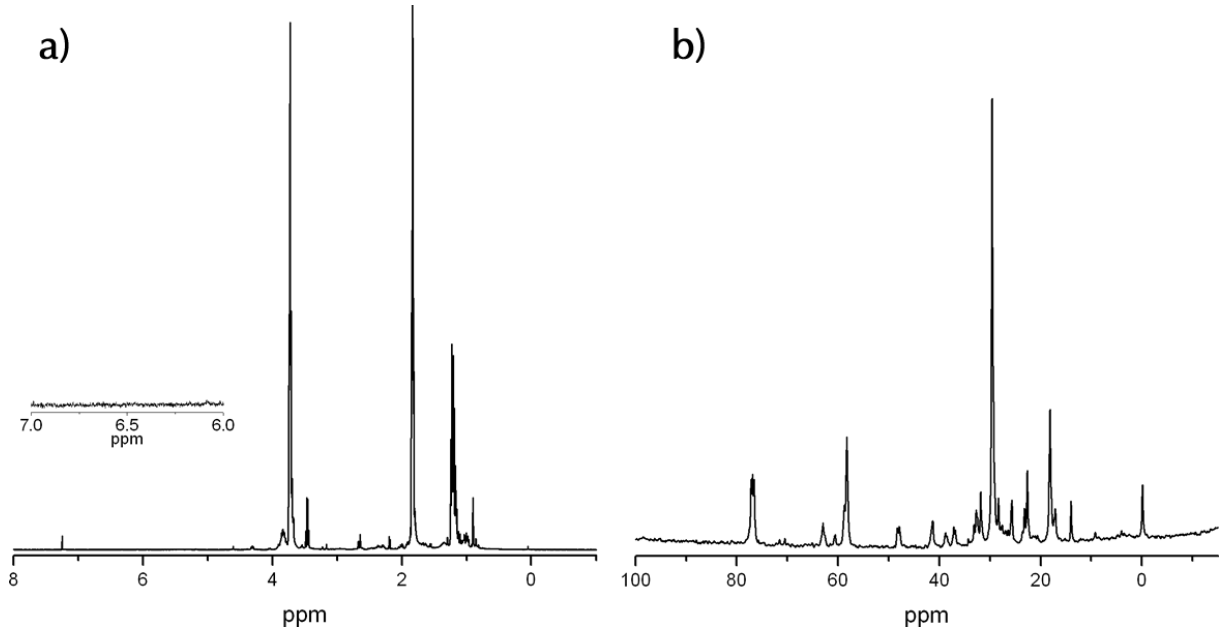

Figure 4-13: A) ^{1}H NMR of the intermediate after the reaction of the unsaturated group. Inset: double bond area. Other peaks are out of proportion, since the intermediate is not purified. B) ^{13}C NMR of the final product. 62.9 and 25.6 ppm: THF; 58.3 and 18.3 ppm: ethoxyl groups; 29.6, 25.6, 22.7 and 14.1 ppm: hexadecanyl; 47.7, 41.7, 38.5, 37.0, 32.8, 31.8, 22.7 and 17.3 ppm: monoisopinocamphenyl.

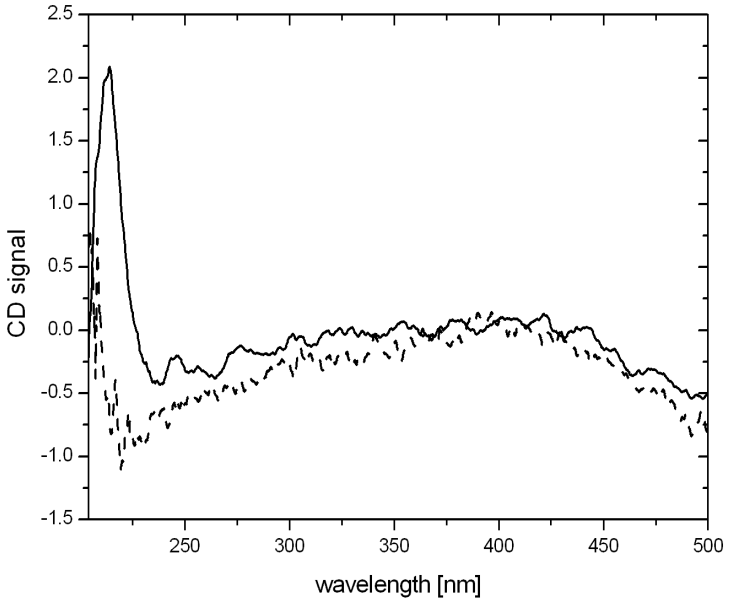

Figure 4-14: CD spectra of the starting hydroboration agent ($IpcBH_2$) shown as the dashed line and the final "all-in-one" chiral precursor (solid line).

In the CD spectra a new peak at 214 nm arises during the hydroboration reaction, belonging to the newly formed chiral center in R-configuration (Figure 4-14). Combining the

results from these two analysis methods it can be concluded that a precursor with a new chiral center at the former double bond is formed in high purity.

4.3.3 MO preparation and analysis

The MO is prepared in the nanocasting procedure under acidic conditions with TEOS or bis(triethoxysilyl)ethane as second precursor in the same procedure as described before (chapter 4.2.2). A second precursor has to be added, since the "all-in-one" silisesquioxane surfactant precursor molecule is not able to form stable walls by itself. During the extraction the boron-carbon bond between the precursor and the surfactant part of the solid is cleaved with hydroxylamine-*O*-sulfonic acid to give primary amine groups on the pore wall surface. It has been shown by Brown *et al.* and others that this reaction can be done without racemization of the compound.[169-171] The chiral center on the pore wall surface of the final material has S-configuration.

The MO is analyzed with TEM, nitrogen and copper adsorption, SAXS and solid state NMR to get information about structure and functionality.

The TEM image (Figure 4-15) of the final amine functionalized material shows a highly porous, wormhole like structure. This is a typical pore system seen for silica solids which are prepared from nonionic surfactants.[3, 153] Such a wormhole like structure should actually give advantage over an ordered structure in catalytic and separation reactions, because in such an unordered system the pores are highly interconnected. A catalytic reaction for example will take place on the first active groups found while entering a pore. In a straight non-interconnected pore system this can mean that the whole pore is blocked by the reaction and all the active centers further down in the voids are not accessible. In an interconnected porous structure however the active centers in one specific pore are reachable through more than one

opening leading to a much better use of active sites and faster reaction times. The same should be true for separation reactions as for example in chromatography.

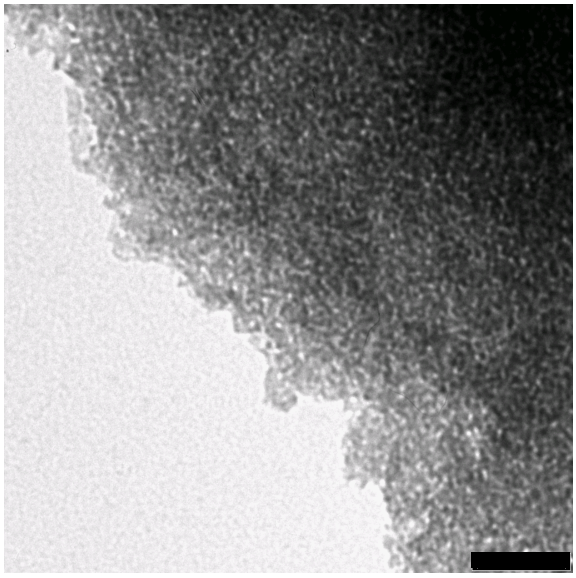

Figure 4-15: TEM image of a chiral MO with TEOS as second precursor. Scale bar 50 nm.

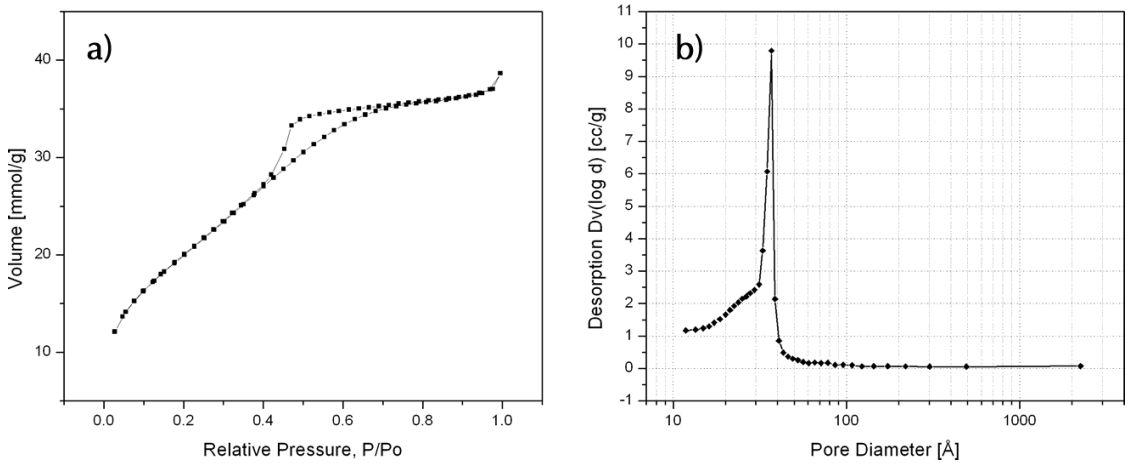

Figure 4-16: Nitrogen adsorption isotherm (a) and BJH pore size distribution (b) of a chiral MO with TEOS as second precursor.

The high porosity is confirmed through nitrogen adsorption (

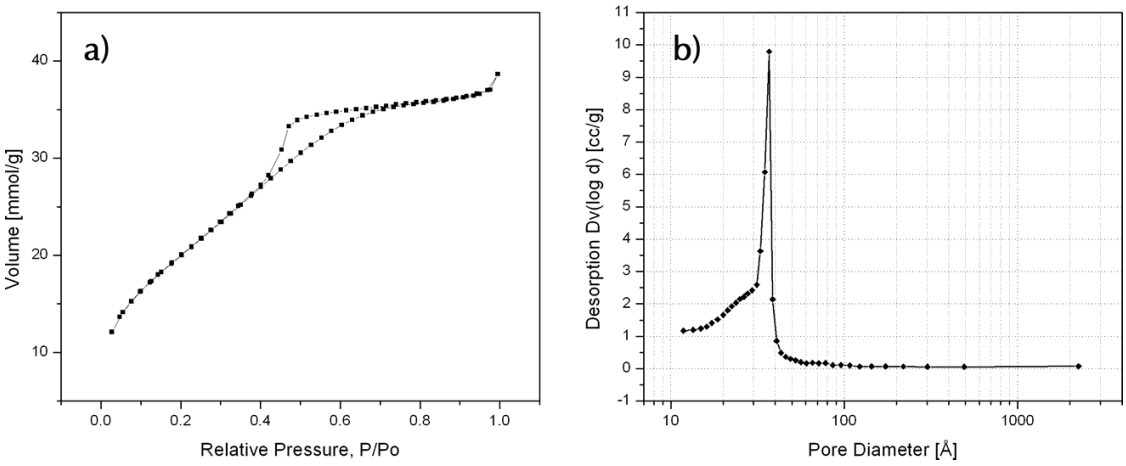

Figure 4-16a) showing an isotherm of type IV with a hysteresis. There is no condensation step in the adsorption branch, which is a usual behavior for a non-ionic T-type surfactant that is similar in form to the "all-in-one" molecule. As already described in chapter 4.2.2 the shape of the curve can be due to a swelling of the MO by nitrogen adsorption. However a definite answer about the adsorption mechanism would require additional experiments and a more in detail characterization, which will be done in the near future. The surface area calculated form the BET equation is 1650 m^2/g, underlining the very high porosity of the material. The pore size distribution evaluated by the BJH method (Figure 4-16b) of the desorption branch has a maximum at 3.7 nm with a narrow pore size distribution in the mesopore range, and the total pore volume is 1.28 cm^3/g.

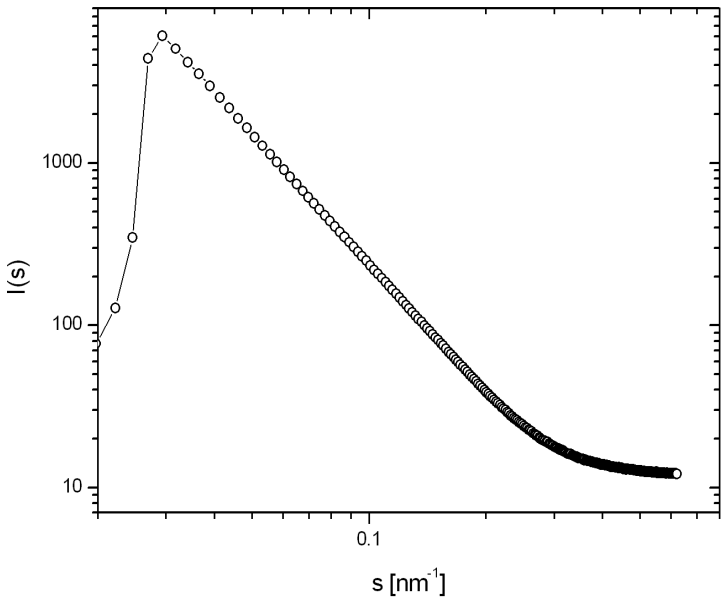

Figure 4-17: SAXS curve of the chiral amine MO in a double logarithmic scale. The first four data points and the lowering of scattering intensity towards very small scattering vectors are due to the beam stop in the instrument.

SAXS measurements have been performed since the few features in the shape of the adsorption isotherm do not allow for a good interpretation of the pore structure. The double logarithmic curve of the scattering data of the chiral amine functionalized MO is shown in Figure 4-17. The scattering intensity of a porous material is due to two different contributions: the structure factor leads to peaks which are corresponding to the d-spacing between the two different phases and indicates the presence of mutual order in the material. The form factor instead relates the data to the shape and size of the pores.

As can be seen in Figure 4-17 our material presents only a featureless linear decrease of the intensity with increasing angle, so that we can conclude that the pores are not arranged with long range order. However the high scattering intensity and its decrease at higher angles show us the presence of a bicontinuous pore system. Information about the shape and size of the pores from such a curve can be deducted from the SAXS spectra by using mathematical algorithms developed in our group.[154] Such algorithms are based on the “Porod theory” and

the calculated values are the cord-length distribution (CLD) and the "Porod-length".[154-157] The CLD curves for the chiral as well as the non-chiral mesoporous organosilica are shown in Figure 4-18.

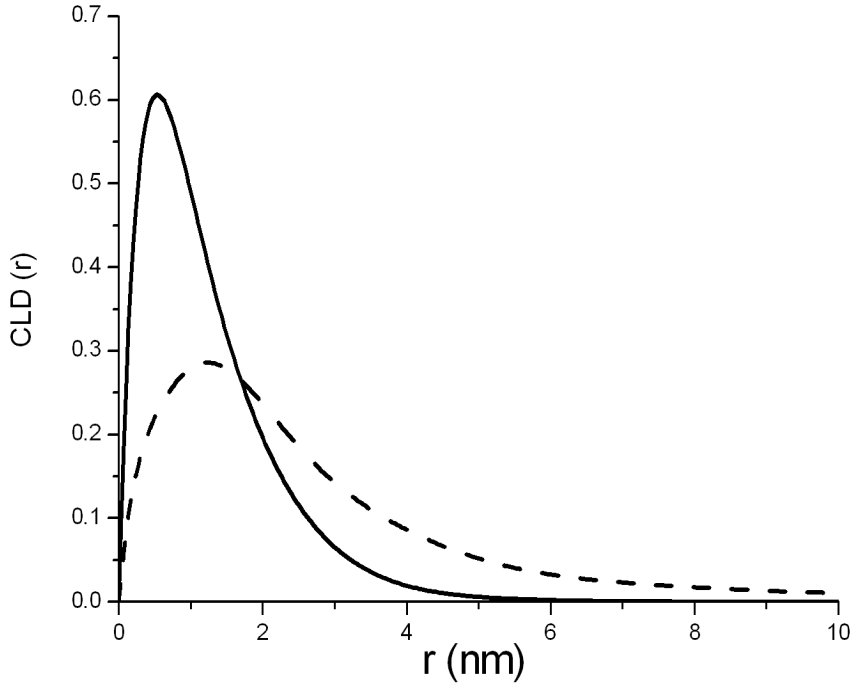

Figure 4-18: CLD curves of the chiral (solid line) and non-chiral amine MO prepared from covalently bonded silsesquioxane surfactant precursor molecules as described in chapter 4.3 and chapter 4.2.

The CLD plots of both materials show that the amount of microporosity is small as the curves go to zero as the radius goes to zero. The average pore diameter, which is independent from the pore shape, can be calculated from the maximum as described in chapter 4.2.2. The "Porod-length" is 2.4 nm for the non-chiral MO and 1.2 nm for the chiral one. By using the value of the total pore volume from nitrogen adsorption and assuming an average density of 1.5 g/cm^3, the average pore diameters are roughly estimated to be 4.7 nm and 3.5 nm respectively. As discussed in chapter 4.2.2 the high value obtained for the non-chiral mesoporous solid is due to an elongated cylinder-like pore system with wormhole structure, which is also reflected in the shape of the CLD. The chiral amine MO shows from this

analysis an average pore diameter of 3.5 nm which is close to the 3.7 nm found from nitrogen adsorption, leading to the conclusion that the pores in this material have a sphere-like or short-cylindrical character. The more spherical character can also be seen in the shape of the CLD, which shows a narrow distribution of the average length of the pore. These different shapes of pores for the two different silsesquioxane surfactant precursors are not surprising since their molecular structure is quite different. The isopinocamphenyl group of the chiral molecule is much bigger than the propyl group of the non-chiral precursor. This presumably leads to a change in the packing parameter of the molecules in the micelles. It is known that a bigger head group in a surfactant leads to more spherical micelles.

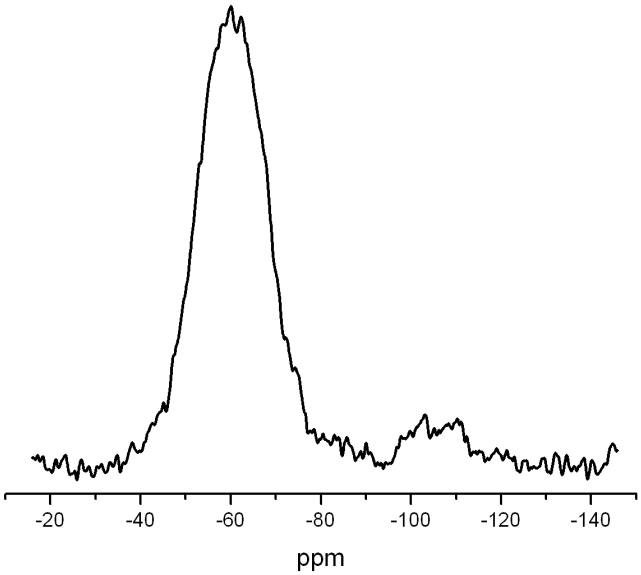

Figure 4-19: ^{29}Si solid state NMR of a chiral MO with BTSE as second precursor after reaction to the amine.

^{29}Si solid state NMR (Figure 4-19) of a MO prepared from the chiral "all-in-one" precursor and bis(triethoxysilyl)ethane shows T-sites centered around -60 ppm as well as some Q-sites at -105 ppm. The Q-sites are due to a 5% of Si-C bond cleavage during preparation, which is not considered to be hampering the applicability of the MO. ^{11}B NMR is used to check the completeness of the surfactant extraction. Figure 4-20 shows one sharp peak at -0.44 ppm for the as synthesized material, which can be assigned to boron atoms attached to two carbon

atoms and one oxygen atom as well as having a water ligand. This peak disappears in the extracted sample, demonstrating a good conversion to the amine.

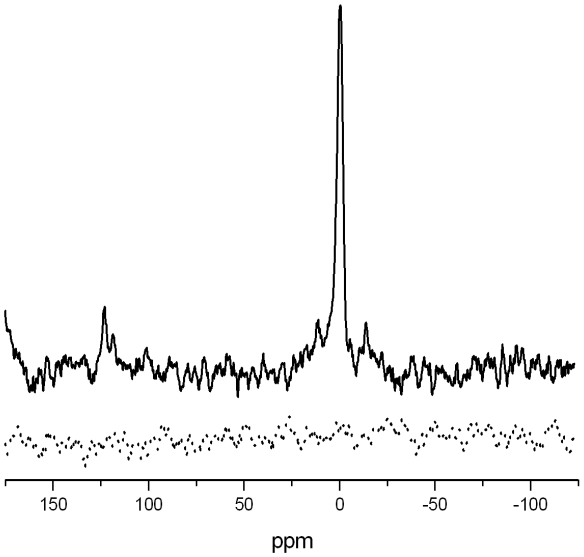

Figure 4-20: ^{11}B NMR of a chiral MO prepared from the "all-in-one" precursor and TEOS. Solid line: as prepared material; doted line: amine functionalized MO.

The primary amine function is qualified with the Kaiser test, [158] which turns deep blue, and is quantified with copper adsorption. After washing the MO with 0.01M ammonia solution and water, aqueous Cu(II) nitrate is added to the material. After 24 hours the solution is filtered off, the solid is washed with water and the residue of Cu(II) in the solution is characterized by AAS. The adsorbed amount is calculated to be 92% of the theoretical amine groups on the pore wall surface in the case the copper ions being in a one to one ratio to amine functions in the starting suspension and 100% if the copper ions are twice as much as the amine groups. Showing that nearly all functional groups are interacting with copper ions, this however also leads to the conclusion that not all four binding sites on the copper are filled with amine groups, which would numerically only lead to an adsorption of 25%. However the presence of tetrahedral complexes formed is seen by the blue coloration of the solid during the adsorption, therefore the other binding sites have to be filled by water or silanol groups. UV/VIS spectroscopy can tell which complexes have actually been formed but this kind of

analysis was not possible on our powders due to experimental reasons, but will be done in the future.

4.3.4 *Analysis of the chirality and the separation mechanism for racemic solutions*

The chiral binding and selectivity for enantiomers of the amine-functionalized chiral mesoporous organosilica are tested with ITC. With this type of measurement the heat of binding can directly be measured, and a complete set of thermodynamic data is generated. ITC is often used to study biological and biomolecular recognition,[172-174] the complexation of molecules in cavities like cyclodextrins[175, 176] and the binding of ions on polyelectrolytes.[177]

Two different small chiral molecules are chosen as representatives for possible interactions with the amine groups on the pore wall surface. First of all cyclohexylethylamine (cyclo-HEA) is taken to probe the specific interactions coming from the chirality of the surface. There should be no strong attraction between the primary amine on the surface of the MO and the primary amine of the small chiral molecule (only some proton exchange seems likely). Mandelic acid is taken as a second molecule, because of the strong and unspecific acid-base interactions between the carboxyl group and the amine group on the surface. Even if the unspecific acid-base interactions are probably much stronger than the specific interactions of the different enantiomers with the amine, it is still interesting to see if there is any influence on the acids by the chirality of the solid surface groups.

For the analysis the solid is suspended in buffer solution at pH 6.9 and filled into the sample cell after degassing. The concentration of amine groups from the MO is kept high (100mM) so that the heat generated by the weak interaction from the small amine molecule is big enough to be measured. The solutions of the pure enantiomers in the same buffer are filled

into the syringe. During the analysis this solution is titrated into the suspension in steps of 10 µl and the heat change is measured with respect to time while the target temperature is kept to 25°C. The total concentration of the enantiomer in the reaction cell is kept low to ensure complete reaction between the small molecules and the surface of the organosilica. If the concentration of the titrant is getting higher it is harder for the enantiomers to reach the active centers on the surface and not all molecules are going to interact. This would make the evaluation of the results more prone to error. The observed heat effects are global values and need to be normalized. Next to desolvation of the surface and the small molecules, the reactions between the surface groups and the enantiomers, there is always dilution taking place in such an experiment. These dilution heat effects can be normalized out by titration of the enantiomers in pure buffer solution and the buffer into the MO slurry. These data are then subtracted from the heat effect determined in the experiment.

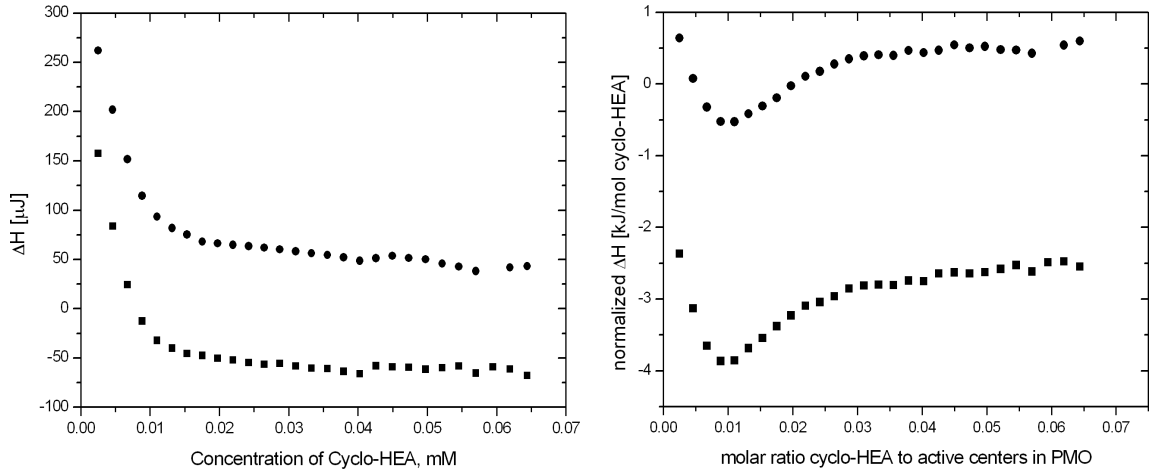

Figure 4-21: ITC curves for the titration of cyclo-HEA into the chiral amine MO. Left: raw data of the titration; right: normalized data; R-cyclo-HEA: squares; S-cyclo-HEA: circles.

The titration of cyclohexylethylamine into the suspension of MO shows an exothermic behavior for the R-enantiomer and an endothermic behavior for the S-enantiomer (Figure 4-21). The reaction steps taking place during the interactions are the desolvation of the cyclohexylethylamine and the MO surface, which are endothermic processes, and then the proton exchange between the different amine/ammonia groups. The endothermic effect from the desolvation of the titrant is not very strong in this case, since the molecule is quite hydrophobic, so that it can be overcome by the exothermic proton exchange if there is an interaction between the functional groups. This is only the case for the R-enantiomer indicating that there are different ways of reaction between the enantiomers and the chiral surface.

From the original data the heat per mole is calculated after normalization (Figure 4-21). It can be seen that the heat decreases steeply at the beginning of the titration. This is due to binding sites having more than one amine group in close proximity, which are often found on functionalized surfaces or macromolecules. After these first two percent of multiple binding sites, the sites only containing one amine group are used and the curve saturates to one value.

This saturation value is then used to determine the enthalpy ΔH, because of its independency from concentration.

The heat seen for the two different enantiomers with the material is quite different. While the ΔH for the S-enantiomer is slightly endothermic (0.46 kJ/mol), the one for the R-enantiomer is exothermic (-2.66 kJ/mol). Both values are small indicating a weak interaction between the small molecule and the surface of the MO, which is expected for the interaction between two amine groups. The values found are close to RT, suggesting a reversible interaction between cyclo-HEA and the MO surface. This is the prerequisite for stationary phases in chromatography, which are relying on adsorption and desorption in near-equilibrium conditions.

As described before the S-form of $IpcBH_2$ (the hydroboration agent) is used, which leads to the formation of a new chiral center with R-configuration in the precursor which is converted into the S-form during the reaction to the primary amine. In this case the different enantiomeric forms in the molecule and on the surface are reacting more strongly with one another. This is most likely due to steric effects on the surface. The surface of the organosilica material is covered with silanol groups as well as the primary amines. An entering cyclo-HEA molecule will not only attractively adsorb on the amine groups, but it also has to avoid the repulsive interactions between the hydrophobic cyclohexyl or methyl groups and the hydrophilic surface. This seems to be only achievable with the R-conformation of the cyclo-HEA.

Similar kind of ITC measurements have been done on molecular imprinted polymers (MIP).[178, 179] Such imprinting into polymers can be done either covalently or non-covalently leading after extraction to polymers which have a cavity presenting selectivity for the molecule used as template. Kirchner *et al*[178] did ITC on a MIP which was synthesized through covalent bonding. A higher affinity for the enantiomeric form used in the preparation

of the MIP can be seen as well as a dependency of the difference in heats of binding between the enantiomers on the concentration. While at low loadings the heats of interaction for the template are much higher than for the other enantiomer the values become more similar when the loading is increased, indicating that there are cavities with different amounts of perfection that interact at different stages. Tovar *et al.*[179, 180] templated an MIP with L-boc-phenylalanine anilide (L-BFA) showing that after extraction the polymer preferably interacts with the L-BFA than with the D-form of the molecule. They explain this behavior with the exact fit of the L-enantiomer into the formed cavity. However the interactions are exothermic in both cases, and the ratio of the heats produced is with about 1.7, small compared to the 5.8 seen here, showing that both enantiomers bind to the polymer. Tovar *et al.* also show that the rebinding of the L-enantiomer is 10 times higher than that of the D-from.[180] Comparing this with the small difference in heats in the ITC the separation factor for the MO material described here should be much higher.

Another disadvantage of such imprinted polymers is that the formed cavity is specific to only one molecule, so that even similar molecules with the correct enantiomeric form show low affinity.[179] A better flexibility on the molecules that can be separated is expected for our MO, since only surface interactions and no inclusions in cavities are involved in the separation. This higher flexibility can already be seen with the cyclo-HEA, which has no similarity to any of the groups in the chiral precursor.

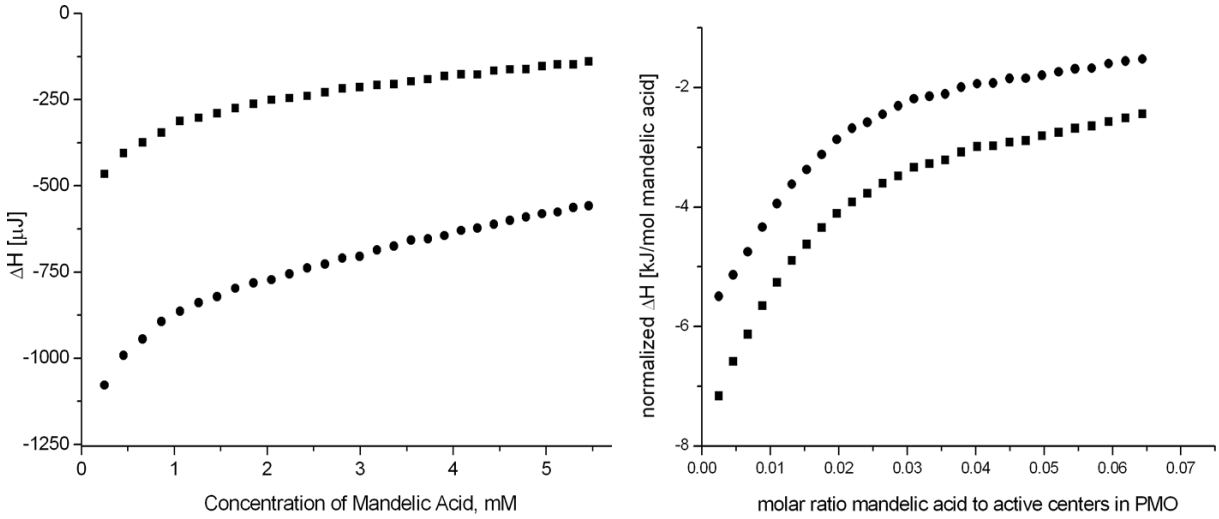

Figure 4-22: ITC spectra for the chiral amine MO with mandelic acid. L-mandelic acid: circles; D-mandelic acid: squares.

The heat released during the titration of mandelic acid into the amine functionalized MO is for both enantiomers exothermic and higher than the one seen in the titration with cyclo-HEA (Figure 4-22). This is not surprising since there is an expected acid-base interaction between the enantiomers of the mandelic acid and the amine surface. The curves of the normalized heats of interaction (Figure 4-22) show an increase at low ratios of acid to amine for both enantiomers, which levels of when more acid is added. As mentioned before in the case of cyclo-HEA, the first steep increase is due to surface sites in which multiple amine are in close proximity and thus able to interact at the same time with the same molecule of adsorbate. Once these sites are saturated the mandelic acid adsorbs on sites bearing an isolated amine group. In this present case though the curve do not saturate so that a concentration-indipendent value for ΔH cannot be reliably determined. The small difference in the heats of interaction observed for the two enantiomers of mandelic acid and the absolute exothermic values (higher than for cyclo-HEA) are consistent with a strong and mostly non-selective acid-base interaction. A qualitative analysis shows that the L-mandelic acid is more strongly adsorbing. We have thus confirmed here that even a typically non-specific interaction like the

an acid-base one can be sensibly influenced by the presence of chiral centers on the surface of a mesoporous material having a mesoporosity compatible with separation devices.

A titration of racemic phenylethylamine into the chiral MO is performed in order to separate a racemic solution and to find the mechanism of the separation of two enantiomers and to estimate the energy and entropy effects involved in the binding of a racemate to the chiral amine surface sites. The chosen molecule was selected for its structural and chemical similarity to the cyclohexylethylamine used in the ITC, but has a phenyl group which is easily detectable by UV/VIS spectroscopy. In a standard experiment, 0.2 g of MO is suspended in 15 ml of water and the racemic phenylethylamine in water is titrated into it (each injection consists of 0.815 ml of a 14.7 mg/ml racemic solution). After every injection the mixture is stirred for 30 minutes and 0.5 ml are taken out, filtered and measured in the HPLC. HPLC is used since it can give the quantitative values for the total amount of racemate in the solution as well as the relative amounts of each enantiomer in the mixture. Crownpak CR(+) from Daniel is selected as column with pH 2 perchloricacid as eluent and a flow rate of 0.7 ml/min. The chromatogram of the racemic starting solution as well as the calibration curves for the enantiomers are shown in Figure 4-23. The elution order is found by analyzing the enantiomeric pure solutions and was determined to be S-phenylethylamine before R-phenylethylamine. The relation between the peak area and the concentration of the racemate for an unknown solution is found by dividing the peak area by the slope of the calibration curve. The “racemic” solution that we are using was found to be not exactly racemic. It contained 54% S- and 46% R-enantiomer, so, appropriate normalization was considered when analyzing the HPLC data.

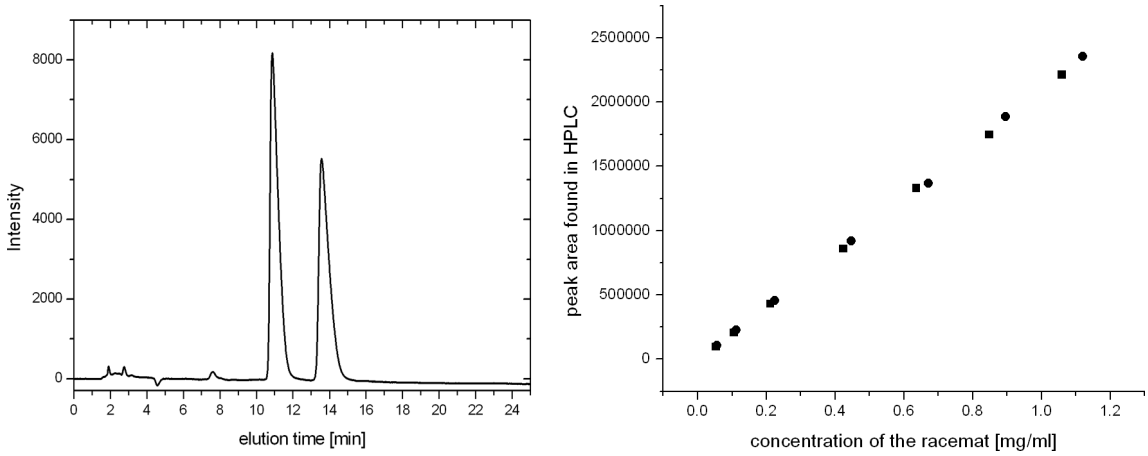

Figure 4-23: Chromatogram of the racemic starting solution of phenylethylamine and the calibration curves for the two enantiomers of the same compound. R-phenylethylamine: squares; S-phenylethylamine: circles.

The HPLC analysis for the titration samples is done under same the conditions as for the calibration samples. Hereby the sample solutions are diluted to approximately 1 mg/ml in order not to overload the column during the measurement. This specific analysis method not only gives the possibility to see the absolute amount of racemate in solution and to compare that with the added amount during titration. It also gives the possibility to check for differences between the adsorption behaviors for the two enantiomers of the compound. Theoretically there are two different mechanisms for the adsorption of a racemate onto a material. First there can be adsorption of both enantiomers in the same amount till all active sites in the material are occupied (ratio of racemate to active centers 1:1) and then a separation starts in which the less favorable enantiomer adsorbed is replaced by the more favorable one till all active centers are filled with the preferred enantiomer (ratio of racemate to active centers 2:1). From here on no further separation takes place. The second possible mechanism for racemates adsorption is the separation from the first addition. Hereby one of the enantiomers preferably adsorbs from the start while the other one is not interacting specifically. So the titration curve increases till all active centers are saturated (ratio of racemate to active centers 2:1). After this the titration curve levels off and there is no further

separation. Specific and non-specific interaction can coexist in our case. An amine on a hydroxylated organosilica surface could show in fact an acid-base interaction between the primary amine of the small molecules and the acidic silanol groups.

The chromatogram of the first sample (concentration 0.76 mg racemate/ml) taken during the titration is shown in Figure 4-24. The peak areas and thus the calculated enantiomers concentrations are very similar. By considering the concentrations of the individual enantiomers in the titrated solution we found that they were much smaller than the ones that we would have found for a non-adsorbing medium. This can be explained with a strong adsorption of the small molecules on the surface. For that specific sample we found that 98.7% of the “racemate” present in the system is actually adsorbed in the material showing no selectivity in the binding.

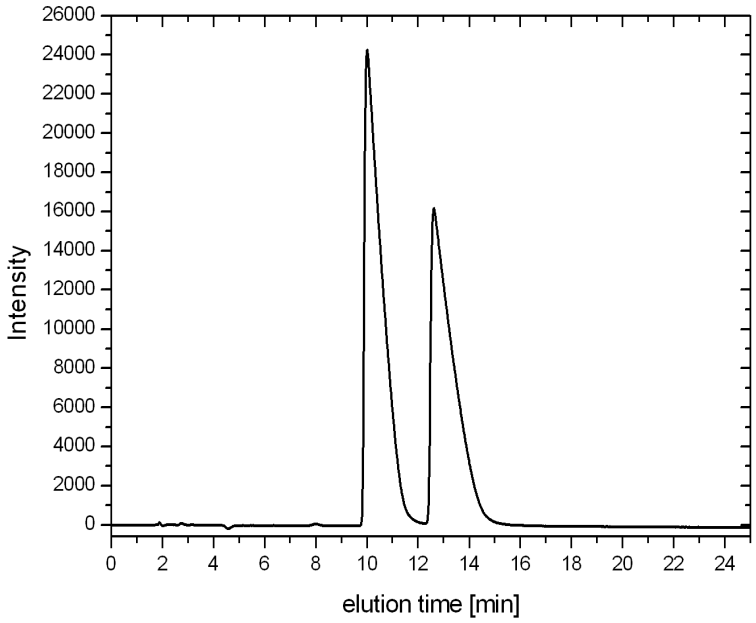

Figure 4-24: Chromatogram of the first sample taken during the titration.

Ratio racemate to active centers	R-phenyl-ethyl-amine in the HPLC (mg/ml)	S-phenyl-ethyl-amine in the HPLC (mg/ml)	R-phenyl-ethyl-amine in the titration mg	S-phenyl-ethyl-amine in the titration mg	ratio of R/S-enantio-mer in the titration	ratio of R/S-enantio-mer in the starting solution	difference between the ratios of enantio-mers	Percent of racemate in the system adsorbed onto the MO
0.19	0.11	0.12	0.07	0.08	0.846	0.843	1.004	98.8
0.37	0.14	0.16	0.18	0.21	0.842	0.843	0.999	98.4
0.56	0.16	0.19	0.32	0.37	0.844	0.843	1.001	98.1
0.74	0.24	0.28	0.47	0.56	0.845	0.843	1.003	97.8
1.30	0.26	0.31	0.93	1.10	0.844	0.843	1.001	97.6
1.49	0.31	0.37	1.12	1.33	0.844	0.843	1.001	97.4
1.67	0.29	0.35	1.28	1.52	0.842	0.843	0.999	97.4
1.86	0.32	0.38	1.44	1.71	0.842	0.843	0.999	97.4
2.23	0.32	0.37	1.71	2.02	0.844	0.843	1.002	97.4
2.60	0.32	0.38	2.02	2.39	0.844	0.843	1.001	97.4
2.79	0.30	0.35	2.16	2.55	0.845	0.843	1.003	97.4
2.97	0.32	0.37	2.33	2.76	0.845	0.843	1.003	97.3
3.16	0.29	0.34	2.41	2.85	0.845	0.843	1.002	97.4
3.34	0.31	0.37	2.65	3.13	0.845	0.843	1.003	97.3
3.53	0.31	0.37	2.68	3.18	0.842	0.843	1.000	97.4
3.71	0.30	0.36	2.88	3.41	0.844	0.843	1.002	97.4
3.90	0.30	0.36	2.95	3.50	0.843	0.843	1.000	97.4
4.09	0.31	0.37	3.09	3.66	0.844	0.843	1.001	97.4

Table 4-1: Values for the calculations of the behavior of phenylethylamine on the chiral amine MO.

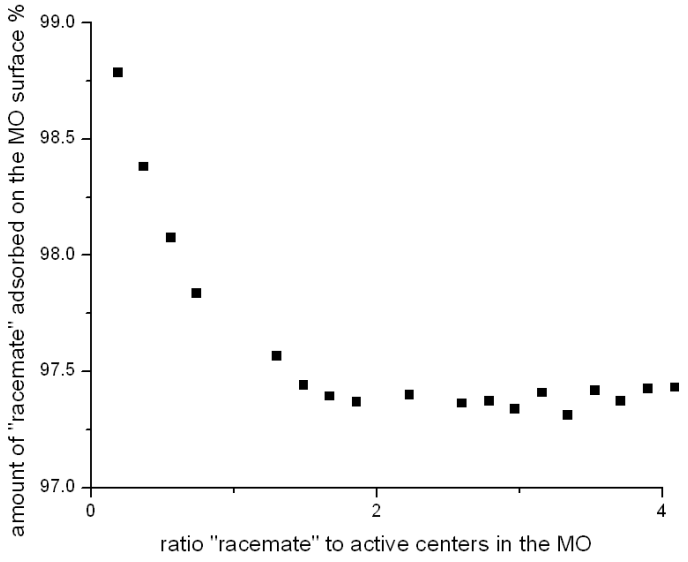

Figure 4-25: Amount of “racemate“ adsorbed on the surface of the chiral amine functionalized MO.

For each sample analyzed by HPLC we calculated the concentrations of the two enantiomers and the obtained values were then converted into a ratio of R- to S-enantiomer found in the solution during the titration. This ratio is then divided by the theoretical ratio in the solution, which comes from ratios of the enantiomers in the starting “racemic” solution. All values are shown in Table 4-1. It can be seen that the difference between these two ratios is minimal, which leads to the conclusion that there is no chiral separation seen for phenylethylamine on the MO under these conditions.

When calculating the amount of racemate adsorbed onto the MO with respect to the total amount of racemate added to the solution a really high adsorption of nearly 99% can be seen in the beginning, which levels of at around 97.4% at the end of the adsorption experiment.

This shows that the chiral MO is strongly adsorbing phenylethylamine in quantities largely exceeding the number of available amine groups on the surface. This can be explained by considering the effect of entropy. In the process of adsorption of the amine to the surface of the MO we have to consider the role of the solvent. Water is solvating the amine molecule in solution and it is adsorbed on the MO surface. The process of amine adsorption is thus releasing water in the solution increasing the entropy of the system and thus driving the process to completion. This is supported by the consideration that our material has a very large surface area (routinely above 1000 m^2/g). The amount of racemate we have used in our titration experiments is obviously not enough to cover the whole available surface of the material, which is explaining why we are not observing any saturation behavior in the range of concentrations we have used. So in our case the adsorption is not an enthalpy driven process, but an entropy driven one.

The material described here is at the moment not suitable for the enantio-specific separation of an amine in water. The strong entropic effects shown in the titration experiments are outweighing the enthalpic effects probed by ITC. There are two possible ways to

compensate for such strong entropic effects. The first one is to modify the chemistry of the surface in order to decrease the strength of its interaction with the solvent. The "all-in-one" methods described herein can be used, since they influence the surface properties of a mesoporous solid without influencing the high stability of organosilica materials. They are also making sure that a large amount of functional groups is accessible from the pores. This change in the surface could also influence the adsorption enthalpies for the enantiomers onto the surface. A second way to compensate for these strong entropic effects it to change the eluent in a HPLC system. This can be obtained by packing the material into a column and the best eluent composition can be found by gradually changing it during the HPLC experiment.

These proposed strategies should show the optimal conditions in which the separation of enantiomers on our MO is possible. This kind of optimization is though beyond the scope of our work and is more suitable for an analytical chemistry environment. Nonetheless, our material will be packed in a HPLC column in the near future and the optimization of the separation conditions for different enantiomers will be attempted.

4.4 Long chain amine precursors for mesoporous materials: A PMO with non-glassy walls

To further extend the "all-in-one" method described in the previous chapters a precursor-surfactant complex bearing a non-covalent bond is examined. The ionic bond between an amine containing precursor and a strongly acidic surfactant is chosen due to its stability under the acidic conditions employed in the nanocasting process. Such interactions have been used before to form PMO materials containing terminal aminosilanes or quaternized aminosilanes and anionic as well as anionic chiral surfactants.[181-183] Also, bridged amine-containing precursors have been assembled into PMOs. For example M. Wahab *et al.* co-assembled

bis(trimethoxysilylpropyl)amine and BTSE containing a maximum of 17.5% of amine groups in the final material.[142] The even longer bridged molecule bis(trimethoxysilylpropyl)ethyldiamine (BTSPEA) has been co-assembled with TEOS in a molar concentration of up to 5% by Mercier *et al.*[12] and in the combination with BTSE with up to 30% of amine containing precursor by Zhu *et al*.[138] PMOs formed in this way showed metal adsorbing properties, but the amount of accessible active sites is lower than what would be attainable by driving the amine-containing precursor to the pore wall surface.

In the work described here, materials with the full range of mixtures from 100% amine precursor to only 20% of amine are prepared. As a second precursor either TEOS (a precursor forming a pure silica material) or BTSE (forming a pure hybrid MO) is used. As a strongly acidic surfactant we chose pentadecafluorooctanonic acid (CF), a C8 perfluorinated anionic molecule. The size of the micelle formed by this template is comparable to the one formed by CTAB, due to the difference in head to tail ratio of two surfactants. The perfluorinated chain is short and thick because of the large size of the fluorine atoms, the hydrocarbon chain is thinner and in a folded conformation. This difference manifests in the behaviours of the two molecules when they are used as surfactants: the perfluorinated chains tend to avoid interdigitation by creating double-layered micelles, while the hydrocarbon chains will interdigitate. The acidic head group of the CF surfactant interacts with the amine group in the precursor driving the functional organic group to the pore wall surface and ensuring its chemical accessibility from the pore. Due to the hydrogen-bonding “sponge” effect, the acid can be used in a much lower concentration than the amine, since it usually interacts with more than one amine at a time.

In a typical synthesis the BTSPA or BTSPEA are diluted in ethanol and the corresponding amount of TEOS or BTSE is added to the solution. Then CF in ethanol is added. For 4.9 mmol of silica in the mixture 0.5 g of 0.01M aqueous HCl are added to the mixture, providing

final molar ratios of precursor:CF:HCl of $8.75:1:4.5*10^{-4}$. The low value for the surfactant is chosen to always keep the amount of amine functions in the sol higher than the acid groups; knowing that this will only lead to unordered diluted micellar structures and pore systems. No long range ordered porous systems can be formed, since the concentration of the surfactant is much lower than the one needed for one of the LC phases. In this case only the L1 phase, but none of the possible hexagonal or cubic phases can be reached. After homogenization the ethanol is removed under vacuum to give a solid, which is dried at 60°C overnight. The extraction is performed in methanol/HCl leading to a porous solid with amine functions on the pore wall surface.

The TEM images of the materials made from BTSPA and TEOS with CF as surfactant are shown in Figure 4-26. For high concentrations on BTSPA no pores can be unequivocally seen. Wormhole structures show up at lower concentrations of amine precursor while at 20% loading the system exhibits a more particle-like structure. No pores can be seen in the pure silica solid indicating that CF cannot act as a template for silica during nanocasting. Only the enlargement of the head group with the condensable organosilane stops the micro-phase separation.

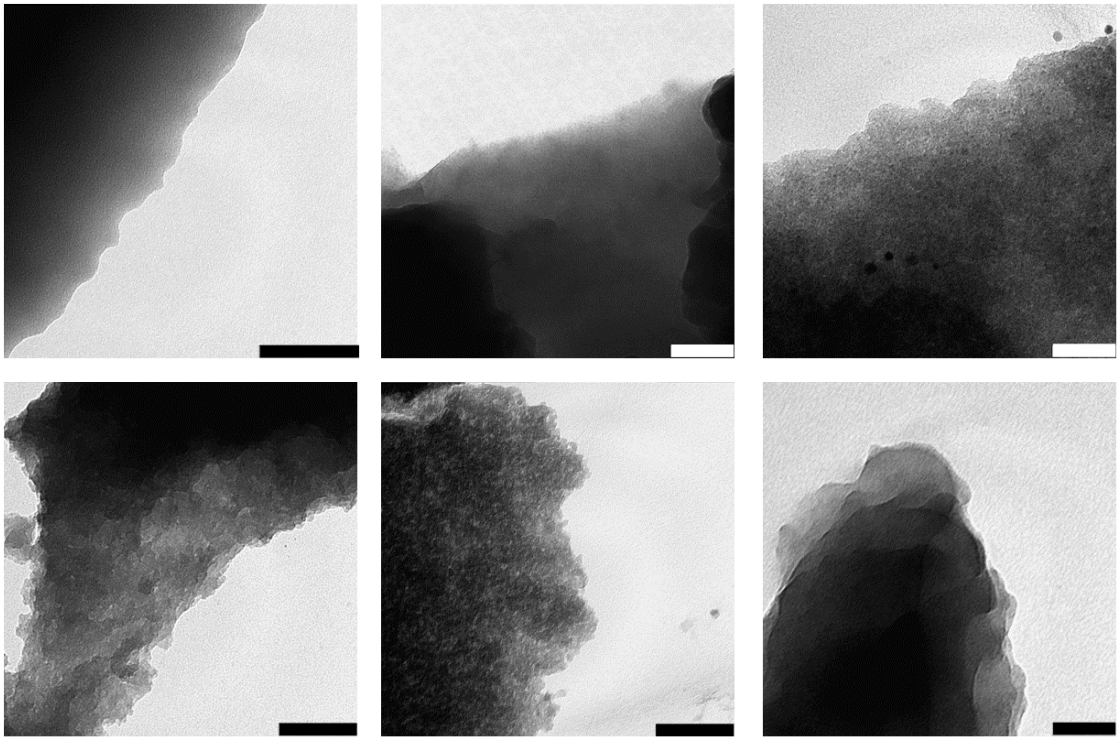

Figure 4-26: TEM images of MOs made from BTSPA/TEOS and CF 100% to 0% of amine in 20% steps from the top left to the bottom right corner. Scale bars for 100%, 80%, 40% and 20% are 100 nm, for 60% and 0% 50 nm.

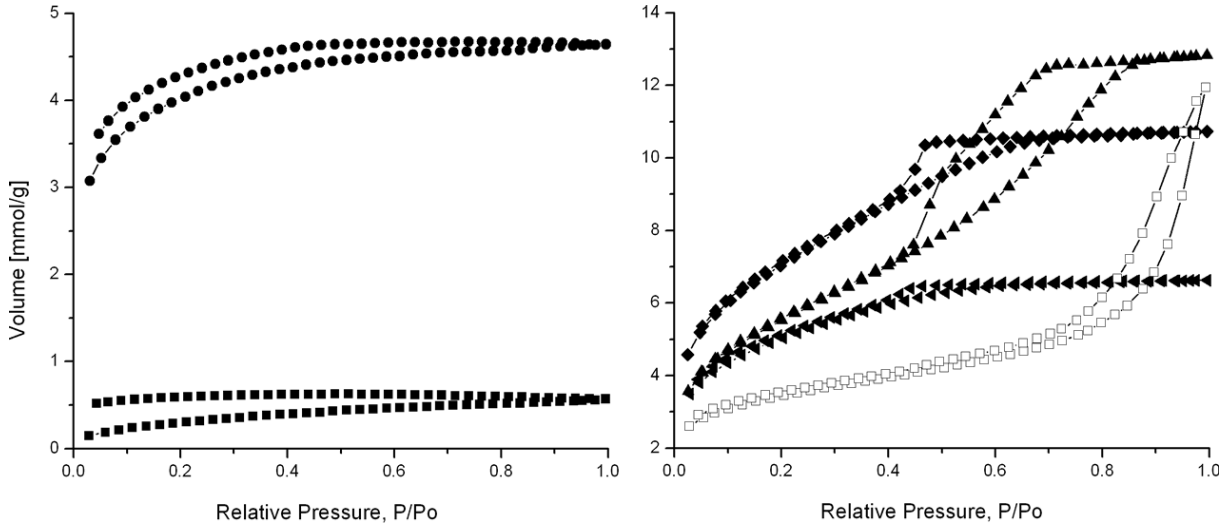

Figure 4-27: Nitrogen adsorption isotherms of MOs synthesized from BTSPA and TEOS CF100: squares; CF75: circle; CF60: triangle left; CF40: rhombs; CF20: triangle top; CF0: open squares.

Mixture	% of amine in the material	BET [m²/g]	BJH [nm]	BJH [nm]	total pore volume [cm³/g]	macroscopic properties
CF/TEOS	0	274	few 3.6	18.9	0.41	micro-phase separation
CF/TEOS	20	445	3.9	broad shoulder at high diameters	0.44	slight micro-phase separation
CF/TEOS	40	568	3.6		0.37	
CF/TEOS	60	403	3.4		0.23	
CF/TEOS	75	326	few 3.1		0.16	
CF/TEOS	100	26.1			0.02	
CF/BTSE	0	-	-	-	-	micro-phase separation
CF/BTSE	34	695	3.9	5.7	0.73	slight micro-phase separation
CF/BTSE	57	614	3.6		0.38	
CF/BTSE	75	383	3.4		0.22	
CF/BTSE	100	26.1			0.02	

Table 4-2: Nitrogen adsorption characteristics of all the MOs formed from BTSPA and CF and their behavior during condensation. The BJH calculation is performed on the desorption branch of the isotherm.

The nitrogen adsorption isotherms for BTSPA combined with TEOS and assembled around CF show different shapes depending on the mixture.

For high concentrations of amine (100% and 75% where all percentages are calculated with respect to molar ratios in the starting solution) the isotherm exhibits a low pressure hysteresis, meaning that not all nitrogen is released during the desorption process. Also the total pore volume and the uptake of nitrogen are small (

Table 4-2). A BET surface area of 326 m^2/g is found for CF75. This large surface with the small total pore volume can be explained by assuming the occurrence of a deformation of the material during the adsorption which is trapping the nitrogen inside. This is the first time that such a flexibility of the pore walls of a MO has been observed. The walls in these materials are usually glass-like, rigid and brittle, which is obviously not the case for this precursor combination. Also the macroscopic mechanical behavior is different: when subject to mechanical grinding these solids are more rubber-like than glass-like.

Starting from 60% of organic in the solid the usual closing type IV isotherm can be seen. The absence of capillary condensation in the adsorption branch is a typical behavior of T-type

non-ionic surfactant templates, which are similar in structure to the precursor-surfactant complex in this work. Also the theory for nitrogen adsorption based on pure silica PMOs might not apply here, because of the flexibility of the walls and the different surfaces of these MOs when compared with pure silica materials. The surface area of CF60 is 403 m^2/g and the total pore volume increases to 0.23 cm^3/g. Both values increase further for CF40 showing the lower flexibility in the material with increasing amount of TEOS.

At low secondary amine concentration (20%) the isotherm shows a bimodal distribution, and the material exhibits micro-phase separation. The combination of BTSPA and CF seems to be able to dissolve large amounts of silicic acid while the organic precursor is too hydrophobic to be dissolved in silicic acid in any quantity.

When pure TEOS is assembled around the CF surfactant no pores in the mesoporous range can be seen and the solid exhibits clean micro-phase separation during the condensation. From this behavior it can be concluded that a perfluorinated acid is not a template for silica.

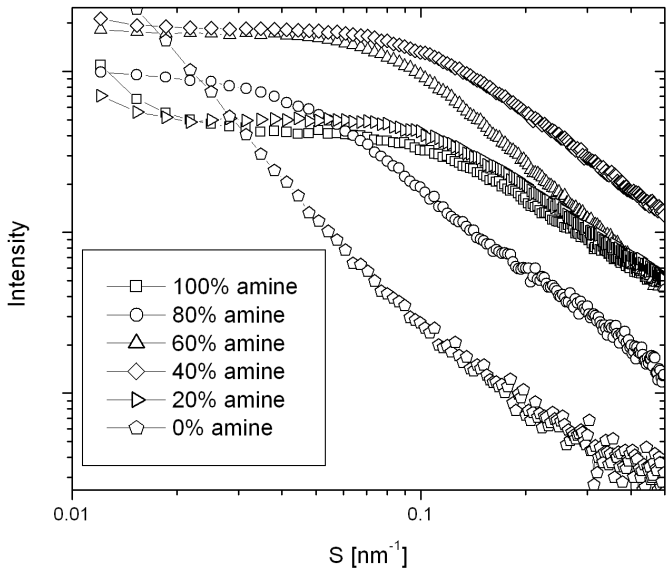

Figure 4-28: SAXS curves of the long chain amine MOs prepared by the "all-in-one" method. Square: 100% amine; triangle to the right: 75% amine; diamond: 60% amine; triangle to the top: 40% amine; circle: 20% amine; five-ring: 0% amine.

The pore structure of the materials can be further analyzed with SAXS measurements (Figure 4-28). The absence of peaks indicating long-range order in the meso length scale is expected, given the dilute template phase during the preparation of these materials. As described before none of the possible LC phases of the surfactant can be reached with the concentrations employed in this work. Scattering curves which are dominated by the form factor can still be used for analysis as has been shown in our group and in previous chapters of this work.[154] It can be seen that all solids show a high X-ray scattering intensity, which implies the existence of a pore system (given the contrast in electron density between the material and the air in the voids). For CF100 and CF75, the two samples having highest organic content, the curves first slightly decrease with increasing scattering angle, then increase going through a broad maximum until they decrease to larger angles. This leads to the conclusion that the pores are in a disordered state with a large variety of inter-pore spacings between them. However the broad peak also suggests the possibility that an increase in template used during the synthesis will lead to the formation of long range order pore systems. For CF60 to CF20 the broad peak vanishes and the curve only exhibits a flat plateau without a maximum, showing that the pore structure is even less ordered. Also these curves steeply decrease at higher angles. It is known that the earlier the decrease starts the more polydisperse a pore system is due to the unproportional scattering of large pores,[154] which is consistent with the nitrogen adsorption data for these organosilicas (Table 4-3). Only the pure inorganic material shows no such plateau in the measured range, which is due to the micro-phase separation.

The shape of the pores can be deduced from the decrease of the scattering curves towards higher angles using “Porods theory”. This theory relates the behavior of the decrease in the scattering curves with the pore shape through an asymptotic fitting with the scattering intensity (I) being proportional to the scattering vector (s) following $I(s) \sim s^{-v}$. For a three

dimensionally extended pore ν = 4 (“Porod law”). In an into the third dimension extended quasi-2D pore ν changes to 3 and if the pore has a thin slit like form the value further decreases to ν = 2. For the Kratky camera used in these measurements the equation changes to $I(s) \sim s^{-(\nu-1)}$ due to slit smearing found in the set up. A value of ν = 3 is thus found for a three dimensional pore, which is extended in all directions of space. For quasi-2D objects the function goes down to ν = 2 and for long and narrow two dimensional pores the values becomes ν = 1. The organosilica materials CF100 and CF75 show a value ν of 1.3 indicating quite narrow two-dimensional pores with a short and wormhole like structure. For the next higher concentration of TEOS the value increases to 1.5 showing a more three-dimensional pore. This increase in size in the third dimension can also be seen in the increase in the pore diameter in nitrogen adsorption (

Table 4-2) and is probably due to the lower flexibility of the material with increasing amount of TEOS. When instead the organic content is high the pores are probably deforming from cylindrical to slit-like during the extraction, given the flexibility of the material. While for lower organic content the walls are glass-like enough to keep the shape of the pore when the template is removed. This hypothesis is further solidified by CF40 which shows another increase in ν to 1.9 indicating a larger extension of the pore into the third dimension. For the solid with only 20% of organic groups this pore shape analysis does not apply, since the pore system in this case is bimodal and there is no way to separate the contributions of the different pore systems in the fitting. Also for the pure inorganic material, such an asymptotic fitting is impossible, since there is no linear decrease to be found in the curve, making the choice of an asymptote impossible.

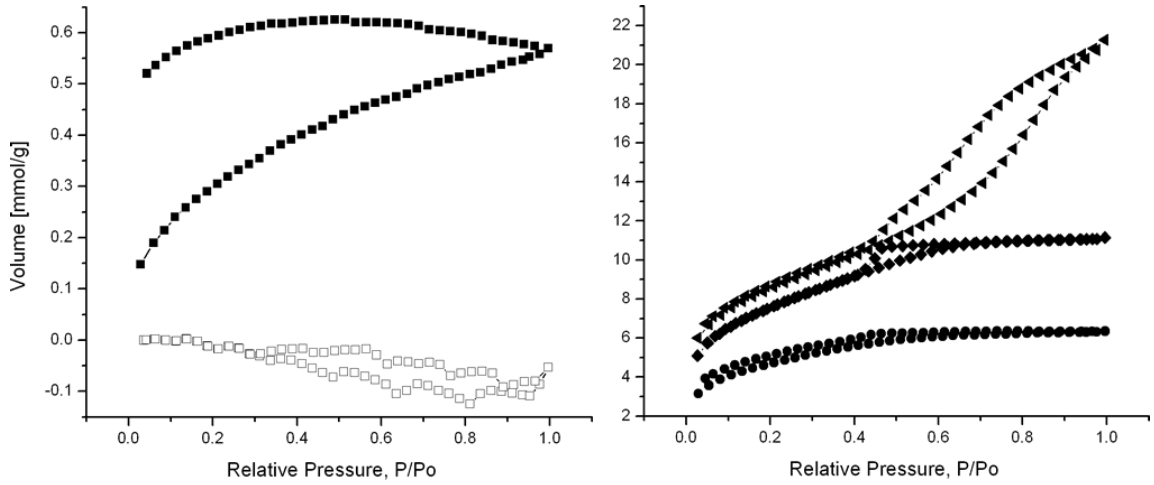

Figure 4-29: Nitrogen adsorption isotherms of MOs from BTSPA and BTSE. 100% amine: squares; 75% amine: circles; 57% amine: rhombs; 34% amine: triangle left; 0% amine: open squares.

In the next series BTSE precursor, containing an ethene bridging group, instead of TEOS is used as a second building block in combination with the amine functionalized BTSPA to form pure organosilica compounds. The adsorption results are similar to the ones described above with the exception that the closing of the low pressure hysteresis starts at lower concentrations of BTSE. This could be due to micro-phase separation occurring during the hydrolytic polycondensation. TEOS and BTSE are both soluble in BTSPA in their non-hydrolized form. A micro-phase separation can happen in multi-precursor systems in the case in which the two precursors are hydrolyzing at very different rates. In these conditions the most reactive precursor forms islands of condensed material before the other precursor start to condense. This can be the case for the TEOS/BTSPA combination since the susceptibility to hydrolysis of TEOS and BTSPA are significantly different. We can thus expect from this system to obtain a not completely homogeneous material in a wide range of conditions. This would then explain the peculiar adsorption properties.

Regions enriched of one precursor will be most likely formed in the mixture of BTSPA with TEOS, leading to highly flexible and highly rigid areas distributed all over the material.

The flexible regions however will be most likely the parts deforming during the nitrogen adsorption conferring an overall flexibility to the material. In the organosilica solid formed from BTSE instead the hydrolization kinetic of the two precursors prevents segregation and thus leads to a more homogeneously rigid material.

At higher concentrations of BTSE micro-phase separation takes place and the system goes from bimodal to non-porous, showing again that CF is not a template for silica mesoporous materials.

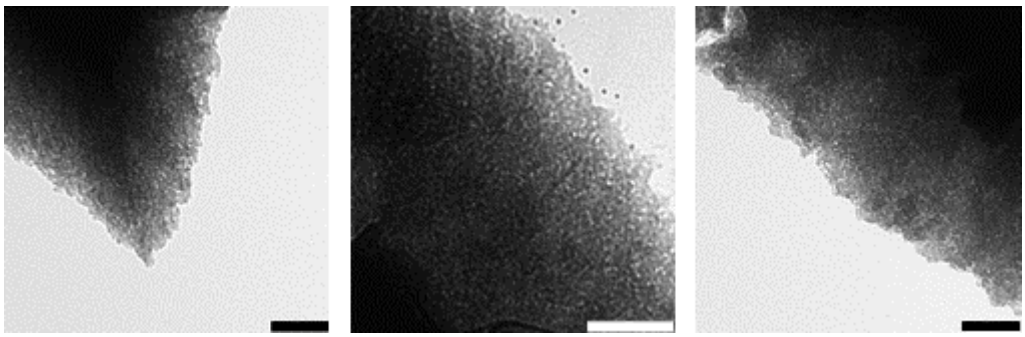

Figure 4-30: TEM images of MOs from BTSPA/TEOS and CTAB containing from right to left 100, 80 and 60% of BTSPA. Scale bars 100 nm.

At this stage it was interesting to understand if such non-glassy behavior for BTSPA could be obtained also with CTAB. As can be seen from the TEM pictures of MOs containing 100%, 80% and 60% BTSPA (Figure 4-30), highly porous solids are formed. These materials show a wormhole like structure with uniform pore size distributions.

Nitrogen adsorption isotherms have been recorded to analyze the mechanical behavior of the walls. They show the same open albeit slightly smaller low pressure hysteresis loop as the ones prepared with CF as surfactant. So both surfactants are able to give mesoporous materials having flexible walls. CF, however, gives materials which show flexibility of the walls over a wider range of concentrations. This could be due to the long chain precursor being more concentrated on the surface of the pore wall because of the interactions with the acidic function of the surfactant. In the case of CTAB this interaction is not present, so that an

even distribution of the precursors in the walls should take place, leading to more uniform walls with more glassy characteristics.

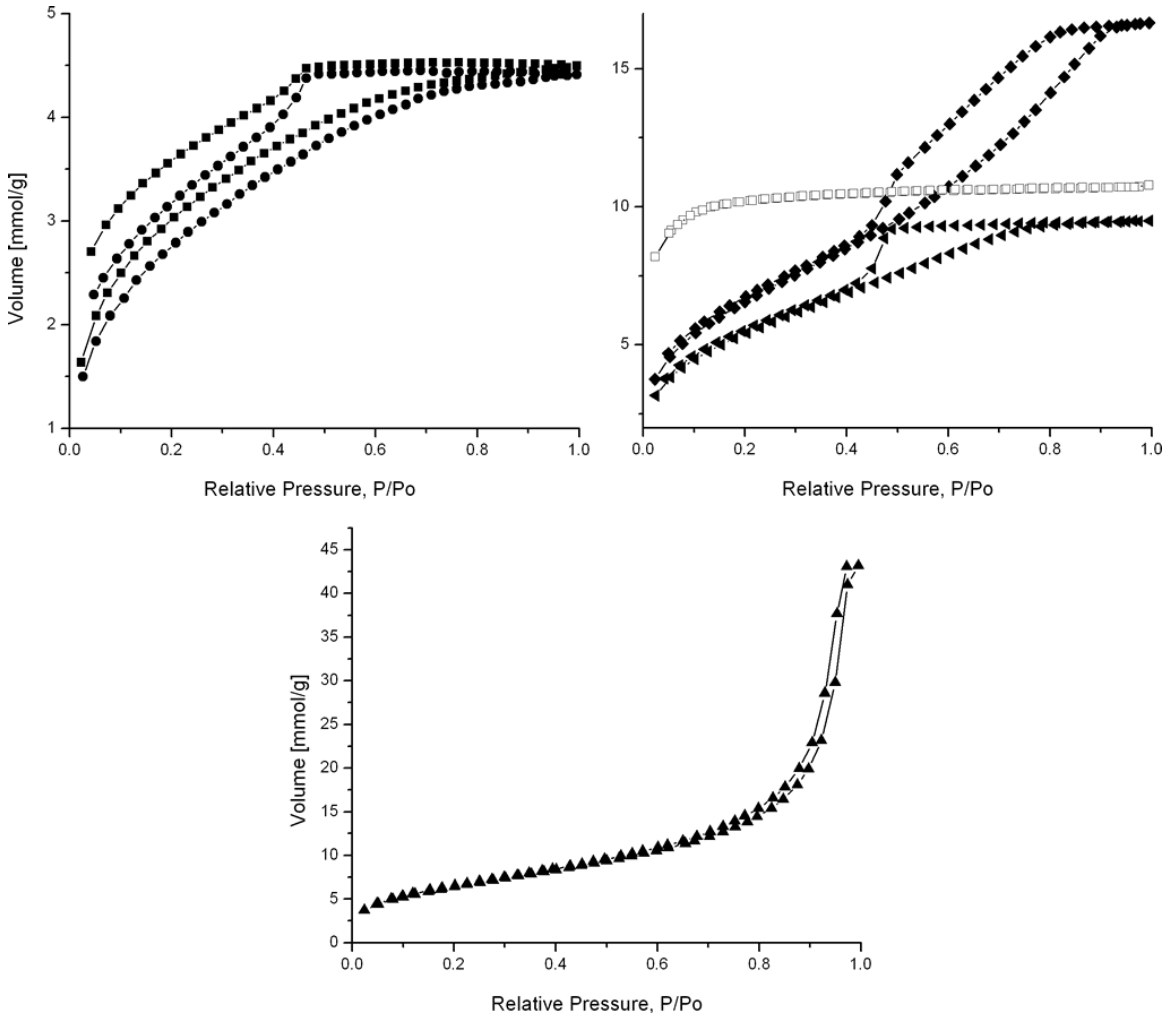

Figure 4-31: Nitrogen adsorption isotherms of MOs from BTSPA, CTAB and TEOS. CT100: squares; CT80: circle; CT60: triangle left; CT40: rhombs; CT20: triangle top; CT0: open squares.

Also the combination of BTSPA, BTSE and CTAB at different ratios was studied. Since these MOs do not behave differently from the ones described above they are not discussed in detail here.

The analysis of the isotherms is done using BET and BJH methods and the resulting values are summarized in Table 4-1. It can be seen that the pore diameter is approximately the same for all amine containing MOs without phase separation. Due to the interactions of the organic group in BTSPA with CTAB the value is with 3.5 nm higher than the 2.2 nm found for CTAB

and TEOS. The propyl groups of the precursor will undergo hydrophobic interactions with the methyl and cetyl groups of the surfactant. The packing parameter of the template is thus changing, leading to a wider spacing between the molecules and an enlarged pore diameter. The surface areas vary from close to zero in phase-separated materials to the high values known for MOs having meso- and micropores. The total pore volume generally increases, because the flexibility of the walls decreases with decreasing amount of BTSPA, so the pore structure will be less deformable and more nitrogen can enter the pores.

Mixture	% of amine in the material	BET [m^2/g]	BJH [nm]	BJH [nm]	total pore volume [cm^3/g]	macroscopic properties
CTAB/ TEOS	0	846	2.2		0.34	
CTAB/ TEOS	20	528	few 3.8	35.7	1.48	micro-phase separation
CTAB/ TEOS	40	541	3.9	broad shoulder at high diameters	0.57	micro-phase separation
CTAB/ TEOS	60	444	3.7		0.33	micro-phase separation
CTAB/ TEOS	80	232	3.6		0.15	
CTAB/ TEOS	100	251	3.5		0.15	
CTAB/ BTSE	0	948	2.2		0.54	
CTAB/ BTSE	34	456	24.7		1.61	micro-phase separation
CTAB/ BTSE	57	508	few 3.7	5.9	0.69	micro-phase separation
CTAB/ BTSE	74	449	3.7		0.36	slight micro-phase separation
CTAB/ BTSE	89	177	3.4		0.11	
CTAB/ BTSE	100	251	3.5		0.15	

Table 4-3: Nitrogen adsorption characteristics of all the MOs formed from BTSPA and their behavior during condensation. The BJH calculation is performed on the desorption branch of the isotherm.

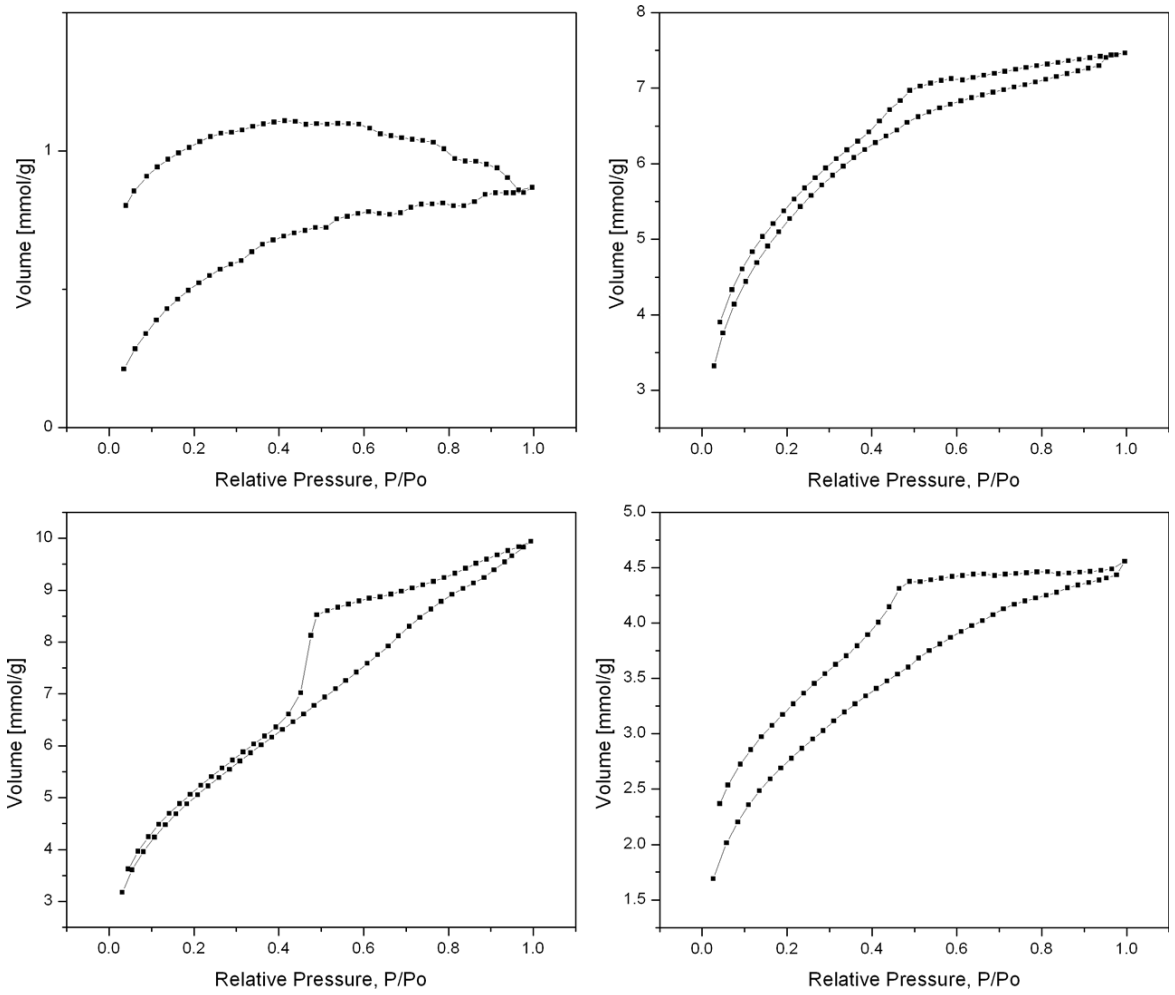

Figure 4-32: Nitrogen adsorption isotherms of MOs from BTSPEA and TEOS. From the top left to bottom right: 59%, 39% and 20% amine with CTAB as surfactant and 19% amine with CF as surfactant. The scales on the y-axis are different for all isotherms to better show their shape. Generally the total uptake on gas adsorption increases with increasing amounts of TEOS.

As an extension of this "all-in-one" method with ionic interactions the longer BTSPEA with two amine groups is investigated. Here even higher flexibility of the walls can be expected as well as better heavy metal binding properties when compared to the single amine group in BTSPA. As can be seen from the adsorption isotherms the amount of TEOS needed to form stable solids is much higher than for the shorter chain precursor. However, to the best of our knowledge, this is the first time this precursor has been assembled in such high concentration into a mesoporous material. Regarding the analysis of these isotherms, the same

trends as for BTSPA can be seen. The surface area is between 49 and 428 m^2/g depending on the composition in the preparation, the pore diameter is around 3.6 nm and the total pore volume is found to increase with decreasing amine content.

mol% amine in the PMO	% Cu(II) adsorbed in respect to amine	
	CF	CTAB
100	23.2	24.0
78/75	20.6	22.3
60	32.1	9.6
40	39.7	16.2
20	40.1	8.9
0	0	0

Table 4-4: Values for Cu(II) nitrate adsorption on different MOs.

For the quantification of the amine content, copper (II) ions can be adsorbed onto PMOs.[138, 159] By using the BTSPA/TEOS series of both surfactants the influence of the "all-in-one" method on the location of the active centers is checked. In the case of the "all-in-one" material more copper should be adsorbed, since the secondary amine functions are directed to the pore wall surface. For the analysis the MO is first suspended in 0.1M ammonia solution for one hour, washed with clean water and dried. Then a 0.1M Cu(II) nitrate solution is added in such a way that the ratio between the amine groups in each solid and copper ions is always 1:1. The Cu-loaded product particles are isolated, rinsed with water two times, dried, and the copper content is determined by AAS. The values are given in Table 4-2. It can be seen that for the purely amine-containing MOs the amount of copper adsorbed is for both surfactants about one quarter of all the amine groups in the solid. This result together with the blue color in the material is a good indication for the formation of tetrahedral copper complexes. That the value for both surfactants is the same is not surprising, since there are 100% of amine groups in the materials. There is no possibility for the CF surfactant to drive all of the

functional groups to the surface, since it is added in much too low a concentration during the preparation. So in both materials there will be some amine groups on the surface and some hidden in the walls. For the next lower concentration the values are quite similar as well, which can be explained with the same arguments as for the purely organic bridge bonded MO material. The amount of CF is still too small to have an effect on the location of the primary amines.

Only starting from 60% of amine groups in the material a clear change in the adsorption behavior of the two solids can be seen. While the value for the acidic surfactant is increasing the one for CTAB is decreasing dramatically. For CF60 the uptake of copper is 32% and the material has a blue color after the adsorption.

Interestingly, the amount of copper adsorbed is further increasing with increasing amount of TEOS, which can be explained with a by the preparation method employed. The amount of acid used as surfactant is kept the same in all materials, so that in the case of lower bridging organic content more acidic groups per amine group can be found driving the active groups more strongly to the pore wall surface. Compared to the CF data, the values for CTAB are quite low and unsystematic, showing that there is no influence of the surfactant in the position of the functional groups. However, in this case there is still a blue coloration in the MOs indicating that the few amines accessible have the right configuration to form four coordinate complexes with copper.

5 Surface properties of the pore walls of MO materials with different organic groups

5.1 Introduction

Water-surface interactions can provide useful information about the nature and local arrangement of surface groups on solid materials. In the case of hydroxyl groups these interactions can either be through electric dipoles or through hydrogen bonding. Considering a porous material there are two 'kinds' of water to be found in the pores. There is one kind bound near the pore surface and another behaving as free water in the pores. In mesoporous silicas, there are isolated and clustered silanol groups, which can be shown by ^{29}Si NMR, FTIR, TGA or TPD.[24] If the silanol groups are close to one another they will from hydrogen-bonds. These interacting surface groups will be the ones mostly adsorbing water vapor. When a monolayer is formed on these patches additional water will preferably adsorb on already existing water molecules, and it will less likely interact with the isolated silanol groups or with the more hydrophobic areas not containing any hydroxyl groups of the material.[104, 121, 184] This kind of de-wetting behavior is well known for purely inorganic silicates as well as for organosilicates. This can go so far that the condensation of water in porous systems starts before a monolayer is formed. The internal water droplet will grow to a point where it touches the opposite surface and with this spontaneously form two menisci, which will rapidly move to fill the pores completely (Figure 5-1).

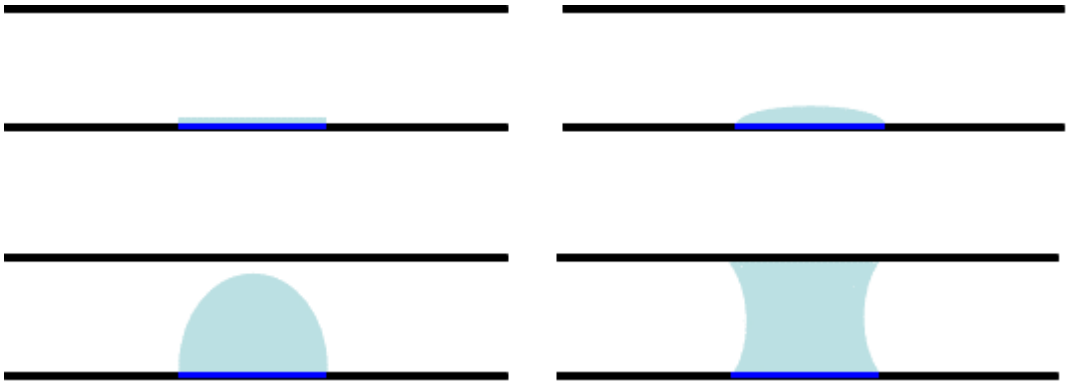

Figure 5-1: Scheme of proposed pore filling mechanism for water (light blue) in pore containing hydrophilic (blue) and hydrophobic parts (black).

So far there have been reports on the hydrophilicity of mesoporous silica materials arising from different organic molecules grafted onto the surface of the pore walls,[107, 184] as well as one report about the influence of the surfactant concentration on the hydrophilicity of a PMO prepared from BTSE and CTAC.[185] Matsumoto *et al.* show in this paper that the materials are generally hydrophobic, but that they get more hydrophilic if the amount of surfactant is increased. This is explained by the interaction between CTAC and the anionic silica species formed during the condensation. The cationic head group of the surfactant will attract anionic charge on the silica surface and these will than form the silanol groups. The capillary condensation seen in the isotherms is due to clustering of water in the most hydrophilic areas.[186]

This chapter describes the behavior of different MOs towards water vapor. Methene, ethene, ethylene, and bis-propylamine are the bridging groups considered as being representative for the commercially available precursors. For purely inorganic silicas the difference in condensation speed due to the alkoxy groups on the hydrophilicity can be checked by comparing TMOS and TEOS precursors. CTAB (a cationic amphiphile), lithium heptadecafluorooctanoic sulfonic acid salt (LiFOS) (an anionic molecule) and CF (a strong acid) are compared as surfactants. The different templates give the possibility to analyze the

influence of the head group and the nature of the chain on the wall surface, while leading to pore-diameters with approximately the same size.

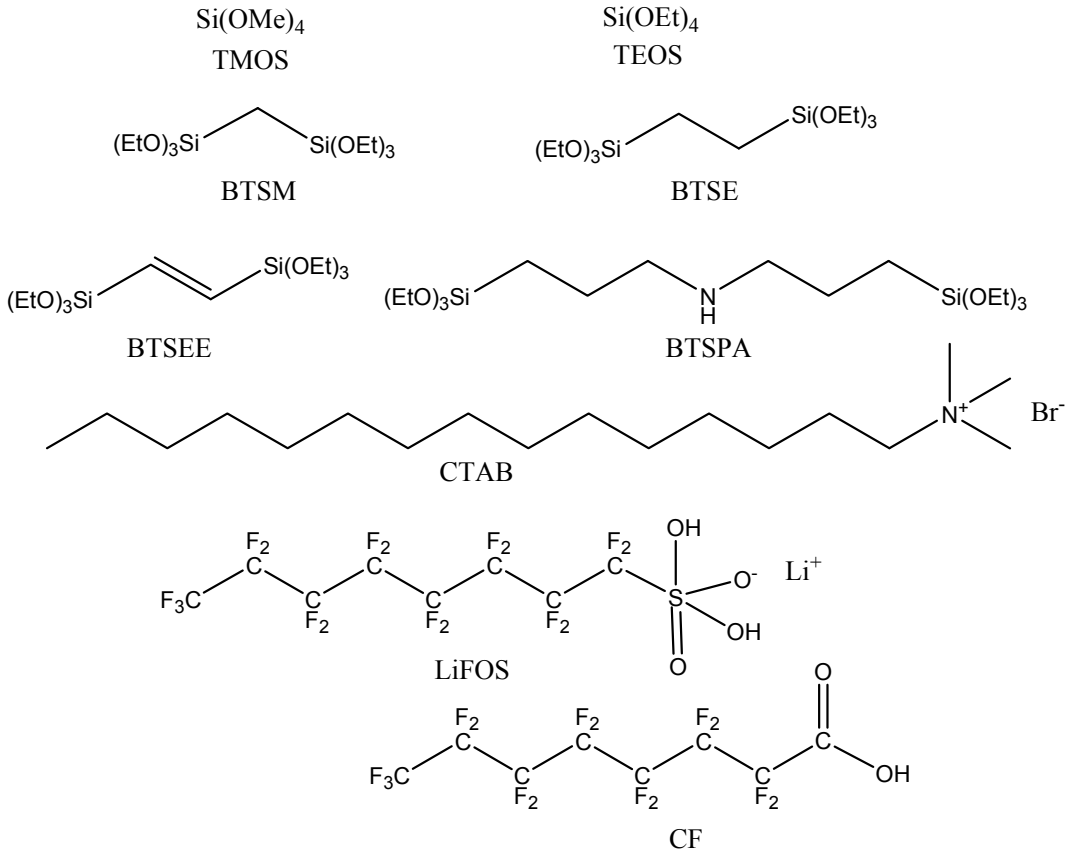

Figure 5-2: Library of molecules used in the water adsorption study.

In a typical synthesis the precursor, ethanol, water and HCl are mixed to form a homogeneous solution and the ethanol is removed under vacuum to give monolithic solids. Our preliminary experiments have shown that the history of a sample strongly influences its behavior towards water. For this reason every sample from one series is prepared in the same way, with all the aging and drying steps performed at the same time. The different series are only partially comparable, since the experimental conditions can vary. All samples are extracted with methanol/HCl for overnight and then dried at ambient pressure and 60°C for at least two days, the last traces of water are removed at 150°C under vacuum for at least 90 minutes, where the time can vary between the series.

5.2 *The influence of different organic groups on the hydrophilicity in MO materials*

In order to study the influence of the different organic groups on the hydrophilicity of the MOs, all the above mentioned precursors are assembled around CTAB. The structural parameters are found by nitrogen adsorption. Only a representative isotherm for TMOS and CTAB and the one for BTSPA are shown in Figure 5-3, since all the other isotherms are type IV.

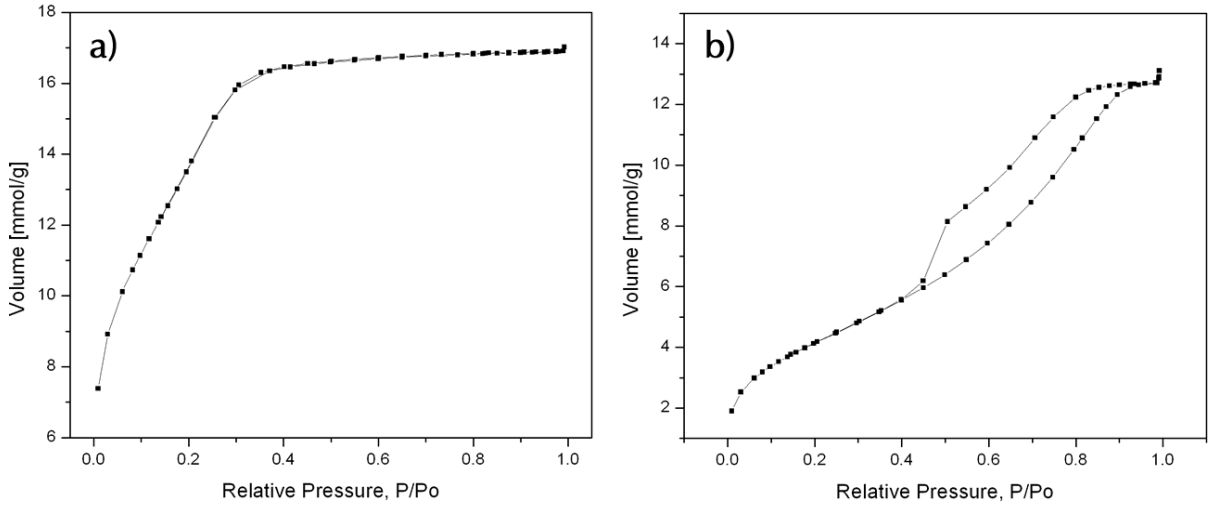

Figure 5-3: Nitrogen isotherm for the extracted MO prepared from a) TMOS and CTAB and b) BTSPA and CTAB.

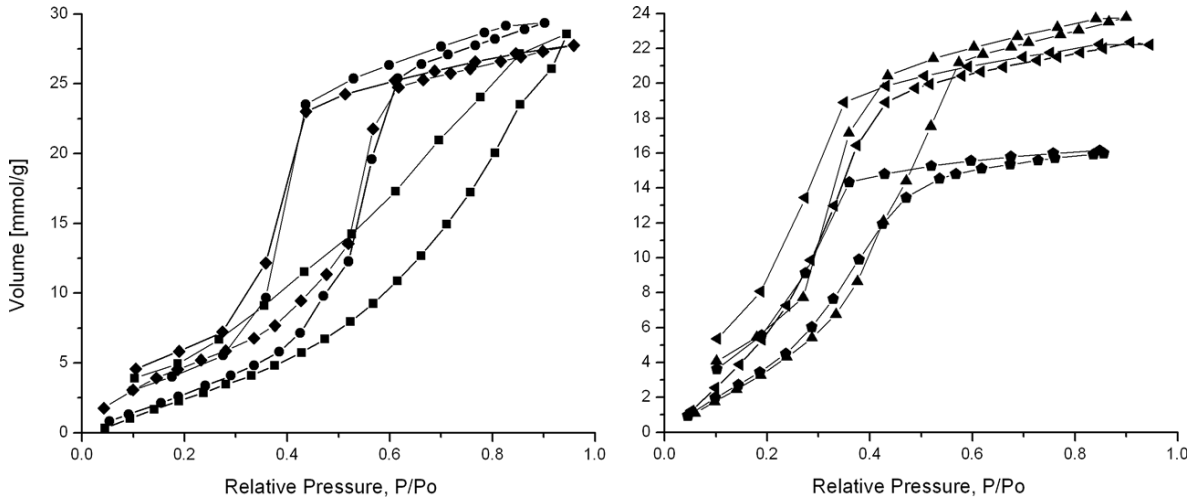

Figure 5-4: Water adsorption isotherms found for different precursors assembled around CTAB measured at 25 °C. TEOS: triangle left; TMOS: pentagons; BTSE: circles; BTSM: rhombs; BTSEE: triangle top; BTSPA: squares.

All values calculated from the nitrogen adsorption are given in Table 5-1. It can be seen that all materials exhibit a high BET surface area with a pore diameter around 2.2 nm calculated from the desorption branch of the isotherm and a high total pore volume.

The water adsorption isotherms measured at 25°C are shown in Figure 5-4. It can be seen that all but one adsorption branches have a type V shape. This comes from the weak interactions between the water vapor and the surface of the MO and is a first indication that the material is to some extent hydrophobic. However, there is capillary condensation taking place for higher pressures filling the mesopores. An exception is the adsorption branch of the material build with bis-propylamine bridging groups. This solid shows a type III branch indicating a different interaction with water. The desorption branch of all materials shows a hysteresis loop due to the mesopores in all but the BTSPA sample and a low pressure hysteresis is present in all samples. This non-closing of the desorption branch can have three explanations: re-hydroxylation of the siloxane bridges (meaning chemical adsorption of water) or physical changes in the adsorbed water as well as some swelling of the walls. The chemisorption is not likely for these materials since there is no calcination step, which would force the de-hydroxylation of the surface putting strain on the siloxane bonds. A physical change of water is most likely: layers of water molecules close to the surface on the hydrophilic patches will be unable to form hydrogen bonds or go into the preferred cage-like structure. If the pore is now filled completely with bulk water the layers close to the surface will undergo conformational changes and the water molecules will be incorporated into the hydrogen bonded network. These interconnected water molecules exhibit a higher surface tension than the one that formed the monolayer during adsorption. This leads to the parallel shift to higher volumes in the desorption branch when compared with the adsorption. In some parts of the material the surface tension is too big or the cavity too small to completely

remove all the water from the solid under low pressure and ambient temperature conditions. Also in some cases water can be incorporated into the walls and be trapped in them.

The hydrophobic behavior of these materials can be also seen in the BET values, which are generally much smaller then the ones measured with nitrogen, indicating that the capillary condensation takes place before a monolayer is formed. This can be explained assuming the specific interaction of water on surfaces that have hydrophilic and hydrophobic domains. Water will first adsorb on the clusters of silanol groups on the surface and after this it will preferably adsorb on the already bound molecules to form water clusters. These clusters will then grow to a point where they start touching the opposite surface and fill the pore diameter completely. From then on the two surfaces of the water will move filling the whole pore independently of the surface (Figure 5-1).[185] The slightly higher surface area for BTSPA can be explained by a swelling of the walls by water. The whole wall of this material contains amine groups, which can interact with water molecules through hydrogen bonding. The higher surface area in the MO prepared from TEOS is due to the size limitations of the water adsorption. Molecular water has a smaller surface area than nitrogen; however water will not be in a molecular state during the adsorption but instead in a clustered form. So it seems that for the quite small pores of the TEOS material (1.9 nm found from nitrogen adsorption) the analysis with water is not anymore possible. This limitation in the size of pores can also be seen in the total pore volumes of this series (Table 5-1). Taking the standard density of bulk water of 1.0 g/ml the calculated total pore volumes are the same within experimental error when comparing the values from nitrogen and water. Only for the purely inorganic samples the values for water are much smaller than the ones found for nitrogen again suggesting that the pores of these MOs are too small for a good analysis with water vapor.

Sample	Surfactant	surface area nitrogen S_{BET} [m^2/g]	pore diameter nitrogen adsorption [nm]	total pore volume nitrogen [cm^3/g]	surface area water S_{BET} [m^2/g]	total pore volume water [cm^3/g]	capillary condensation start at P/P_0
TEOS	CTAB	1101	1.9	0.59	1458	0.40	0.15
TMOS	CTAB	1117	1.9	0.59	442	0.29	0.18
BTSEE	CTAB	820	2.2	0.45	497	0.43	0.19
BTSE	CTAB	948	2.2	0.54	342	0.53	0.25
BTSM	CTAB	938	2.5	0.56	401	0.50	0.28
BTSPA	CTAB	346	3.5/5.8	0.44	401	0.52	0.34
TEOS	LiFOS	925	3.3	0.52	430	0.29	0.21
TMOS	LiFOS	964	3.3	0.56	472	0.41	0.24
BTSEE	LiFOS	654	3.3	0.41	285	0.36	0.31
BTSM	LiFOS	848	3.3	0.55	477	0.46	0.34
BTSPA	LiFOS	300	3.6	0.28	355	0.41	0.39
BTSE	LiFOS	444	3.8	0.37	205	0.38	0.42

Table 5-1: Values for nitrogen and water adsorption for the combination of different precursors with CTAB or LiFOS.

The point at which the capillary condensation starts can also be used for characterization, which is depended on the hydrophilicity of the surface and the pore diameter. A more hydrophilic surface will lead to a better spreading of the water on top of it and therefore the formation of water clusters and inner droplets will occur at much higher pressures, which in turn will lead to a delayed capillary condensation. The smaller the pore, the faster the water clusters formed around the hydrophilic patches will completely fill the diameter.

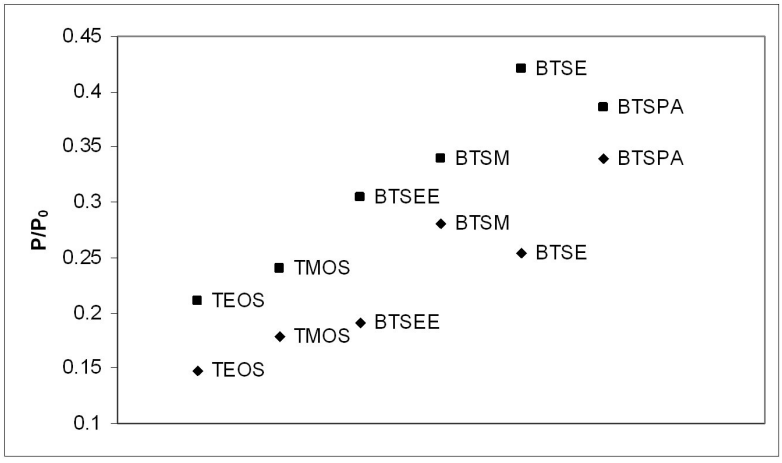

Figure 5-5: Relationship between the type of bridging organic group and the point of capillary condensation for MOs. Diamond: CTAB series; square: LiFOS series.

As can be seen from Table 5-1 as well as in Figure 5-5 there is an increase in the values for the starting points of capillary condensation in the following order TEOS<TMOS<BTSEE< BTSE<BTSM<BTSPA. This order is equivalent to the increase in pore diameter in these samples and can be purely explained by this effect. So considering this series alone the organic group has no direct influence on the hydrophilicity of the surface of a MO material found by water adsorption. It only indirectly influences the condensation with changing the packing parameters of the templating CTAB and with this the pore diameter of the extracted sample. As seen from the comparison of data found by two different surfactants below, there might however be a small influence of the organic. Only a material strongly interacting with water like BTSPA shows a differently shaped isotherm, which comes from the inclusion of water into the walls. In that case the values found cannot be due to the pore size of the material alone.

5.3 *The influence of the surfactant on a series of MO materials prepared from different precursors*

To check the influence of the surfactant the same precursors as mentioned above are assembled around LiFOS and water is adsorbed onto them at 25°C.

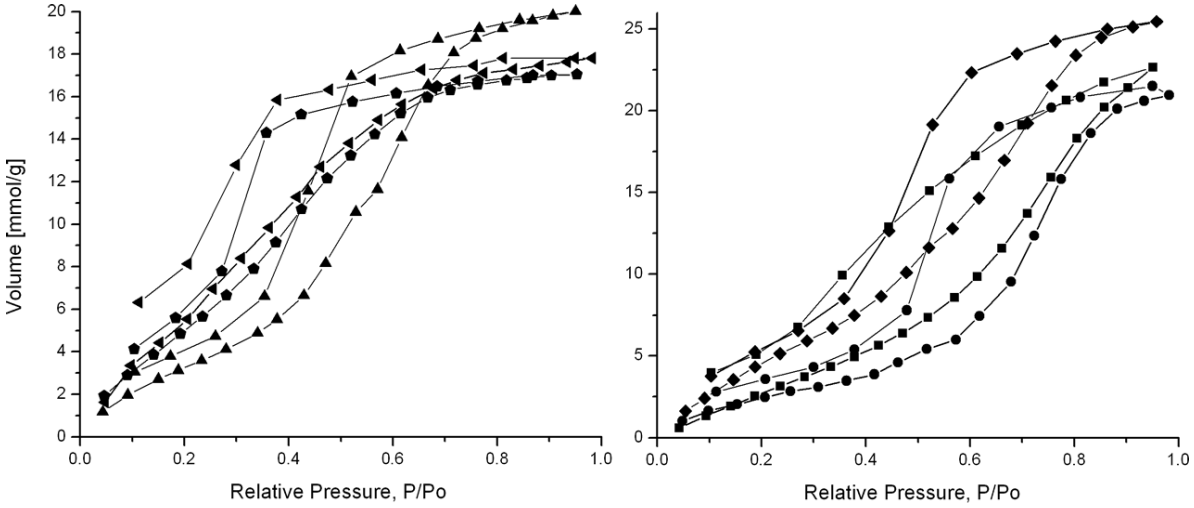

Figure 5-6: Water adsorption isotherms for different precursor assembled around LiFOS measured at 25 °C. TEOS: triangle left; TMOS: pentagons; BTSE: circles; BTSM: rhombs; BTSEE: triangle top; BTSPA: squares.

Here all isotherms show a type V adsorption branch and a capillary condensation step as well as a hysteresis loop in the desorption branch. Also all samples exhibit a low pressure hysteresis, which is again due to the conversion of the first adsorbed water layers into bulk water when the pores are completely filled. The hydrophilic surface areas are smaller then the ones found for nitrogen adsorption with the exception of the solid prepared from BTSPA, which again shows a higher hydrophilic area due to inclusion of water molecules into the walls. So in this case, the area found by BET is more a mixture of the hydrophilic patches on the surface as well as the probability of the walls to incorporate water. The total pore volumes for nitrogen and water are identical within the experimental errors showing a complete filling

of the MOs. Only in the case of BTSPA the value 0.41 cm^3/g for water and 0.28 cm^3/g for nitrogen is much higher, showing that more water is adsorbed into the material than there is pore volume. This excess water has to go into the walls. It can also be seen that the capillary condensation in this series is generally later than in the materials prepared with CTAB (Figure 5-5). This is first of all due to the bigger pore diameters in this series, which leads to a later change over from water droplets into void filling. However there are also changes in the order of the capillary condensation compared to the materials prepared by CTAB. Here the condensation value increases in the following order TEOS<TMOS<BTSEE<BTSM≈BTSPA <BTSE. The most interesting changes are the switch of BTSM and BTSE, which is coupled with a bigger pore size for the BTSE sample in the LiFOS series than the one of BTSM, and the quite low value for BTSPA. This can be explained with the ionic interaction between the anionic head group of the surfactant and the amine group in the precursor. Even so the fluorocarbon will repel the hydrocarbon chains in the precursor and the negatively charged head groups, which are on the surface of the micelles, are driving the organic function to the surface. This leads to a more hydrophobic material, which is showing earlier capillary condensation than a more hydrophilic material having the same pore diameter.

Comparing the materials with the same precursor but different surfactants with one another it can be seen that the difference in P/P_0 at the starting point of condensation for TEOS, TMOS and BTSM materials are the same and quite small. The higher values found in the case of LiFOS are due to the larger pore sizes and with this the later condensation of water in them. For BTSEE the difference between CTAB and LiFOS surfactant is slightly higher than the pure inorganic solids. This can be explained first of all with the larger pore diameter, but also with the different interactions of the surfactants with the precursors. CTAB with its hydrocarbon chain is interacting attractively with the hydrocarbons of the bridging group and therefore allowing them on the surface. This makes the material more hydrophobic and thus

forces water into cluster formation leading to an early capillary condensation. The fluorocarbon chain of the LiFOS surfactant instead repels the hydrocarbons into the wall interior and makes the surface more hydrophilic. So water can cover more surface area and the capillary condensation takes place at a later relative pressure. This effect can be seen even more strongly in the BTSE mesoporous organosilica, because the bridging group is more flexible then the one mentioned before and it can therefore be more easily drawn to the surface by CTAB or pushed into the wall by LiFOS. This higher flexibility can also lead to a better condensation of the silanol groups, because they can more easily achieve the right conformation for tetrahedral network formation. BTSPA again is an exception showing a small difference in capillary condensation with changing surfactants. This can be explained by the inclusion of water into the walls. Both compounds are formed with pure organic precursor and therefore contain the same amount of amine groups in the material so that the same amount of water can be incorporated into them. The slightly higher value for LiFOS is, as explained above, due to the interaction of the anionic head group and the basic amine function.

5.4 The influence of mixing two precursors on the hydrophilicity of a MO as well as the influence of the "all-in-one" method compared to usual templating

After analyzing the influence of different precursors on the hydrophilicity a closer look is taken into the mixing of two precursors at different concentrations with respect to the hydrophilicity of MOs. For this study BTSPA is chosen as precursor, because it did show this interesting behavior of water incorporation in the walls and the functional group can be directed to the surface with the "all-in-one" method. TEOS is taken as a second precursor, because it contains no organic group. CTAB and CF are used as surfactants, since the first has

no influence on the position of the organic group and the second will drive the amine function to the wall surface due to ionic interactions.

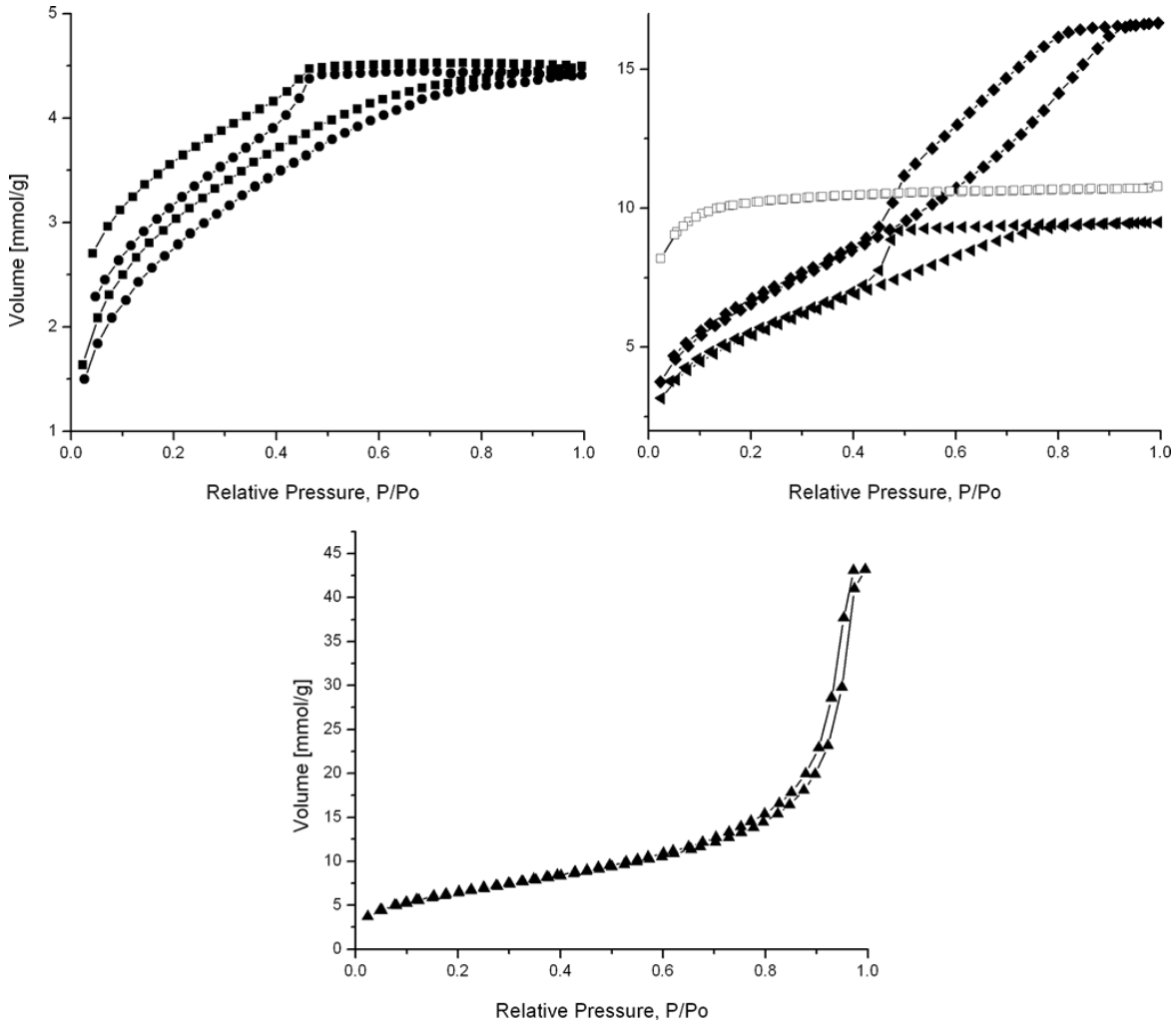

Figure 5-7: Nitrogen adsorption spectra of MOs from BTSPA and TEOS. CT100: squares; CT80: circle; CT60: triangle left; CT40: rhombs; CT20: triangle top; CT0: open squares.

In Figure 5-7 the nitrogen adsorption isotherms for the combination of BTSPA with TEOS and CTAB as surfactant are shown. As described in chapter 4.4 these materials exhibit interesting mechanical behavior of the walls due to the long bridging group with its flexibility. This can be seen from the low pressure hysteresis in nitrogen adsorption for high concentrations of organic precursor. In these solids nitrogen is incorporated into the walls and they are deformed at high nitrogen pressures trapping the gas in the material. This also leads

to low total uptakes and with this to small total pore volumes (Table 5-2). Standard type IV isotherms with closing hysteresis loops and reasonable high total pore volumes can be found by increasing the amount of TEOS and with further increase bimodal systems and then macroporous materials will be seen, until for pure TEOS the material goes back to the type IV isotherm type.

sample	surfactant /% amine in MO	pore diameter [nm]	surface area nitrogen S_{BET} [m^2/g]	total pore volume nitrogen adsorption [cm^3/g]	surface area water S_{BET} [m^2/g]	total pore volume water adsorption [cm^3/g]	capillary condensation start at P/P_0
CT100	CTAB/100	3.5	251	0.15	1430	0.16	0.472
CT80	CTAB/80	3.6	232	0.15	242	0.20	0.519
CT60	CTAB/60	3.7	444	0.33	358	0.29	0.469
CT40	CTAB/40	3.9	541	0.57	234	0.53	0.438
CT20	CTAB/20	3.8/35.7	528	1.48	173	0.49	0.473
CT0	CTAB/0	1.2	846	0.34	955	0.21	0.114
CF100	CF/100		26	0.02	293	0.18	0.483
CF80	CF/80	few 3.1	326	0.16	228	0.15	0.414
CF60	CF/60	3.4	403	0.23	392	0.28	0.370
CF40	CF/40	3.6	568	0.37	404	0.34	0.363
CF20	CF/20	3.9/5.4	445	0.44	198	0.28	0.420
CF0	CF/0	3.6/18.9	274	0.41	207	0.16	0.559

Table 5-2: Water and nitrogen adsorption values for the combinations of BTSPA and TEOS with CTAB or CF as surfactant.

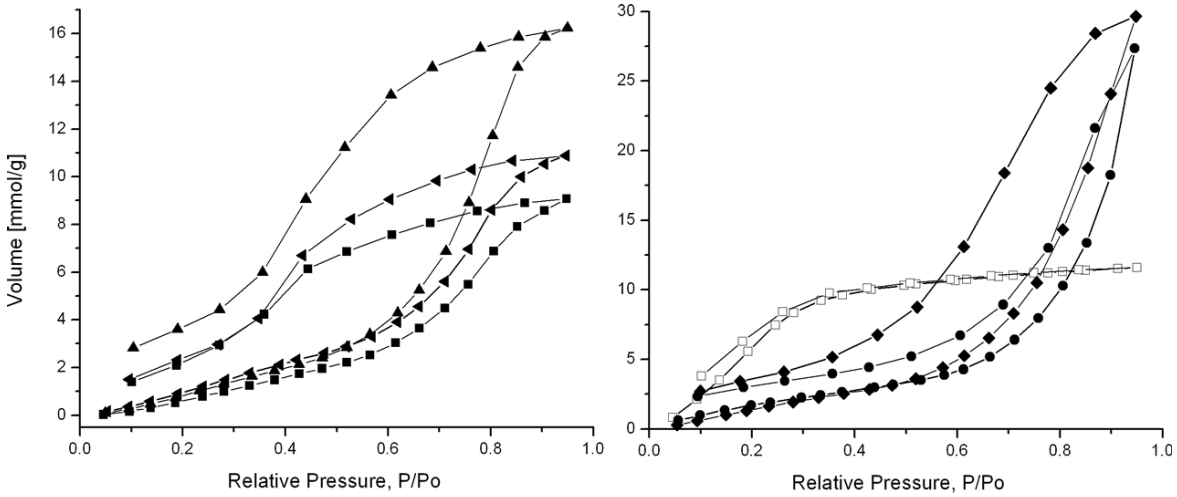

Figure 5-8: Water adsorption isotherms from BTSPA, TEOS and CTAB measured at 25 °C. CT100: squares; CT80: circle; CT60: triangle left; CT40: rhombs; CT20: triangle top; CT0: open squares.

For water adsorption on these MOs the isotherms all show a type V shape characteristic of hydrophobic materials. However the form of the hysteresis loop for high concentrations of BTSPA is completely different from all the others seen before. The shifts between the relative

pressures for the adsorption branch and the desorption one are much bigger. This cannot only be due to the change from surface water to bulk water with its increase in surface tension at high relative pressures. As already seen in the nitrogen adsorption of these samples and the water adsorption of the two pure BTSPA samples described above, this material is able to incorporate nitrogen and more so water vapor into the walls. This is what happens here as well, water goes into the walls spreading the organic groups further apart, so that more water can be adsorbed than expected from the pure pore volume or diameter. As the amount of TEOS increases the hysteresis is closing till at 20% of amine when it comes back to the size corresponding to conversion of water molecules into bulk water. The isotherm for the pure inorganic compound is different from the one prepared with TEOS in the above series. This shows again that the series are only partially comparable as well as the limitation of the model of water vapor analysis for small pore diameter materials.

All organosilicas in this series have about the same pore diameter, so that in this case differences in the BET area, total pore volume and capillary condensation point cannot be due to size effects. The BET areas for CT100 and CT80 from water adsorption are bigger than the ones found from nitrogen, which is due to the incorporation of water molecules into the wall. So this area is more a value for the inclusion of water into the walls. The value is especially high for the purely organic containing MO, which shows the highest flexibility of the walls. For the intermediate combinations the surface areas are smaller than the ones found in nitrogen, measuring only the hydrophilic surface. The value found for pure TEOS is higher for water, which is physically impossible and again shows the limits of water adsorption as an analytical tool.

The total uptake in molecules and the total pore volume increase from CT100 till CT40 and then decreases again to CT0. This is due to the higher surfaces of the mixed solids as well as the flexibility of the walls. For high organic content the walls are the most flexible ones,

however the overall pore volume is quite small. With increasing amount of TEOS the total pore volume increases leading to more surface area, but at the same time the wall gets less flexible making the incorporation of water harder. At the point of 80% TEOS in the material the walls are glassy as in a "normal" PMO materials and no water can enter them. Even if this material has the highest uptake and the largest total pore volume in nitrogen the values for water are quite small because the walls show none of the interesting mechanical behavior and a bigger pore system which might not fill completely.

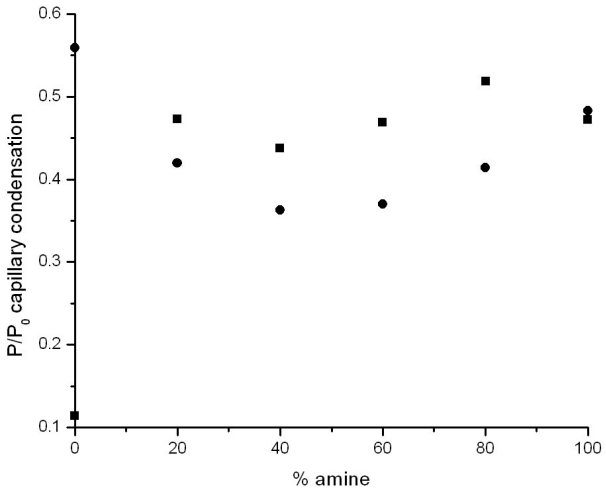

Figure 5-9: Points of capillary condensation for BTSPA assembled around different surfactants. Squares: CTAB, circles: LiFOS.

There are no big differences in the starting points of the capillary condensation for all the MOs containing organic function in this series (Figure 5-9) (with TEOS being an exception for the described reasons). With all solids having approximately the same pore diameter, the small variation of the values can be explained with their hydrophilicity and probability to incorporate water. CT80 has the highest relative pressure for condensation, because of its probability to incorporate water molecules into the framework. CT100 and CT60 have the same values, which are slightly smaller. This is due to the high flexibility of the walls in CT100 with its low porosity and the lower flexibility but higher porosity of CT60. CT40

cannot include water into the walls any more and therefore the condensation point is earlier. The slightly higher value for CT20 comes from the bigger pores, which have a later jump over point for the inner water droplets.

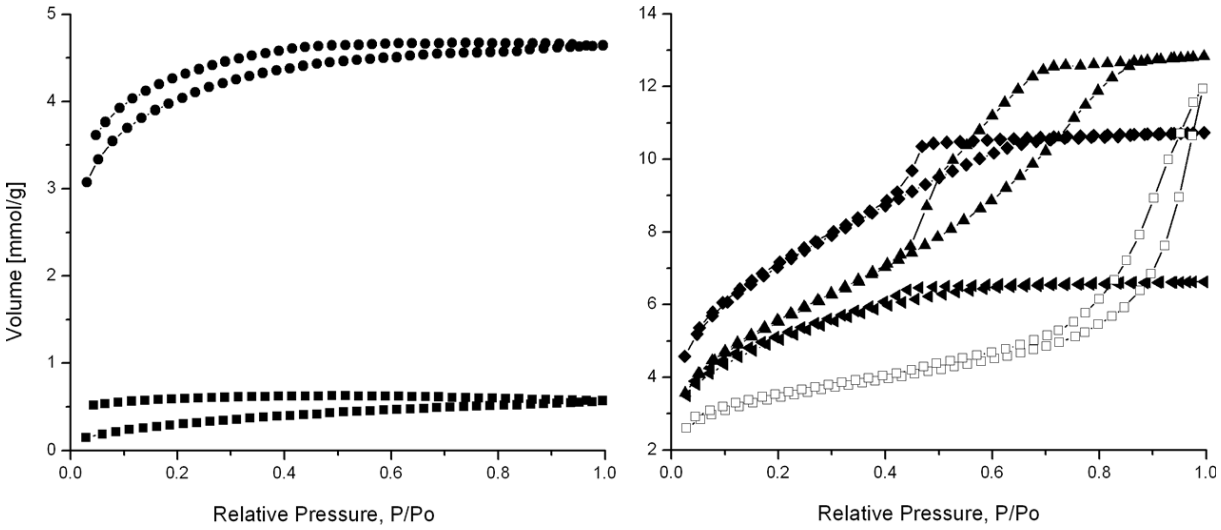

Figure 5-10: Nitrogen adsorption spectra of MOs from BTSPA, CF and TEOS. CF100: squares; CF75: circle; CF60: triangle left; CF40: rhombs; CF20: triangle top; CF0: open squares.

For BTSPA and TEOS assembled around CF the nitrogen isotherms are shown in Figure 5-10. As described in chapter 1 they exhibit interesting mechanical behavior like the materials assembled around CTAB. For high organic content the walls are flexible and nitrogen swells the walls and deforms the pore system and is trapped in the solid. By increasing the inorganic fraction the materials become glassier and even phase separate leading to type IV isotherms for CF60 and CF40 and mixed mesoporous systems for the lowest concentrations of organic function.

The special feature of the combination with BTSPA and CF is that the acidic group of the surfactant interacts with the amine function of the precursor in the “all-in-one” fashion. This drives the organic functions to the surface and makes them more accessible from the pore space.

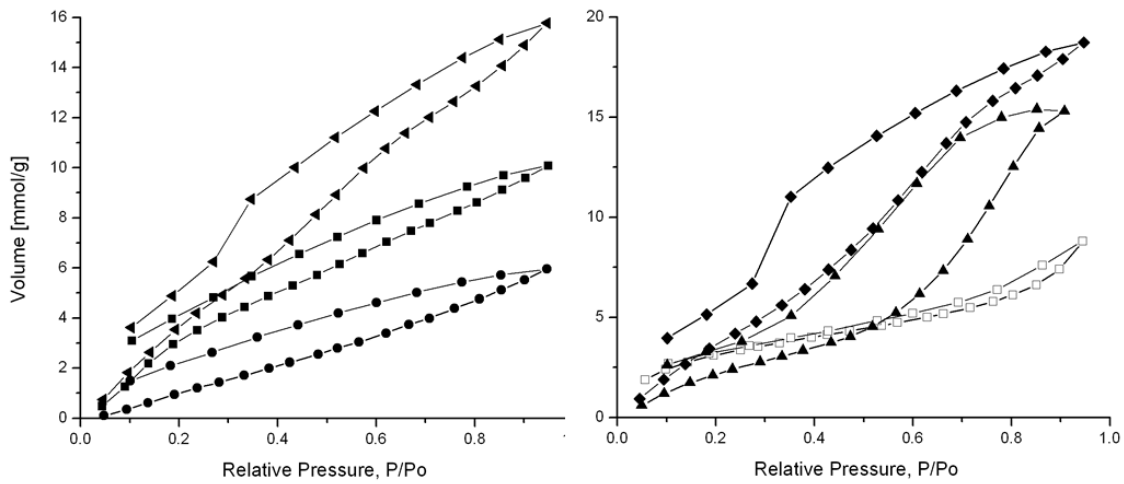

Figure 5-11: Water adsorption isotherms from BTSPA, TEOS and CF measured at 25 °C. CF100: squares; CF75: circle; CF60: triangle left; CF40: rhombs; CF20: triangle top; CF0: open squares.

The isotherms found from water adsorption (Figure 5-11) all show type IV shape for more hydrophilic materials with low pressure hysteresis. This is due to the amine function, which in this case is on the surface of the material and leads to more hydrophilic areas, so that more water can be incorporated into pores at low relative pressures. CF100 and CF80 show featureless adsorption branches with no real capillary condensation steps, which is due to the low porosities and the incorporation of some water into the walls of these materials. For CF60 to CF20 the isotherms show capillary condensation and a shift between adsorption and desorption coming from the conversion of surface water to bulk water at high pressures. For the purely inorganic compound the isotherm shows late capillary condensation and near-closing of the desorption branch onto the adsorption branch, which can be explained by the larger pore structure of CF0. The generally smaller shifts between the branches compared to the materials prepared by CTAB are due to the position of the amine functions. In the CF materials the organic functions are brought to the surface of the pore walls and so there is no large driving force for water to go into the walls, whereas in the series assembled around CTAB the amine is homogenously distributed in the material and water is more prone to diffuse into the walls.

The surface area found for the highest concentration of organic in the MOs is bigger then the ones seen in nitrogen adsorption (Table 5-2). This comes from the specific interaction with water. Since it will adsorb only on the hydrophilic patches of the material the pores will be filled with droplets and therefore the walls cannot deform as much as in nitrogen adsorption experiments and also some water molecules will be incorporated into the walls. For all the other samples the surface area found from water is smaller than the one from nitrogen and corresponds to the pure hydrophilic surface.

The total pore volume for the pure amine containing MO is bigger for water than the one found from nitrogen. which can be explained again with the deformation of the walls and some water incorporation (Table 5-2). For CF80 to CF40 the total pore volume is the same for water and nitrogen indicating a complete filling of the pores. CF20 and CF0 show a smaller total uptake, which is due to a very high capillary condensation point because of the bigger pores and an incomplete filling of them. Since nitrogen adsorbs on the whole surface from the beginning and than adds, layer-by-layer, over the whole material the total pore volume seems bigger than in the case of water, which forms isolated droplets that are not able to fuse due to the high distance between opposite walls in the bigger pores.

For the capillary condensation points (Table 5-2 and Figure 5-9) again a trend with changing composition can be seen. For the two lowest concentrations of organic precursor the values for the condensation step are high, due to the larger pores with their later change from inner water droplets to bulk water. CF40 and CF60 show identical relative pressures for the condensation even though the pore diameter for CF60 is slightly smaller and so an earlier start would be expected. However, in this material not only the size but also the flexibility of the walls matters, which increases with higher organic content interfering with the nitrogen adsorption and may be giving too small values, e.g. for the pore diameter. With a further increase in organic precursor the capillary condensation is even later. This can be explained

with some inclusion of water into the walls. Even so, the shape of the isotherms suggests no high amount of inclusion and some water might get into the walls for high concentrations of amine functions. In the case of CF80 and CF100 the concentration of amine groups is much higher than that of the acidic groups of the surfactant, so that not all of the amine functions are on the wall surface. Even a very high concentration of amines on the surface would likely not prevent water to squeeze through the flexible hydrocarbon chains to reach the amine groups inside the walls. The general earlier capillary condensation of the CF materials when compared to the CTAB ones can again be explained with the "all-in-one" interaction between the CF surfactant and the precursor. The acid group forms ion-pair bonds with the amine bringing it closer to the surface making it more hydrophilic. However, the amine is bound to long hydrocarbon chains, which are hydrophobic. These are also forced to the surface leading to fewer hydrophilic patches on it. Fewer internal droplets will form, which are then increasing in size more rapidly with increasing relative pressure and the capillary condensation will occur earlier.

5.5 Conclusion

Water adsorption is an interesting method for the analysis of mesoporous organosilica materials however, the data so-obtained are not easy to interpret. There are always different factors influencing the behavior of water on surfaces of organo-silicas: the amount of hydrophilic interaction sites and the positions and type of organic groups. However, in a porous material there are also purely structural factors like the diameter of the pore and the mechanical behavior of the walls, which can sensitively influence the structure of the isotherms and the values that can be calculated from them. Nevertheless it is possible to see that the amount of organic has little influence on the total uptake of water into the materials

and differences in behavior can be seen only as relative pressure differences around the capillary condensation point. The more a precursor increases the pore size the later water will start condensing in the pores. An influence of the precursor is also present because for longer and more flexible hydrocarbon chains a perfluorinated surfactant will tend to push the organic into the walls making the surface more hydrophilic. For flexible precursors with functional groups that can interact with water the adsorption depends on the behavior of the wall, the pore diameter and the position of the functional group. Only in this special case a direct influence of the precursor is found.

All the differences in the analyzed samples are much smaller than the ones seen for organosilicas in which the functional group has been grafted onto the surface.[187-189] These differences arise because the organic group, which is attached in a post-synthetic way, is definitely on the wall surface as well as blocking the silanol groups, whereas organics from a bridged precursor can be hidden in the walls without hampering the access of water to the surface silanol groups.

6 Summary and future work

The primary objective of this work was the preparation of new functional MO materials their characterization, including novel techniques like quantitative X-ray scattering or water vapor adsorption.

In chapter 4.2 the fabrication of amine functionalized mesoporous materials with high surface areas as well as narrow pore size distributions was described. The materials were prepared from silsesquioxane surfactant precursors, which direct the functional groups to the surface by a novel “all-in-one” synthesis method. In contrast with the usual chemical strategy of mixing a precursor with a template, so very typical of many mesoporous materials preparations, we synthesized and used bridged hydrolizable precursors having surfactant-like behavior. In this way the function embedded in the bridge of the precursor is forced to hydrolyze at the surface of the walls. The following cleavage of the covalent bond between the hydrophobic chain and the condensed hydrophilic head enables the extraction of the template to give mesoporous materials with controllably functionalized surface. Beside the obvious advantage of having the functionality right at the chemically accessible pore wall surface, this approach also decreases the amount of functional precursor needed in the preparation. As well as the conversion of the as-synthesized “all-in-one” MO to an amine functionality during the extraction process other functional groups can be incorporated into these organosilica materials through straightforward reactions. The analysis of the MO product using copper coordination demonstrates spatial and chemical accessibility of the amine groups.

Amine functions have the advantage of being versatile starting groups for a large library of other reactions. Future work on these amine functionalized MOs can focus on solid state reactions of primary amine groups to create materials with hydrophobic or fluorophobic

surfaces as well as anchored metal complexes for catalysis, sensing and separations. Reactions of this genre could be combined with grafting of terminal silsesquioxane precursors to give bi-functional pore surfaces. By exploiting reactivity differences of surface amine and silanol groups such functionalization might be achievable in “one-pot” reactions.

Another direction for future work could be to vary the mesopore size. So far only a single kind of silsesquioxane surfactant precursor has been used, giving a pore size of 3.9 nm. Through the use of different hydroboration agents as well as other double bond containing molecules the pore size of these “all-in-one” MOs could be dramatically enlarged. First of all there is the possibility to use longer 1-en hydrocarbons, but also polymers or naturally occurring compounds with terminally double-bounds could be used.

In chapter 4.3 a similar preparation method to the one described in chapter 4.2 has been used to form mesoporous hybrid materials with chiral amine functions on the pore surface. These materials also have a high surface area and display efficient coordination to added copper ions. The chirality of the surface was demonstrated with ITC and HPLC measurements, which indicated a substantial difference in the heat of interaction between two enantiomers devoid of non-specific interactions with primary amines and the possibility to separate a racemic solution on the MO, respectively.

As well as the experiments described for the non-chiral amine MO more tests need to be performed on the separation of mixtures of racemates using “all-in-one” MOs with different functional groups to discover the strengths and weakness of this new class of materials for chiral separations and catalysis.

In chapter 4.4 ion-pair interactions have been used to create secondary amine MO with the amine functionality on the pore surface. Since the bridge-bonded group in the precursor is quite long and flexible the solids so-formed exhibit interesting macroscopic mechanical behavior with distinctive properties to those of the “typical” PMOs. In particular, this can be

seen by the incorporation of nitrogen and water into the pore wall in an adsorption experiment. Also the nature of the surfactant template influences the location of the functional group in the MO, when assembling precursors around CTAB and then CF in the “all-in-one” fashion. The latter combination leads to much higher accessibility of the amine groups in the pores, seen by copper ion adsorption.

In future work is will be important to measure the mechanical properties of a wide range of flexible MOs using nano-indentation. A notable advantage of the ion-pair interaction compared to the covalent bonding one described in chapter 4.2 and 4.3 is that the amount of surfactant can be reduced with respect to the functional groups to a value below unity plus the fact that the functional group is already present in the precursor. This gives the chance to react the amine further during the condensation procedure. For example a short chain perfluorinated carboxylic acid could be used in combination with a perfluorinated non-carboxylic acid. The solid product can than be heated to 100ºC or more to transform the ion-pair bond to an amide group. The longer chain non-carboxylic acid is then extracted to give a fluorophobic MO material in one step.

Such materials could be used as stationary phases in chromatography or as storage materials for gaseous materials providing they behave towards them in a similar way as they do towards nitrogen and water.

In chapter 5 water adsorption was described as an analytical tool for defining the hydrophilicity of surfaces. Different organic groups were incorporated into PMOs and their influence on the pore surface properties was checked. It could be seen that short non-interacting organic groups have no direct influence on the total uptake of water, but they shift the point of capillary condensation to higher relative pressures because of the increase in pore size and the amount of water needed for pore filling. Only for longer more flexible chains the surfactant can influence the behavior of water in the pores. A perfluorinated surfactant will

repel hydrocarbon groups, which will be incorporated into the walls and therefore are not found so much on the wall surface. This makes these materials more hydrophilic.

The largest influence on water vapor was seen with a flexible hydrogen bonding precursor. Here the amount of organic function as well as its location in the pore wall has an influence on its water adsorption. It can be seen that water can penetrate the walls of these MOs at higher pressures and the materials start to swell.

In future work better care has to be taken to ensure all the pores in the MOs that are analyzed have exactly the same diameter to eliminate the influence of size differences on the adsorption of water. Also the concentration of surface hydroxyl groups needs to be considered, since the number and location of surface silanol groups is expected to influence the mechanism of water adsorption and the structure of confined water molecules.

Also larger and more hydrophobic bridging groups like benzyl or phenyl should be included into PMOs and used for water adsorption measurements. As well, some low dielectric constant PMO materials, like the ones synthesized be Ozin *et al.*,[190, 191] which show a temperature induced switch of bridging methene to terminal methyl groups with a concomitant increase in the resistance to water adsorption, need to be investigated in detail.

7 Appendices

7.1 Instruments

Adsorption measurements

The nitrogen adsorption measurements are done on either a Tristar3000 from MicroMeritics or an Autosorb1 from Quantachrome. All samples are out-gassed at 150ºC under vacuum and the measurements are done at liquid nitrogen temperature. The data analysis is done with the instrument software.

Water adsorption measurements are taken on a Hydrosorb from Quantachrome. The samples are out-gassed at 150ºC under vacuum and the measurements are done at 25ºC in water.

Transmission electron microscopy (TEM)

TEM analysis is done on an electron microscope Omega 912 from Carl Zeiss with an acceleration speed of 120 kV. The samples are prepared through grinding the solid in acetone and giving one drop onto a carbon coated copper grid.

Small angle x-ray scattering

The measurements are either done with a Kratky camera or with a Nonius rotating anode *(U* = 40 kV, *I* = 100 mA, λ = 0.154 nm) using image plates. With the image plates placed at a distance of 40 cm from the sample, a scattering vector range of s = 0.07-1.6 nm^{-1} was available. 2D diffraction patterns were trans-formed into 1D radial averages. The data noise

was calculated according to Poisson statistics, which is a valid approach for scattering experiments.

Nuclear magnetic resonance (NMR)

Solution NMR spectra are taken on a Bruker Avance DPX 400 spectrometer. The solid state measurements are done on a Bruker DSX 400 spectrometer.

Circular dichroism (CD)

Circular dichroism spectra are taken on a Jasco J715 instrument.

HPLC analysis

HPLC analysis is done on a Shimadzu LC-10AD system with a SPD-10AD UV/VIS detector from the same company and a Jasco AS-950 auto-sampler under the in chapter 4.3.4 described conditions.

7.2 Chemicals used

All starting materials and solvents are commercially available and are used without further purification. The preparation methods for the precursors are described in the respective chapters.

7.3 Abbreviations

α	separation on HPLC
BET	Brunauer-Emmet-Teller
AAS	atomic adsorption spectroscopy
BJH	Barrett-Joyer-Halenda
BTSE	bis(triethoxysilyl)ethane

BTSEE	bis(triethoxysilyl)ethene
BTSM	bis(triethoxysilyl)methane
BTSPA	bis(triethoxysilylpropyl)amine
BTSPEA	bis(triethoxysilylpropyl)ethyldiamine
c	concentration
CD	circular dichroism
CF	pentadecafluorooctanonic acid
CFx	CF preparation with x% of amine groups
CLD	cord-length distribution
cmc	critical micelle concentration
CSP	chiral stationary phase
CTAB	cetyltrimethylammonium bromide
CTAC	cetyltrimethylammonium chloride
CTx	CTAB preparation with x% of amine groups
ΔH	calorimetric enthalpy change
HPLC	high pressure liquid chromatography
$IpcBH_2$	monoisopinocampheylborane
ITC	isothermal titration calorimetry
K_B	equilibrium binding constant
λ	wavelength
LC	liquid crystalline
LiFOS	heptadecafluorooctanoic sulfonic acid salt
l_P	Porod-length
NMR	nuclear magneton resonance
PMO	periodic mesoporous silica
T	temperature
TEM	trans electron micrsocopy
TEOS	tetraethoxysilane
THF	tetrahydrofuran
TMOS	tetramethoxysilane
V_{Pore}	total pore volume

8 Literature

[1] J. S. Beck, J. C. Vartuli, W. J. Roth, M. E. Leonowicz, C. T. Kresge, K. D. Schmitt, C. T. W. Chu, D. H. Olson, E. W. Sheppard, S. B. McCullen, J. B. Higgins, J. L. Schlenker, in *Journal of the American Chemical Society, Vol. 114*, **1992**, pp. 10834.

[2] S. Polarz, M. Antonietti, *Chemical Communications (Cambridge, United Kingdom)* **2002**, 2593.

[3] B. Smarsly, S. Polarz, M. Antonietti, *Journal of Physical Chemistry B* **2001**, *105*, 10473.

[4] A. Thomas, H. Schlaad, B. Smarsly, M. Antonietti, *Langmuir* **2003**, *19*, 4455.

[5] C. G. Goltner, B. Berton, E. Kramer, M. Antonietti, *Advanced Materials (Weinheim, Germany)* **1999**, *11*, 395.

[6] D. Zhao, J. Feng, Q. Huo, N. Melosh, G. H. Frederickson, B. F. Chmelka, G. D. Stucky, *Science (Washington, D. C.)* **1998**, *279*, 548.

[7] A. Stein, in *Microporous and Mesoporous Materials, Vol. 44*, **2001**, pp. 227.

[8] Y. Zhou, S. H. Yu, A. Thomas, B. H. Han, *Chemical Communications* **2003**, 262.

[9] S. M. Yang, N. Coombs, G. A. Ozin, *Advanced Materials (Weinheim, Germany)* **2000**, *12*, 1940.

[10] T. Asefa, M. J. MacLachan, N. Coombs, G. A. Ozin, in *Nature, Vol. 402*, **1999**, pp. 867.

[11] T. Asefa, M. Kruk, M. J. MacLachlan, N. Coombs, H. Grondey, M. Jaroniec, G. A. Ozin, *Journal of the American Chemical Society* **2001**, *123*, 8520.

[12] K. Z. Hossain, L. Mercier, *Advanced Materials* **2002**, *14*, 1053.

[13] S. Inagaki, S. Guan, T. Ohsuna, O. Terasaki, *Nature (London, United Kingdom)* **2002**, *416*, 304.

[14] H. Hata, S. Saeki, T. Kimura, Y. Sugahara, K. Kuroda, *Chemistry of Materials* **1999**, *11*, 1110.

[15] D. Y. Zhao, P. D. Yang, Q. S. Huo, B. F. Chmelka, G. D. Stucky, *Current Opinion in Solid State & Materials Science* **1998**, *3*, 111.

[16] B. L. Newalkar, N. V. Choudary, P. Kumar, S. Komarneni, T. S. G. Bhat, *Chemistry of Materials* **2002**, *14*, 304.

[17] R. I. Nooney, E. Maginn, D. Moore, *Abstracts of Papers of the American Chemical Society* **2000**, *219*, U321.

[18] S. V. Mattigod, X. D. Feng, G. E. Fryxell, J. Liu, M. L. Gong, *Separation Science and Technology* **1999**, *34*, 2329.

[19] J. Liu, X. Feng, G. E. Fryxell, X. Chen, M. Gong, L. Wang, K. M. Kemner, *Abstracts of Papers of the American Chemical Society* **1997**, *214*, 344.

[20] L. Mercier, T. J. Pinnavaia, *Advanced Materials* **1997**, *9*, 500.

[21] J. Y. Ying, C. P. Mehnert, M. S. Wong, *Angewandte Chemie-International Edition* **1999**, *38*, 56.

[22] L. Bois, A. Bonhomme, A. Ribes, B. Pais, G. Raffin, F. Tessier, *Colloids and Surfaces a-Physicochemical and Engineering Aspects* **2003**, *221*, 221.

[23] A. Sayari, S. Hamoudi, Y. Yang, *Chemistry of Materials* **2005**, *17*, 212.

[24] X. S. Zhao, G. Q. Lu, in *Journal of Physical Chemistry B, Vol. 102*, **1998**, pp. 1556.

[25] J. P. G. Pater, P. A. Jacobs, J. A. Martens, *Journal of Catalysis* **1999**, *184*, 262.

[26] M. S. Morey, A. Davidson, G. D. Stucky, *Journal of Porous Materials* **1998**, *5*, 195.

[27] E. Armengol, A. Corma, H. Garcia, J. Primo, *Applied Catalysis a-General* **1995**, *126*, 391.
[28] E. A. Gunnewegh, S. S. Gopie, H. vanBekkum, *Journal of Molecular Catalysis a-Chemical* **1996**, *106*, 151.
[29] K. R. Kloestra, J. C. Jensen, H. Vanbekkum, *Abstracts of Papers of the American Chemical Society* **1996**, *211*, 68.
[30] H. Vanbekkum, A. J. Hoefnagel, M. A. Vankoten, E. A. Gunnewegh, A. H. G. Vogt, H. W. Kouwenhoven, in *Zeolites and Microporous Crystals, Vol. 83*, ELSEVIER SCIENCE PUBL B V, Amsterdam, **1994**, pp. 379.
[31] E. Armengol, A. Corma, L. Fernandez, H. Garcia, J. Primo, *Applied Catalysis a-General* **1997**, *158*, 323.
[32] E. Armengol, A. Corma, H. Garcia, J. Primo, *Applied Catalysis a-General* **1997**, *149*, 411.
[33] J. S. Beck, J. C. Vartuli, W. J. Roth, M. E. Leonowicz, C. T. Kresge, K. D. Schmitt, C. T. W. Chu, D. H. Olson, E. W. Sheppard, S. B. McCullen, J. B. Higgins, J. L. Schlenker, *Journal of the American Chemical Society* **1992**, *114*, 10834.
[34] J. H. Clark, J. C. Ross, D. J. Macquarrie, S. J. Barlow, T. W. Bastock, *Chemical Communications* **1997**, 1203.
[35] M. A. Marshall, H. A. Mottola, *Analytical Chemistry* **1983**, *55*, 2089.
[36] P. M. Price, J. H. Clark, D. J. Macquarrie, in *Journal of the Chemical Society-Dalton Transactions*, **2000**, pp. 101.
[37] A. J. Butterworth, J. H. Clark, P. H. Walton, S. J. Barlow, *Chemical Communications* **1996**, 1859.
[38] D. Brunel, N. Bellocq, P. Sutra, A. Cauvel, M. Lasperas, P. Moreau, F. Di Renzo, A. Galarneau, F. Fajula, *Coordination Chemistry Reviews* **1998**, *180*, 1085.
[39] M. Lasperas, N. Bellocq, D. Brunel, P. Moreau, *Tetrahedron-Asymmetry* **1998**, *9*, 3053.
[40] T. Maschmeyer, F. Rey, G. Sankar, J. M. Thomas, *Nature* **1995**, *378*, 159.
[41] G. A. Ozin, E. Chomski, D. Khushalani, M. J. MacLachlan, *Current Opinion in Colloid & Interface Science* **1998**, *3*, 181.
[42] K. Moller, T. Bein, *Chemistry of Materials* **1998**, *10*, 2950.
[43] S. L. Burkett, S. D. Sims, S. Mann, *Chemical Communications* **1996**, 1367.
[44] M. Koya, H. Nakajima, in *Mesoporous Molecular Sieves 1998, Vol. 117*, ELSEVIER SCIENCE PUBL B V, Amsterdam, **1998**, pp. 243.
[45] M. H. Lim, C. F. Blanford, A. Stein, *Journal of the American Chemical Society* **1997**, *119*, 4090.
[46] R. J. P. Corriu, A. Mehdi, C. Reye, C. Thieuleux, in *Chemical Communications*, **2002**, pp. 1382.
[47] C. H. Lee, S. S. Park, S. J. Choe, D. H. Park, in *Microporous and Mesoporous Materials, Vol. 46*, **2001**, pp. 257.
[48] M. Alvaro, M. Benitez, D. Das, B. Ferrer, H. Garcia, *Chemistry of Materials* **2004**, *16*, 2222.
[49] M. C. Burleigh, M. A. Markowitz, M. S. Spector, B. P. Gaber, *Journal of Physical Chemistry B* **2001**, *105*, 9935.
[50] M. J. MacLachlan, T. Asefa, G. A. Ozin, *Chemistry-a European Journal* **2000**, *6*, 2507.
[51] T. Asefa, M. J. MacLachan, N. Coombs, G. A. Ozin, *Nature* **1999**, *402*, 867.
[52] S. Inagaki, S. Guan, Y. Fukushima, T. Ohsuna, O. Terasaki, *Journal of the American Chemical Society* **1999**, *121*, 9611.

[53] C. Yoshina-Ishii, T. Asefa, N. Coombs, M. J. MacLachlan, G. A. Ozin, *Chemical Communications* **1999**, 2539.
[54] T. Asefa, C. Yoshina-Ishii, M. J. MacLachlan, G. A. Ozin, *Journal of Materials Chemistry* **2000**, *10*, 1751.
[55] B. J. Melde, B. T. Holland, C. F. Blanford, A. Stein, *Chemistry of Materials* **1999**, *11*, 3302.
[56] W. J. Hunks, G. A. Ozin, *Chemistry of Materials* **2004**, *16*, 5465.
[57] W. J. Hunks, G. A. Ozin, *Chemical Communications (Cambridge, United Kingdom)* **2004**, 2426.
[58] H. Fan, Y. Lu, A. Stump, S. T. Reed, T. Baer, R. Schunk, V. Perez-Luna, G. P. Lopez, C. J. Brinker, *Nature (London)* **2000**, *405*, 56.
[59] G. Temtsin, T. Asefa, S. Bittner, G. A. Ozin, *Journal of Materials Chemistry* **2001**, *11*, 3202.
[60] M. Kuroki, T. Asefa, W. Whitnal, M. Kruk, C. Yoshina-Ishii, M. Jaroniec, G. A. Ozin, *Journal of the American Chemical Society* **2002**, *124*, 13886.
[61] G. J. D. Soler-illia, C. Sanchez, B. Lebeau, J. Patarin, *Chemical Reviews* **2002**, *102*, 4093.
[62] N. K. Raman, M. T. Anderson, C. J. Brinker, *Chemistry of Materials* **1996**, *8*, 1682.
[63] J. C. Vartuli, K. D. Schmitt, C. T. Kresge, W. J. Roth, M. E. Leonowicz, S. B. McCullen, S. D. Hellring, J. S. Beck, J. L. Schlenker, D. H. Olson, E. W. Sheppard, *Chemistry of Materials* **1994**, *6*, 2317.
[64] G. S. Attard, C. G. Goltner, J. M. Corker, S. Henke, R. H. Templer, *Angewandte Chemie-International Edition in English* **1997**, *36*, 1315.
[65] G. S. Attard, J. C. Glyde, C. G. Goltner, *Nature* **1995**, *378*, 366.
[66] C. G. Goltner, M. Antonietti, *Advanced Materials (Weinheim, Germany)* **1997**, *9*, 431.
[67] C. G. Goltner, S. Henke, M. C. Weissenberger, M. Antonietti, *Angewandte Chemie, International Edition* **1998**, *37*, 613.
[68] N. Husing, U. Schubert, *Angewandte Chemie-International Edition* **1998**, *37*, 23.
[69] D. W. Schaefer, *Science* **1989**, *243*, 1023.
[70] D. W. Schaefer, K. D. Keefer, *Physical Review Letters* **1984**, *53*, 1383.
[71] K. D. Keefer, D. W. Schaefer, *Physical Review Letters* **1986**, *56*, 2376.
[72] M. Kruk, M. Jaroniec, *Chemistry of Materials* **2001**, *13*, 3169.
[73] R. S. Mikhail, T. Elakkad, *Journal of Colloid and Interface Science* **1975**, *51*, 260.
[74] C. M. Bambrough, R. C. T. Slade, R. T. Williams, S. L. Burkett, S. D. Sims, S. Mann, *Journal of Colloid and Interface Science* **1998**, *201*, 220.
[75] C. M. Bambrough, R. C. T. Slade, R. T. Williams, *Journal of Materials Chemistry* **1998**, *8*, 569.
[76] C. M. Bambrough, R. C. T. Slade, R. T. Williams, *Physical Chemistry Chemical Physics* **2000**, *2*, 3499.
[77] F. Rouquerol, J. Rouquerol, K. Sing, *Adsorption by Powders and Porous Solids: Principles, Methodology and Applications*, **1999**.
[78] K. S. W. Sing, D. H. Everett, R. A. W. Haul, L. Moscou, R. A. Pierotti, J. Rouquerol, T. Siemieniewska, *Pure and Applied Chemistry* **1985**, *57*, 603.
[79] M. Kruk, M. Jaroniec, A. Sayari, *Langmuir* **1997**, *13*, 6267.
[80] S. J. Gregg, K. S. W. Sing, *Adsorption, Surface Area and Porosity. 2nd Ed*, **1982**.
[81] P. C. Ball, R. Evans, *Langmuir* **1989**, *5*, 714.
[82] M. D. LeVan, Editor, *Fundamentals of Adsorption. (Proceedings of the Fifth International Conference on Fundamentals of Adsorption held May 13-18, 1995 in Pacific Grove, California.)*, **1996**.

[83] H. L. Liu, L. Zhang, N. A. Seaton, *Journal of Colloid and Interface Science* **1993**, *156*, 285.
[84] P. I. Ravikovitch, S. C. Odomhnaill, A. V. Neimark, F. Schuth, K. K. Unger, *Langmuir* **1995**, *11*, 4765.
[85] Q. S. Huo, D. I. Margolese, G. D. Stucky, *Chemistry of Materials* **1996**, *8*, 1147.
[86] H. P. Lin, S. T. Wong, C. Y. Mou, C. Y. Tang, *Journal of Physical Chemistry B* **2000**, *104*, 8967.
[87] P. J. Kooyman, M. J. Verhoef, E. Prouzet, *Studies in Surface Science and Catalysis* **2000**, *129*, 535.
[88] M. Jaroniec, R. Madey, *Studies in Physical and Theoretical Chemistry. 59. Physical Adsorption on Heterogeneous Solids*, **1988**.
[89] J. Rouquerol, D. Avnir, C. W. Fairbridge, D. H. Everett, J. H. Haynes, N. Pernicone, J. D. F. Ramsay, K. S. W. Sing, K. K. Unger, *Pure and Applied Chemistry* **1994**, *66*, 1739.
[90] M. Kruk, M. Jaroniec, *Chemistry of Materials* **2000**, *12*, 222.
[91] E. P. Barrett, L. G. Joyner, P. P. Halenda, *Journal of the American Chemical Society* **1951**, *73*, 373.
[92] Broekhof.Jc, J. H. Deboer, *Journal of Catalysis* **1967**, *9*, 8.
[93] Broekhof.Jc, J. H. Deboer, *Journal of Catalysis* **1967**, *9*, 15.
[94] Broekhof.Jc, J. H. Deboer, *Journal of Catalysis* **1968**, *10*, 368.
[95] Broekhof.Jc, J. H. Deboer, *Journal of Catalysis* **1968**, *10*, 377.
[96] R. W. Cranston, F. A. Inkley, *Advances in Catalysis* **1957**, *9*, 143.
[97] D. Dollimore, G. R. Heal, *Journal of Applied Chemistry* **1964**, *14*, 109.
[98] G. Horvath, K. Kawazoe, *Journal of Chemical Engineering of Japan* **1983**, *16*, 470.
[99] A. Saito, H. C. Foley, *AIChE Journal* **1991**, *37*, 429.
[100] A. V. Kiselev, *Quart. Rev. (London)* **1961**, *15*, 99.
[101] A. V. Kiselev, B. V. Kuznetsov, S. N. Lanin, *Journal of Colloid and Interface Science* **1979**, *69*, 148.
[102] A. V. Kiselev, *Journal of Colloid and Interface Science* **1968**, *28*, 430.
[103] L. Alzamora, S. Contreras, J. Cortes, *Journal of Colloid and Interface Science* **1975**, *50*, 503.
[104] A. C. Zettlemoyer, H. H. Hsing, *Journal of Colloid and Interface Science* **1977**, *58*, 263.
[105] P. B. Barraclough, P. G. Hall, *Journal of the Chemical Society-Faraday Transactions I* **1978**, *74*, 1360.
[106] A. Cauvel, D. Brunel, F. DiRenzo, E. Garrone, B. Fubini, *Langmuir* **1997**, *13*, 2773.
[107] H. Naono, M. Hakuman, T. Tanaka, N. Tamura, K. Nakai, *Journal of Colloid and Interface Science* **2000**, *225*, 411.
[108] R. K. Iler, *The Chemistry of Silica: Solubility, Polymerization, Colloid and Surface Properties and Biochemistry*, **1979**.
[109] W. K. Lowen, E. C. Broge, *Journal of Physical Chemistry* **1961**, *65*, 16.
[110] R. E. Day, G. D. Parfitt, J. Peacock, *Journal of Colloid and Interface Science* **1979**, *70*, 130.
[111] F. S. Baker, K. S. W. Sing, *Journal of Colloid and Interface Science* **1976**, *55*, 605.
[112] M. Park, S. Komarneni, *Microporous and Mesoporous Materials* **1998**, *25*, 75.
[113] X. S. Zhao, G. Q. Lu, *Journal of Physical Chemistry B* **1998**, *102*, 1556.
[114] T. Kimura, S. Saeki, Y. Sugahara, K. Kuroda, *Langmuir* **1999**, *15*, 2794.
[115] T. Kimura, K. Kuroda, Y. Sugahara, *Journal of Porous Materials* **1998**, *5*, 127.

[116] P. Van Der Voort, M. Baltes, E. F. Vansant, *Journal of Physical Chemistry B* **1999**, *103*, 10102.
[117] X. S. Zhao, G. Q. Lu, X. Hu, *Microporous and Mesoporous Materials* **2000**, *41*, 37.
[118] C. M. Bambrough, R. C. T. Slade, R. T. Williams, *Studies in Surface Science and Catalysis* **2000**, *129*, 617.
[119] R. B. Gammage, S. J. Gregg, *Journal of Colloid and Interface Science* **1972**, *38*, 118.
[120] Hagymass.J, S. Brunauer, R. S. Mikhail, *Journal of Colloid and Interface Science* **1969**, *29*, 485.
[121] K. Klier, J. H. Shen, Zettlemo.Ac, *Journal of Physical Chemistry* **1973**, *77*, 1458.
[122] J. Teixeira, M. C. Bellissentfunel, S. H. Chen, A. J. Dianoux, *Physical Review A* **1985**, *31*, 1913.
[123] J. Dore, *Chemical Physics* **2000**, *258*, 327.
[124] M. C. Bellissent-Funel, *European Physical Journal E* **2003**, *12*, 83.
[125] M. Rovere, P. Gallo, *European Physical Journal E* **2003**, *12*, 77.
[126] G. Barut, P. Pissis, R. Pelster, G. Nimtz, *Physical Review Letters* **1998**, *80*, 3543.
[127] J. Y. Park, G. B. McKenna, *Physical Review B* **2000**, *61*, 6667.
[128] J. E. Ladbury, B. Z. Chowdhry, *Chemistry & Biology* **1996**, *3*, 791.
[129] T. Wiseman, S. Williston, J. F. Brandts, L. N. Lin, *Analytical Biochemistry* **1989**, *179*, 131.
[130] E. Freire, O. L. Mayorga, M. Straume, *Analytical Chemistry* **1990**, *62*, A950.
[131] S. Inagaki, S. Guan, Y. Fukushima, T. Ohsuna, O. Terasaki, in *Journal of the American Chemical Society, Vol. 121*, **1999**, pp. 9611.
[132] B. J. Melde, B. T. Holland, C. F. Blanford, A. Stein, in *Chemistry of Materials, Vol. 11*, **1999**, pp. 3302.
[133] T. Asefa, M. J. MacLachlan, H. Grondey, N. Coombs, G. A. Ozin, *Angewandte Chemie, International Edition* **2000**, *39*, 2389.
[134] C. Baleizao, B. Gigante, D. Das, M. Alvaro, H. Garcia, A. Corma, *Chemical Communications (Cambridge, United Kingdom)* **2003**, 1860.
[135] Y. Goto, S. Inagaki, *Chemical Communications (Cambridge, United Kingdom)* **2002**, 2410.
[136] M. Kuroki, T. Asefa, W. Whitnal, M. Kruk, C. Yoshina-Ishii, M. Jaroniec, G. A. Ozin, in *Journal of the American Chemical Society, Vol. 124*, **2002**, pp. 13886.
[137] C. Yoshina-Ishii, T. Asefa, N. Coombs, M. J. MacLachlan, G. A. Ozin, in *Chemical Communications*, **1999**, pp. 2539.
[138] H. G. Zhu, D. J. Jones, J. Zajac, R. Dutartre, M. Rhomari, J. Roziere, *Chemistry of Materials* **2002**, *14*, 4886.
[139] T. Asefa, M. Kruk, N. Coombs, H. Grondey, M. J. MacLachlan, M. Jaroniec, G. A. Ozin, *Journal of the American Chemical Society* **2003**, *125*, 11662.
[140] R. J. P. Corriu, A. Mehdi, C. Reye, C. Thieuleux, *Chemical Communications (Cambridge, United Kingdom)* **2002**, 1382.
[141] R. J. P. Corriu, A. Mehdi, C. Reye, C. Thieuleux, *New Journal of Chemistry* **2003**, *27*, 905.
[142] M. A. Wahab, I. Kim, C. S. Ha, *Journal of Solid State Chemistry* **2004**, *177*, 3439.
[143] P. M. Price, J. H. Clark, D. J. Macquarrie, *Journal of the Chemical Society-Dalton Transactions* **2000**, 101.
[144] M. Lasperas, N. Bellocq, D. Brunel, P. Moreau, in *Tetrahedron-Asymmetry, Vol. 9*, **1998**, pp. 3053.
[145] D. Brunel, N. Bellocq, P. Sutra, A. Cauvel, M. Lasperas, P. Moreau, F. Di Renzo, A. Galarneau, F. Fajula, in *Coordination Chemistry Reviews, Vol. 180*, **1998**, pp. 1085.

[146] M. H. Lim, A. Stein, *Chemistry of Materials* **1999**, *11*, 3285.
[147] M. H. Lim, C. F. Blanford, A. Stein, *Chemistry of Materials* **1998**, *10*, 467.
[148] T. A. Wesley Whitnall, Geoffrey A. Ozin, *Journal of the American Chemical Society, submitted*.
[149] D. A. Loy, J. P. Carpenter, S. A. Yamanaka, M. D. McClain, J. Greaves, S. Hobson, K. J. Shea, in *Chemistry of Materials, Vol. 10*, **1998**, pp. 4129.
[150] H. C. Brown, S. K. Gupta, *Journal of the American Chemical Society* **1971**, *93*, 4062.
[151] G. W. Kabalka, H. C. Hedgecock, *Journal of Organic Chemistry* **1975**, *40*, 1776.
[152] G. W. Kabalka, E. E. Gooch, *Journal of Organic Chemistry* **1980**, *45*, 3578.
[153] S. A. Bagshaw, E. Prouzet, T. J. Pinnavaia, *Science* **1995**, *269*, 1242.
[154] B. Smarsly, M. Antonietti, T. Wolff, *Journal of Chemical Physics* **2002**, *116*, 2618.
[155] G. Porod, *Kolloid-Zeitschrift and Zeitschrift Fur Polymere* **1951**, *124*, 83.
[156] G. Porod, *Kolloid-Zeitschrift and Zeitschrift Fur Polymere* **1952**, *125*, 51.
[157] G. Porod, *Kolloid-Zeitschrift and Zeitschrift Fur Polymere* **1952**, *125*, 108.
[158] E. Kaiser, Colescot.Rl, Bossinge.Cd, P. I. Cook, *Analytical Biochemistry* **1970**, *34*, 595.
[159] S. Dai, M. C. Burleigh, Y. Shin, C. C. Morrow, C. E. Barnes, Z. L. Xue, *Angewandte Chemie-International Edition* **1999**, *38*, 1235.
[160] N. M. Maier, P. Franco, W. Lindner, *Journal of Chromatography A* **2001**, *906*, 3.
[161] B. Sellergren, K. J. Shea, *Journal of Chromatography A* **1993**, *654*, 17.
[162] G. Cavazzini, G. Nadalini, F. Dondi, F. Gasparrini, A. Ciogli, C. Villani, *Journal of Chromatography A* **2004**, *1031*, 143.
[163] B. Sellergren, *Journal of Chromatography A* **2001**, *906*, 227.
[164] A. Corma, S. Iborra, I. Rodriguez, M. Iglesias, F. Sanchez, *Catalysis Letters* **2002**, *82*, 237.
[165] C. Baleizao, B. Gigante, H. Garcia, A. Corma, *Journal of Catalysis* **2003**, *215*, 199.
[166] C. Perez, S. Perez, G. A. Fuentes, A. Corma, *Journal of Molecular Catalysis A: Chemical* **2003**, *197*, 275.
[167] C. Baleizao, B. Gigante, M. J. Sabater, H. Garcia, A. Corma, *Applied Catalysis, A: General* **2002**, *228*, 279.
[168] H. C. Brown, P. V. Ramachandran, *Journal of Organometallic Chemistry* **1995**, *500*, 1.
[169] L. Verbit, P. J. Heffron, *Journal of Organic Chemistry* **1967**, *32*, 3199.
[170] M. V. Rangaishenvi, B. Singaram, H. C. Brown, *Journal of Organic Chemistry* **1991**, *56*, 3286.
[171] H. C. Brown, K. W. Kim, T. E. Cole, B. Singaram, *Journal of the American Chemical Society* **1986**, *108*, 6761.
[172] M. L. Doyle, *Current Opinion in Biotechnology* **1997**, *8*, 31.
[173] I. Jelesarov, H. R. Bosshard, *Journal of Molecular Recognition* **1999**, *12*, 3.
[174] M. M. Pierce, C. S. Raman, B. T. Nall, *Methods-a Companion to Methods in Enzymology* **1999**, *19*, 213.
[175] M. Rekharsky, Y. Inoue, *Journal of the American Chemical Society* **2000**, *122*, 4418.
[176] M. V. Rekharsky, Y. Inoue, *Journal of the American Chemical Society* **2002**, *124*, 813.
[177] C. G. Sinn, R. Dimova, M. Antonietti, *Macromolecules* **2004**, *37*, 3444.
[178] R. Kirchner, J. Seidel, G. Wolf, G. Wulff, *Journal of Inclusion Phenomena and Macrocyclic Chemistry* **2002**, *43*, 279.
[179] A. Weber, M. Dettling, H. Brunner, G. E. M. Tovar, *Macromolecular Rapid Communications* **2002**, *23*, 824.

[180] D. Vaihinger, K. Landfester, I. Krauter, H. Brunner, G. E. M. Tovar, *Macromolecular Chemistry and Physics* **2002**, *203*, 1965.
[181] S. Che, A. E. Garcia-Bennett, T. Yokoi, K. Sakamoto, H. Kunieda, O. Terasaki, T. Tatsumi, in *Nature Materials, Vol. 2*, **2003**, pp. 801.
[182] T. Yokoi, H. Yoshitake, T. Tatsumi, *Chemistry of Materials* **2003**, *15*, 4536.
[183] S. Che, Z. Liu, T. Ohsuna, K. Sakamoto, O. Terasaki, T. Tatsumi, *Nature* **2004**, *429*, 281.
[184] A. Cauvel, D. Brunel, F. DiRenzo, E. Garrone, B. Fubini, in *Langmuir, Vol. 13*, **1997**, pp. 2773.
[185] A. Matsumoto, H. Misran, K. Tsutsumi, *Langmuir* **2004**, *20*, 7139.
[186] A. Matsumoto, K. Tsutsumi, K. Schumacher, K. K. Unger, *Langmuir* **2002**, *18*, 4014.
[187] P. Van Der Voort, M. Baltes, E. F. Vansant, in *Journal of Physical Chemistry B, Vol. 103*, **1999**, pp. 10102.
[188] M. Park, S. Komarneni, in *Microporous and Mesoporous Materials, Vol. 25*, **1998**, pp. 75.
[189] C. M. Bambrough, R. C. T. Slade, R. T. Williams, S. L. Burkett, S. D. Sims, S. Mann, in *Journal of Colloid and Interface Science, Vol. 201*, **1998**, pp. 220.
[190] K. Landskron, B. D. Hatton, G. A. Ozin, D. D. Perovic, *Polymeric Materials Science and Engineering* **2004**, *90*, 733.
[191] T. Asefa, M. J. MacLachlan, H. Grondey, N. Coombs, G. A. Ozin, *Angewandte Chemie, International Edition* **2000**, *39*, 1808.

Acknowledgments

First of all I like to thank Prof. Geoffrey Ozin and Prof. Markus Antonietti for the possibility to do my doctorate in two countries with two great supervisors. For all the ideas and support during my stays in their groups as well as the possibility to travel back to the other group if need be.

I would like to thank the two great groups I have worked with during this time. Most of all I would like to thank Sung Yeun Choi, Alexei Esmanski and Mark Mamak, with whom I shared a funny time in my office in Toronto. As well as Wesley Whitnall, William Hunks, Kai Landskron and Corinna Freitag, for the nice time in the lab as well as all the help with small and bigger problems. From Golm I most of all thank Matthjis Gronewolt, for standing my stupid questions and the great team work in the lab and office, Arne Thomas for the introduction to chiral PMOs and the great work already done in this field as well as Torsten Brezesinski for distracting me from work as well as giving good suggestions and changing samples on the weekends and Hartmut Rettig for supplying nice conversations as well as good books to read.

I would like to thank Bernd Smarsly to whom I could come with all the little problems and who treated me as one of his students even so I was not.

Then I would like to thank all the technicians for helping me with measurements. Specially Andrew Baer for solid state NMR, Olaf Niemeyer for solution NMR, Regina Rothe for gas and vapor adsorption and Marlies Gräwert for the chiral separation. The last two I also thank for the nice talks.

I also thank Sue Mamiche the “group mom” in Toronto. She always knew where to find the things in the lab and who is a great person to spend time with.

I thank the coffee group in Toronto as well as Samira Nozari for the nice tea brakes in Golm.

Then I would like to thank all the people who are not mentioned here in name, for the great working conditions in Toronto and in Golm.

In the end I like to thank my parents who have helped me through all this time at university; thank you mom for kicking me out and thanks dad for always reminding me that it was me who choose to do chemistry. I also thank my grandparents who made the first stay in Canada possible for me; without them I would never have gotten this great opportunity.

Last but not least I like to thank Ludovico Cademartiri not only for reading the whole thesis and listening to all my talk about it, no I thank him most of all for finding the right words to make me smile and go on again, whenever I thought it not possible to do so.